MECHANISMS, OPTIMIZATION, AND IMPLEMENTATION OF WAVELENGTH SPECIFIC ULTRAVIOLET WATER DISINFECTION

by

NATALIE MARIE HULL

B.S. Civil Engineering, University of Kentucky, 2010

M.S. Civil Engineering, University of Colorado Boulder, 2013

for

A dissertation submitted to the

Faculty of the Graduate School of the

University of Colorado in partial fulfillment

of the requirements for the degree of

Doctor of Philosophy

Department of Civil, Environmental, and Architectural Engineering

2018

This dissertation entitled:

Mechanisms, Optimization, and Implementation of Wavelength Specific Ultraviolet Water Disinfection

written by Natalie Marie Hull

has been approved for the University of Colorado
Department of Civil, Environmental, and Architectural Engineering

Dr. Karl G. Linden (Chair)
University of Colorado Boulder
Department of Civil, Environmental, and Architectural Engineering

Dr. R. Scott Summers
University of Colorado Boulder
Department of Civil, Environmental, and Architectural Engineering

Dr. Mark T. Hernandez
University of Colorado Boulder
Department of Civil, Environmental, and Architectural Engineering

Dr. Norman R. Pace
University of Colorado Boulder
Department of Molecular, Cellular, and Developmental Biology

Dr. Gail M. Brion
University of Kentucky
Department of Civil Engineering

Date_____

The final copy of this dissertation has been examined by the signatories, and we find that both the content and the form meet acceptable presentation standards of scholarly work in the above-mentioned discipline.

ABSTRACT

Hull, Natalie Marie (Ph.D. Environmental Engineering)

Mechanisms, Optimization, and Implementation of Wavelength Specific Ultraviolet Water Disinfection

Dissertation directed by Professor Karl G. Linden, Ph.D.

The variability of ultraviolet (UV) disinfection efficacy with wavelength and the emerging regulatory guidance accounting for this variability offer opportunities for wavelength specific optimization. Wavelength selectable mercury-free UV sources including light emitting diodes (LEDs) and excilamps were tested alone and with traditional low-pressure mercury lamps to demonstrate synergy in maximizing viral inactivation while minimizing UV dose. Additionally, biomolecular damage and repair were quantified to provide mechanistic evidence for wavelength specific UV disinfection optimization and monitoring. The disinfection performance of the first commercial flow-through UV LED reactor was evaluated at various UV transmittances and flowrates before demonstrating resilience and continued efficacy at low operating cost in a year-long demonstration study at a local small drinking water system (SDWS). By mechanistically optimizing wavelength selection of mercury-free UV sources, equivalent or better disinfection performance can be achieved with lower doses and electricity input to improve sustainability of UV disinfection, especially for SDWSs.

ACKNOWLEDGEMENTS

To my committee: I am so grateful for your input, advice, and mentoring time and energy. I deeply respect and have learned so much from all of you, and cannot stress enough your influence inspiring me to be a high quality and personable educator and researcher. All of you were indispensable in helping me get a job as an assistant professor. I offer special gratitude to each of you in order of appearance.

To Gail: For my first research experience. For nudging me out of the nest. For being there when I was crushed. For the email that I couldn't seem to move out of the inbox encouraging me to go for a PhD opportunity I had declined. For continually, fearlessly, and selflessly inspiring me.

To Mark: For mentoring me in teaching, and allowing me many useful and unique teaching experiences. For being unapologetically real. For believing in me.

To Scott: For help navigating bureaucracy. For your grounding presence and perspective. For practical, vital coordination to move from the bench to the field.

To Norm: For a life boat to a continent of uncharted territory. For hiring me when I was wounded, grading for another job, taking a class, trying to finish my MS, and facing a steep learning curve before I could start contributing in the lab. For sending me on water sampling expeditions. For stories and shooting the breeze. For allowing and teaching me to write papers. For continued support and inspiration.

To Karl: For sending email requests for new students, and for responding to those and most other emails. For far exceeding my expectations of a PhD adviser. For really listening to me and understanding the DeRISK project was a great fit for my career goals. For showing up at the New Brew Fest which was the defining moment when I knew it would be OK to be your PhD student. For giving me space to learn from mistakes. For sending me to many fun places to present and conduct research, and introducing me to many interesting colleagues.

I can't imagine attempting this research without the support of the Linden Lab (including all my peers, predecessors, and superiors who are too numerous to list), the labs with whom we share space and equipment, and the Environmental Engineering Department. The undergrads I mentored including Nathan Simpson, Dustin Levine, Armand Ngassam, Mythili Isola, and William Herold were rewarding to train and invaluable help. Special thanks to Dorothy Noble and Erin Printy for making things work.

Several partnerships were essential for this research: Aquisense (Oliver Lawal and Jennifer Pagan) provided bench-top and flow-through UV-C LED systems and technical support, USHIO (Shawn Malek and Michael Clark) provided the KrCl excimer lamp, Trojan Technologies (Brian Petri and Po-Shun Chan) provided algae and technical support, and US EPA researchers (Hodon Ryu and Jennifer Cashdollar) provided adenovirus stocks.

This research was funded by the US EPA Science to Achieve Results (STAR) Grant 83560301 to the Design of Risk-reducing Innovative-Implementable Small System Knowledge (DeRISK) Center at the University of Colorado Boulder. I was also partially supported by a National Water Research Institute (NWRI) Graduate Fellowship. The mention of certain commercial products is for information purposes only and does not constitute an endorsement

by the authors or their institutions. This dissertation has not been subjected to EPA or NWRI review and does not necessarily reflect the views of the agencies.

I would not be at CU working toward my dream of earning a PhD and becoming a professor without a family that valued education. Thanks to my parents Mark and Pat Gooch for raising me to be independent and work hard, and being proud of me. Thanks to my big brother Gabe Gooch for calling me “Meathead” since middle school – you realized I was heading for academia long before I did. Thanks to my baby sister Stacie Taylor for suffering through my teaching when you were a toddler during ‘school’. Thanks to uncle Matt Gooch for ceaselessly advising me to ‘stay in school as long as possible’. Thanks to my in-laws for being supportive even when that meant your son/brother moved over a thousand miles away.

Thanks to my KY and CO friends that helped me survive, especially when ringing in each new year, celebrating marriages, trying out new breweries, going on outdoor adventures, or going to live music shows. I couldn’t have persevered without my book club ladies, especially Carolina and Lane and their families.

Endless thanks to my dog Betty for brightening my life every. single. day.

Finally, and most of all, thank you to my husband, Michael Hull. For your love and support. For your partnership, respect, and pride. For your adventurous spirit. For listening to, questioning, and providing unique perspectives on my research. For making me laugh. For fixing things and managing our money. For your hard work and sacrifices. For putting up with me. For persevering, dreaming and growing with me. Yours always, Natalie.

CONTENTS

FIGURES

TABLES

EQUATIONS

1. Introduction

1.1 Motivation

In some small towns across the United States, the three pillars of sustainability are impaired. Economies that once boomed have been left to bust. Communities that were or could be cultural hubs are withering. Environmental neglect and irresponsible practices have polluted surface and ground water, affecting human health and putting the public at risk. These factors demand that innovative solutions be put forward to support communities like these, including sustainable technologies for drinking water treatment. Non-mercury sources of ultraviolet (UV) light, including light emitting diodes (LEDs) and excimer lamps, have promise as more sustainable disinfection alternatives (versus chlorine or traditional mercury UV lamps) to protect human health and the environment. Increased mechanistic understanding of wavelength specific UV disinfection will inform optimization and design of wavelength-tailored systems, made possible using these novel UV sources. Providing proof of concept for a demonstration study for one of these technologies in a real-world small system will instill hope that there are effective, affordable solutions for treating water (and other issues) in underserved areas, inspiring investment in small communities.

1.2 UV Disinfection Fundamentals

Before optimizing UV disinfection for specific wavelengths for any scale UV disinfection application, the fundamental mechanisms of how UV light is absorbed and inactivates infectious agents must be understood. Additionally, historical application of UV disinfection by traditional UV lamps must provide the foundation for advancement.

1.2.1 Ultraviolet Light and Photochemistry

Light has properties of a wave and a particle, and the quantum energy packets delivered by light waves are contained in massless photon particles. The energy contained in a photon is determined by its wavelength, or frequency. Ultraviolet light is emitted in the region of the electromagnetic spectrum of wavelengths from 100 nm (higher energy) to 400 nm (lower energy), as shown in Figure 1 (US EPA, 2006a). Vacuum UV is generated at wavelengths from 100 – 200 nm. Germicidal UV, from 200 nm – 300 nm, encompasses UV-C (200 nm – 280 nm) and UV-B (280 nm – 315 nm). Finally, UV-A spans wavelengths from 315 nm to 400 nm. The first law of photochemistry (Grotthus-Draper) states that only photons that are absorbed can produce photochemical change. The second law (Stark-Einstein) states that only one molecule can absorb one photon. These fundamental properties and laws of photochemistry inform the mechanistic understanding of UV disinfection.

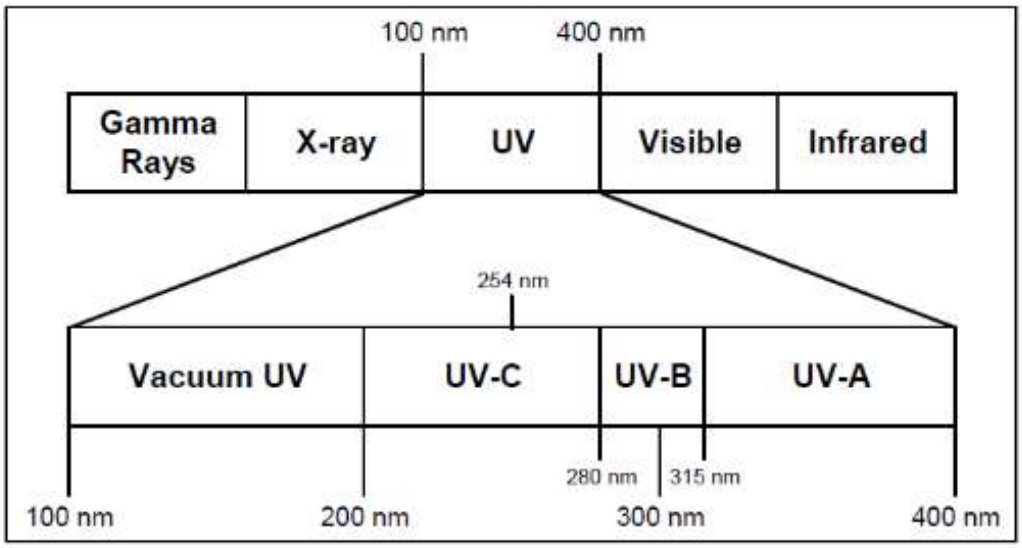

Figure 1 The Electromagnetic Spectrum and Ultraviolet (UV) wavelengths (US EPA, 2006a)**.**

1.2.2 UV-Induced Damage

The main targets for UV disinfection are nucleic acids (DNA or RNA), which strongly absorb light in the 200 to 300 nm germicidal region, as shown in Figure 2 (Harm, 1980). The most common damage is production of pyrimidine dimers, which are covalent bonds that form between adjacent thymine or cytosine bases in DNA and uracil or cytosine bases in RNA. These dimers inhibit nucleic acid replication and therefore the infective potential of infectious agents. Other potential types of nucleic acid damage include production of pyrimidine photoproducts, pyrimidine hydrates, cross links between nucleic acids or nucleic acids and proteins, and single- or double-stranded breaks. Proteins also strongly absorb light in the germicidal region (especially at wavelengths below 240 nm), as shown in Figure 2. Absorption of light by proteins can lead to

their damage (assumed to be mainly due to cross links which disrupt protein structure and function, or fragmentation), therefore disrupting stability and function of protein capsids, cell membrane proteins, and/or enzymes. UV light can also be absorbed by particles in solution, such as colloidal organic matter, that can act as photosensitizers that enhance the formation of reactive oxygen species, which non-selectively oxidize biomolecules (Lester et al., 2013; Mostafa and Rosario-Ortiz, 2013), leading to enhanced disinfection.

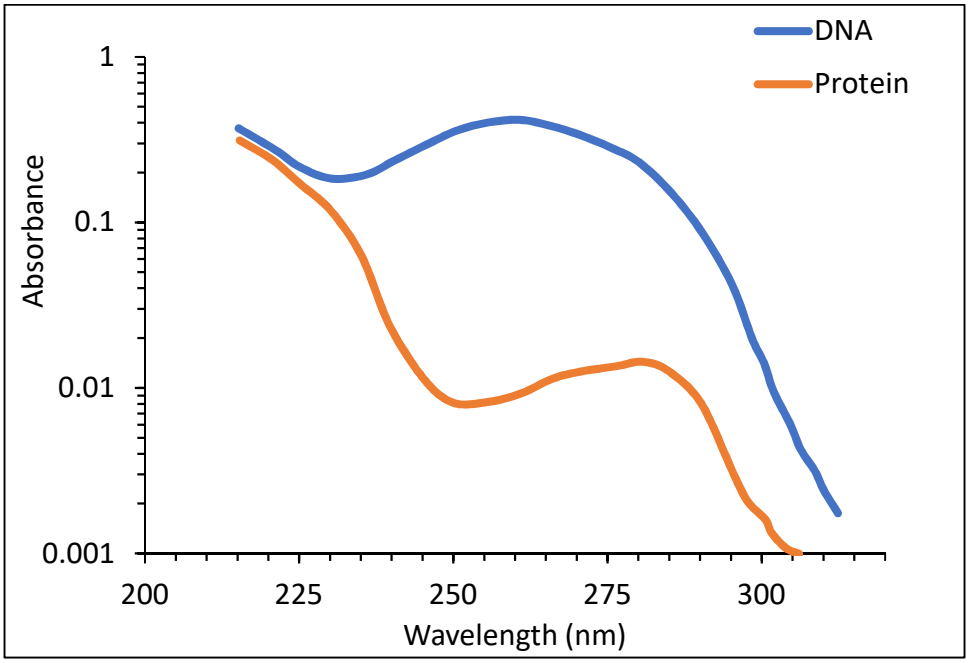

Figure 2 Comparative UV absorbance of equal concentrations of protein and DNA (Harm, 1980)**.**

1.2.3 History of UV Disinfection

The germicidal properties of sunlight were discovered in 1877, followed by the first use of UV for drinking water disinfection in 1910 (US EPA, 2006a). Although much fundamental research on UV for disinfection was carried out in the following decades, UV was not widely implemented for water disinfection until the 1960s, due to chlorine's low cost and ease of use (US EPA, 2006a). UV disinfection gained popularity as an alternative to oxidative disinfection technologies such as chlorine and ozone when the chemicals were discovered to produce hazardous disinfection-by-products (DBPs). Additional momentum was gained by UV upon the US EPA passing the suite of regulations known as the Microbial and Disinfection Byproducts Rules (MDBPR), which required utilities to simultaneously disinfect and reduce risk from disinfection byproduct formation (US EPA, 1999). Discovery of the effectiveness of UV against chlorine-resistant protozoa such as *Cryptosporidium* and *Giardia* (Clancy et al., 1998; Linden et al., 2002) led to even greater widespread acceptance and implementation of UV for water disinfection.

1.2.4 Conventional UV Sources

Conventional UV disinfection technology utilizes either low pressure (LP) or medium pressure (MP) mercury vapor lamp sources. The characteristics of these lamps are compared in Table 1 (US EPA, 2006a). Because of the difference in mercury vapor pressure, MP lamps emit many more wavelengths of light, produce more waste heat, have shorter lifespans, require more energy to operate and produce more light, and achieve lower overall efficiency of

conversion of input electricity into useful germicidal photons in the UV-C region. Most small systems use LP lamps that can be easily integrated with typical electrical systems.

Table 1 Characteristics of conventional mercury vapor UV lamps (US EPA, 2006a)**.**

Parameter	Low pressure	Medium pressure
Mercury Vapor Pressure (Pa)	~0.93 (1.35 X 10^{-4} psi)	40,000 – 4,000,000 (5.8 – 580 psi)
Lamp Emission Spectrum	Monochromatic 254 nm	Polychromatic UV + Visible light
Operating Temperature (°C)	~40	600 - 900
Electrical Input (W/cm)	0.5	50 - 250
Germicidal Output (W/cm)	0.2	5 - 30
Germicidal Electrical Conversion Efficiency (%)	35 - 38	10 - 20
Lifetime (hr)	8,000 – 10,000	4,000 – 8,000

1.3 UV Disinfection Efficacy

1.3.1 Advantages

Many advantages could be gained by systems by using UV disinfection instead of or to minimize use of chemical oxidants such as chlorine. UV has been proven effective against bacteria, protozoa, and viruses and is commonly used for drinking water treatment in the US and Europe (Clancy et al., 1998; Linden et al., 2002, 2001, Shin et al., 2009, 2001; US EPA, 2006a). UV doesn't cause taste or odor issues, and there are no harmful effects of overdosing (Chatterley et al., 2010). UV doesn't require addition of chemicals. LP UV does not induce

formation of disinfection byproducts (DBPs). UV doesn't apply pressure to select for chlorine- or antibiotic-resistant microbes (Guo et al., 2013).

1.3.2 Disadvantages

Like any technology, UV has drawbacks that present opportunities for engineering solutions or optimizations. The biggest drawback to utilizing UV alone for disinfection of drinking water is lack of disinfectant residual, which could result in light and dark repair, reactivation, and regrowth of microbes in distribution and storage systems (Bohrerova et al., 2015; Clauß et al., 2005; Kang et al., 2018a; Kollu and Örmeci, 2015; Oguma et al., 2002; Poepping et al., 2014; Quek and Hu, 2008; Rodriguez et al., 2014; Shin et al., 2010). Although these and other studies have examined photoreactivation after exposure to LP, MP, LEDs, and excilamps, the mechanisms and kinetics of repair after exposure to specific UV wavelengths needs to be more fully understood to enable rapid validation and monitoring. Better understanding of repair kinetics may inform rapid techniques for molecular-based inactivation testing that accounts for repair.

Additionally, absorbance of water and its constituents can impact disinfection efficacy. Shielding, leading to decreased inactivation, has been observed when iron or humic material was present in the water matrix (Cantwell et al., 2008; Templeton et al., 2006). Water matrix absorbance affects light penetration to target microbes (Loge et al., 1999), but turbidity up to 10 NTU has been reported to have no effect on dose-responses (Passantino et al., 2004; US EPA, 2006a). Aggregation of microbes together or with particles can also lead to lower disinfection efficacy and tailing effects (Mamane and Linden, 2006). The low wavelengths

emitted by MP UV have been shown to induce photolysis of nitrate to nitrite, but the products were below regulatory limits even at high initial concentrations of nitrate (Sharpless and Linden, 2001). MP UV has also been shown to induce formation of genotoxic compounds in nitrate- and organic carbon-rich waters (Martijn et al., 2015).

Poor reactor design could lead to non-uniform dose distributions, and certain water matrixes can lead to premature lamp fouling by minerals or biofilms, resulting in lower dose delivery or false sensor readings. Even though LP UV efficiently disinfects antibiotic resistant bacteria, their antibiotic resistance genes have been shown to be not completely destroyed by UV, resulting in potential for horizontal gene transfer after disinfection (McKinney and Pruden, 2012; Pang et al., 2015). Using a wavelength-targeted strategy to target infectious agents or genes of interest may alleviate some of these issues by avoiding using UV sources that emit wavelengths where the water matrix has high background absorbance.

1.3.3 Wavelength Issues

One area with opportunity for great improvement is the wavelength specific enhancement of UV disinfection efficacy, especially for UV-resistant infectious agents. Viruses (especially the human pathogen, adenovirus), spores, and eukaryotes (like yeast and pathogenic amoeba that can also host intracellular pathogens) tend to be more resistant to LP UV than bacteria (Aksozek et al., 2002; Bounty et al., 2012; Kollu and Örmeci, 2015; Pereira et al., 2013; Sökmen et al., 2008; US EPA, 2006a; Wang et al., 2010). Adenoviruses and *B. pumilus* spores, which are resistant to LP UV, have been shown to be significantly more sensitive to disinfection at wavelengths below 254 nm due to enhanced protein damage at low

wavelengths (Beck et al., 2017a, 2014b, 2014a; Chen et al., 2009; Rodríguez et al., 2013; Vazquez-Bravo et al., 2018). Damage to protein by higher wavelengths around 280 nm can also prevent repair in bacteria and viruses after UV irradiation (Li et al., 2017a; Vazquez-Bravo et al., 2018).

1.3.4 Regulatory Issues

While LP sources are more efficient at converting electricity to germicidal energy because their emission is narrowly focused in the UV-C region, MP sources have disinfection advantages due to their polychromatic emission for inactivation of UV-resistant pathogens such as adenoviruses and spores (Beck et al., 2014b; Linden et al., 2007; Yates et al., 2006). Federal regulations in the Long Term 2 Surface Water Treatment Rule (LT2SWTR) require a LP dose of 186 mJ/cm^2 for 4-log inactivation of viruses (US EPA, 2006b), but MP can achieve the same inactivation at a lower dose ranging from 60 to 100 mJ/cm^2 (Linden et al., 2009). The high dose requirement for adenovirus inactivation to validate a UV system, coupled with the Groundwater Rule statement that it is not possible to validate UV systems for such a high dose (US EPA, 2006c), has handicapped the use of UV for small systems. A recent life cycle assessment comparing UV and chlorine found that the high dose requirements to achieve 4-log virus inactivation limited the sustainability of UV disinfection for small systems (Jones et al., 2018). Emerging regulatory guidance for validation and implementation of UV reactors (US EPA, 2017) will provide methods for crediting reactors for all wavelengths emitted that play a role in disinfection, and will allow validation with a single test organism (US EPA, 2006a), reducing validation costs and eliminating overly conservative validation factors that were detrimental to

UV in the life cycle analysis (Jones et al., 2018). For example, the guidance document states that a two to three-fold reduction in capital and operating costs could be achieved by using MP for adenovirus disinfection along with the new approach, increasing the attainability and sustainability of UV disinfection. This advantage is largely due to the increased sensitivity of viruses at low wavelengths (Bolton, 2017). In order to fully take advantage of the emerging regulations in tailored wavelength reactors with confidence in providing public health protection, the mechanisms of inactivation at all relevant wavelengths need to be understood to ensure that commonly used surrogates (such as MS2 bacteriophage) accurately represent pathogen (such as adenovirus) disinfection processes.

1.4 New UV Sources and Operation

The demonstration of increased efficiency for low-wavelength UV offers small systems the possibility to incorporate UV as a potentially standalone primary disinfection technology (especially for groundwater systems where maintaining a disinfectant residual is not required) because of the ability to achieve greater inactivation of resistant organisms, such as adenovirus, with a lower UV dose. Recent advances in UV LED and excimer lamp technologies now offer the opportunity to gain efficiency over MP systems by utilizing tailored wavelength disinfection systems, with greatly improved electrical and cost-efficiency compared to early models, no use of mercury in the lamp construction, and ease of architecture optimization due to their small size (Crook et al., 2015; Ibrahim et al., 2013; Lawal, 2012; Lui et al., 2014; Nelson et al., 2013; Würtele et al., 2011). Recently, the ratification of the international Minamata Convention set the goal of phasing out mercury production, which provides further motivation for future UV

disinfection to use wavelength specific light sources that do not contain toxic mercury (Lawal et al., 2018).

1.4.1 Ultraviolet Light Emitting Diodes

UV LEDs emit photons when voltage is applied to the leads of a semiconductor with a p–n junction, where electrons recombine with electron holes causing electroluminescence. The wavelength emitted is determined by the energy band gap (and therefore materials) of the semiconductor in the chip. The most common UV LED chips are made of aluminum gallium nitride (AlGaN) and aluminum gallium indium nitride (AlGaIN), and are fabricated by vapor deposition of GaN crystal layers on to sapphire (Muramoto et al., 2014). Advantages of UV LEDs, aside from lack of mercury, include nearly instantaneous powering on, unlimited cycling, long lifespan, small size, and greater efficiency at light production versus mercury UV sources (Nelson et al., 2013). The PearlAqua is the world's first commercially available UV-C LED system designed for water disinfection (Aquisense, Erlanger, KY).

Researchers have already considered the particular suitability of small, sturdy UV-C LEDs for small system water disinfection (Oguma and Mohseni, 2015). Their circuitry is also amenable to integration with photovoltaic (solar) power (Lui et al., 2014) that may be used in remote systems. Previous work has demonstrated in a flow-through reactor that 285 nm UV-LEDs were efficient at bacterial and adenovirus inactivation in water (Oguma et al., 2015). Similar research using batch and flow-through reactors found time-based inactivation efficiency to be greater for 285 nm versus 265 nm LEDs, due to higher output at higher wavelengths, even though fluence-based efficiency was greatest for lower wavelengths (Oguma et al., 2013).

Previous research found 265 nm and 280 nm LEDs to be effective at microbial disinfection, but not yet more efficient than LP UV or MP UV when normalized to energy use (Beck et al., 2017b). The proven efficacy of UV-C LEDs against a variety of bacterial, viral, and protozoan agents has been recently reviewed (Song et al., 2016), and the body of literature has grown rapidly since the review (Beck et al., 2017b; Chen et al., 2017a; Li et al., 2017a; Rattanakul and Oguma, 2018; Sholtes et al., 2016; Vazquez-Bravo et al., 2018). The feasibility and positive outlook for UV LEDs as a water disinfection technology, including considerations for design optimizations, was recently extensively reviewed in a special journal edition (Beck, 2018; Jasenak, 2018; Oguma, 2018; Taghipour, 2018). While UV-C LEDs with wavelengths greater than 240 nm are currently most feasible for disinfection due to their long lifespans (up to 10,000 hours), lower cost, higher output, and external quantum efficiencies (EQE) ranging from <1 % up to (rarely) 20 %, LEDs with very low EQE and lifetimes have been manufactured with wavelengths as low as 222 nm (Lawal et al., 2018).

1.4.2 Excimer Lamps

Excimer lamps may be useful as low-wavelength emitters while the LED industry continues to develop more efficient and long-lasting sources at all UV wavelengths. Generation of UV photons in excimer lamps occurs through dielectric barrier discharge (DBD) when excited dimers, halogen excited dimers, or rare gas halide excited complexes transition back to the ground state, emitting a photon whose wavelength is dependent on the complex elemental composition (Oppenländer, 2007; Qian et al., 2005). The light emitted from these complexes is nearly monochromatic across the UV spectrum (Matafonova and Batoev, 2012). Complexes can

be housed in quartz sleeves and excited by electricity, similar to the process of emission for mercury-vapor lamps. Advantages of excimer lamps, other than lack of hazardous mercury, include powering on nearly instantaneously with no negative impact of on/off cycling, functioning in cold temperatures, lack of heat production, compact size, easy installation, narrow emission spectrum, and nearly 10% energy efficiency conversion (USHIO communication). Though many elements have been demonstrated for excimer lamp use, KrCl excimer lamps are particularly relevant for disinfection due to their emission near the peak of protein absorbance at 222 nm. KrCl excilamps with output power up to 100 W have been described (Lomaev et al., 2002).

The disinfection efficacy for KrCl excimer lamps was first observed in 1996, and has been further demonstrated in recent years, even at high initial microbe concentrations (Matafonova and Batoev, 2012; Matafonova et al., 2008). Their applicability for water and air treatment has been reviewed in the past (Oppenländer, 2007; Oppenlander and Sonsin, 2005; Sosnin et al., 2006) and more recently (Avdeev et al., 2017; Lomaev et al., 2016, 2012; Sosnin et al., 2015). One study showed exposure to a 222 nm excimer lamp to be more efficient for inactivation of *B. subtilis* spores than exposure to a 254 nm LP UV lamp (Wang et al., 2010). Additionally, excilamp exposure was found to limit bacterial photorepair better than LP exposure (Clauß et al., 2005). Excilamps have been shown to be more efficient than LP in inactivating both gram negative and positive bacteria, and toxin-producing foodborne pathogens (Kang et al., 2018b; Orlowska et al., 2015). In these studies, excilamps were found to affect proteins, cell membrane integrity, and DNA (by direct absorption and indirect photolysis leading to ROS production),

where LP only damaged DNA through direct absorption. No one has examined the efficiency of combining LEDs and excilamps for a wavelength-tailored, mercury-free disinfection system.

1.4.3 Design Considerations

In addition to using novel non-mercury UV sources, operational factors can also be optimized. Operating reactors in pulsed rather than continuous mode has shown promise for increasing disinfection efficiency, even if the only benefit was shown to be better management of waste heat (Bohrerova et al., 2008; Kim et al., 2013; Lamont et al., 2007; Li et al., 2010; Song et al., 2018; Wengraitis et al., 2013; Willert et al., 2010). However, in one study, authors found that microbes were able to develop resistance to polychromatic pulsed light (Massier et al., 2013). Finally, LED placement must be carefully considered because of waste-heat generation and reductions in output, leading to decreased efficiency in combined-wavelength reactors (Oguma, 2015). Placing LEDs and/or other UV sources of similar or varying wavelengths in series may be useful for waste-heat management because neither synergy nor detriment has been noted for simultaneous irradiation of viruses or bacteria with different wavelengths of UV-C LEDs (Beck et al., 2017b; Li et al., 2017a). However, in natural water matrices containing organic matter, synergy has been observed from combining UV-A wavelengths with UV-C LEDs, presumably due to photosensitization of organic matter by the higher wavelength and higher output UV-A LEDs (Chevremont et al., 2012a, 2012b). One early study even demonstrated disinfection synergy for bacteria after combining a KrCl excilamp in series with LP UV in a flow-through reactor (Ramsay et al., 2000). Finally, because of the nature of DBD in excilamps and the very small size of LED chips, these technologies offer vast opportunities in terms of reactor

architecture. For example, in a DBD excilamp, the water flowing through the reactor can serve as one dielectric.

1.5 Research Needs

This research sought to capitalize on these opportunities to optimize UV disinfection based on mechanistic knowledge of inactivation and repair using novel, wavelength selectable, mercury-free sources. A wavelength-tailored UV disinfection module could be a sustainable strategy for small systems to utilize UV disinfection. Design and optimization of such a technology requires understanding of molecular damage, molecular repair, and inactivation efficacy of disinfection of UV-resistant microbes at each wavelength alone and in various wavelength combinations, while using novel, tailored wavelength UV sources without mercury. Sustainable implementation of this technology in small systems also requires understanding of system-level effects such as costs of installation and maintenance, reliability for operation, longitudinal disinfection performance, lifespan, and ease of use. Understanding these factors will enable life cycle analysis of the sustainability of implementing wavelength specific UV disinfection for small systems, and will drive technology advancement.

1.6 Hypotheses

Based on the literature and research needs, the following hypotheses were tested:

1. Molecular Damage: Spectral molecular mechanisms of inactivation are similar between viral surrogate (MS2 bacteriophage) and pathogen (adenovirus).

2. Molecular Repair: Repair of DNA damage (measured in a marina alga *Tetraselmis suecica*) is a rapid enzymatic process that is unaffected by culture conditions.
3. Wavelength Specific Strategies: Sequential combination of tailored UV wavelengths can be optimized to achieve more efficient virus disinfection than any source alone.
4. UV LED Demonstration: A novel UV LED reactor run in a year-long demonstration study for drinking water treatment at a small system will be inexpensive and easy to operate, and will maintain disinfection performance over time.

1.7 Research Overview

Enhanced disinfection of UV-resistant infectious agents at low wavelengths, and the potential for increased electrical efficiency and sustainability from using a combination of non-mercury UV-LEDs and excimer lamps in wavelength-tailored reactor, are the driving forces for the hypotheses proposed to be tested here. Understanding these mechanisms of damage and repair will enable wavelength optimization that will result in more sustainable UV disinfection reactor implementations and monitoring at all scales to better protect public health, including in small systems.

A tailored reactor would ideally combine wavelengths from peak DNA absorbance (250 - 280 nm) with peak protein absorbance below 240 nm. This combination would simulate the advantages of polychromatic UV emissions from a MP lamp, yet be more efficient and targeted for inactivation. Targeting different biomolecules will provide a mechanistic multibarrier approach to improve efficacy of UV disinfection over traditional monochromatic LP UV. UV LEDs emitting at nominal peak wavelengths of 255, 265, and 285 nm were used to target the

maximum absorbance of DNA and the secondary peak of protein absorbance in the UV-C range. A benchtop UV LED system capable of emitting at these wavelengths was supplied through a partnership with Aquisense (Earlanger, KY). A KrCl excimer lamp emitting at 222 nm was used to target the maximum protein absorbance in the UV-C region, and was supplied through a partnership with USHIO (Cypress, CA). These LEDs and the excilamp were tested in comparison to traditional LP mercury UV lamps.

1.7.1 Hypothesis 1 (Molecular Damage)

1.7.1.1 Approach

Chapter 2 describes how the spectral molecular mechanisms of viral inactivation were compared between pathogenic adenovirus and the commonly used validation surrogate MS2 bacteriophage. After exposure to the UV sources emitting various wavelengths, MS2 protein damage was quantified by image densitometry of SYPRO Ruby stained sodium dodecyl sulfate polyacrylamide gel electrophoresis (SDS-PAGE) gels. Results for MS2 spectral protein damage were compared to adenovirus spectral protein damage measured previously by similar methods (Beck et al., 2017a). Using the spectrally irradiated adenovirus and MS2 samples, the cyclobutane pyrimidine dimer (CPD) concentration was quantified in nucleic acids of both adenovirus (DNA) and MS2 bacteriophage (RNA) using an enzyme linked immunosorbent assay (ELISA) with monoclonal antibodies specific to the structure of CPDs.

1.7.1.2 Results

Damage of MS2 and adenovirus viral proteins was greatest at wavelengths below 240 nm and near 280 nm where protein absorbance is greatest. The least significant protein damage was inflicted on both viruses by LP UV. Enhanced adenovirus and MS2 inactivation at low wavelengths correlates with protein damage at those wavelengths. Wavelength dependent adenovirus DNA damage was similar to the spectral absorbance of DNA (with peaks at low and high UV-C wavelengths), while MS2 RNA damage was greater at higher wavelengths (near ~260 nm). Spectral differences in nucleic acid damage were hypothesized to be due to the structure of the viruses, where MS2 is much smaller and simpler and has its RNA genome closely associated with its capsid, while adenovirus is larger and more complex and has its DNA genome sequestered within a thicker capsid. These direct quantification assays of nucleic acid damage provided context and complementary information to previous research using long range qPCR to indirectly (using the polymerase enzyme) quantify dose-dependent and wavelength specific nucleic acid damage in these viruses (Beck et al., 2015, 2014a). Wavelength specific CPD formation in the current study of adenovirus was similar to genome damage previously measured by PCR. Low wavelength inactivation of MS2 was attributed solely to genome damage when previously measured by PCR, but in the current study, protein damage was also determined to be a major contributor, suggesting that a combination of mechanisms (RNA-protein cross-linking) may drive MS2 inactivation at low wavelengths.

These results confirm Hypothesis 1 that the dominant spectral molecular mechanisms of inactivation are similar between adenovirus and MS2 bacteriophage for UV-C disinfection,

indicating that protein damage is a significant contributor to increased low UV-C wavelength sensitivity for viruses and that genome damage is more significant at higher UV-C wavelengths. These data provide mechanistic confidence for using MS2 alone as a viral surrogate to more easily validate UV reactors, and point toward potential molecular tools that could eventually be used for more rapid testing and direct quantitation of UV disinfection-relevant products.

1.7.2 Hypothesis 2 (Molecular Repair)

1.7.2.1 Approach

Chapter 3 describes how UV dose-dependent molecular DNA damage and kinetics of repair were quantified for a marine alga, *Tetraselmis suecica*. This alga was tested to provide mechanistic evidence for validation of UV disinfection for ship ballast water treatment systems (BWTS). Ballast water was considered as a tangential type of small system because BWTS operators and technology developers face many of the same challenges: difficulty of validations within current regulatory frameworks, and lack of capacity for continued disinfection monitoring. The same ELISA approach applied in Chapter 2 was used to measure CPDs in *T. suecica* DNA after irradiation with LP UV, the most commonly applied BWTS lamp type, providing a basis of comparison to past studies using other techniques to measure efficacy of BWTS (including techniques such as staining permeabilized cells that are inappropriate for assessing UV disinfection). The DNA repair kinetics of the alga were quantified over a range of conditions simulating varying levels of natural sunlight in the marine and freshwater environment that would induce photolyase activation and photorepair.

1.7.2.2 Results

Most *T. suecica* DNA repair occurred within 6 hr after LP UV exposure, was essentially complete within 24 hr, and was insensitive to light or nutrient conditions during incubation. Asymptotic repair kinetics indicated a maximum of 67% of DNA damage inflicted by 300 mJ/cm^2 LP UV was repairable. These data provided a novel UV dose response for DNA damage in *T. suecica* and indicated that enzymatic DNA repair kinetics were unaffected by culture conditions. Because DNA photorepair is an enzymatic process driven by the photolyase enzyme, the kinetic information is likely widely applicable to other (micro)organisms with the same enzyme. Considering the rapid DNA repair kinetics alongside slow algae growth rates (doubling time of 24 hr) revealed that almost 4 additional days of monitoring would be required to detect all repairable cells in a culture based multiple dilution most probable number enumeration assay.

These results confirm hypothesis 2 that DNA photorepair is a rapid, enzymatic process that is unaffected by culture conditions. Additionally, these data indicate that incorporating a culturing step with photorepair conditions may be necessary to account for growth of repairable (and potentially infective in the case of pathogens or ecologically invasive species) cells before enumeration using molecular techniques. Incorporating a brief culture step before applying molecular monitoring tools may help calibrate the assays so that all infectious agents are quantified.

1.7.3 Hypothesis 3 (Wavelength Specific Strategies)

1.7.3.1 Approach

As described in Chapter 4, MS2 bacteriophage was exposed to the LEDs, excilamp, and LP lamp individually and in sequential exposures to determine the optimum wavelength tailored disinfection strategy or strategies. The ability to disinfect was measured via MS2 bacteriophage infectivity. Disinfection efficacy was quantified over a range of doses for each UV source or combination of sources to determine disinfection dose responses. Responses were normalized to fluence (UV dose) and electrical energy requirements, enabling direct comparisons between UV source combinations on these two bases.

1.7.3.2 Results

Among the excimer lamp, LEDs, and the LP lamp, the excimer lamp was most effective at inactivating MS2 on a fluence basis, in concurrence with the action spectrum of this virus where low wavelengths are most effective for disinfection. This is the first reported dose response for any virus exposed to a KrCl excimer lamp. Sequential exposures incorporating the excimer lamp resulted in greater inactivation at a lower total UV dose versus single exposure to any non-excimer source alone. Sequential exposure dose responses indicated synergy from exposures to the LP or excimer lamps before UV LEDs. Sequential exposure to the LP and excilamps in either order of exposure was competitive on an electrical basis with current medium pressure (MP) disinfection (at all scenarios of wall plug efficiencies reported in the

literature), indicating the plausibility of retrofitting existing LP systems with upstream or downstream excilamps to achieve equal performance as could be achieved by replacement with MP. Best-case scenarios for electrical efficiency also showed all sequential exposures (with LEDs, excilamps, and LP lamps) to be competitive with MP UV disinfection, indicating further the current plausibility of achieving more efficient and targeted wavelength specific disinfection than MP, even with the burgeoning technologies of excilamps and LEDs. Predictive models for sequential exposure dose responses were assessed to support the current feasibility of incorporating sequential UV exposures to optimize tailored wavelength viral disinfection.

These results confirm hypothesis 3, indicating that electrical efficiency of UV disinfection using novel, wavelength specific, mercury free sources already rivals that of current mercury-based polychromatic lamps.

1.7.4 Hypothesis 4 (UV LED Demonstration)

1.7.4.1 Approach

As described in Chapter 5, the first commercially available UV-C LED disinfection system (PearlAqua, Aquisense) was chosen as the test subject for the UV LED small system demonstration study. The disinfection efficacy of the reactor was validated at the bench over a range of flowrates and UV transmittances (UVTs). The reactor was validated according to standard UV reactor validation protocols by MS2 challenge testing and biodosimetry. After validation, the reactor was installed downstream of sand filtration at a local small drinking water treatment system (Jamestown, CO). The reactor was immediately challenge tested with

MS2 to verify the installed performance against the bench validation. Over the course of 1 year, the UV transmittance (UVT) in the UV reactor influent was measured daily, and correlated with temperature, pH, and turbidity which were measured in the chlorinated effluent. Bi-weekly samples were collected in the treatment plant influent, slow sand filter effluent, and existing chlorine disinfection effluent for comparison to the demonstration study UV LED disinfection. Analytes for bi-weekly samples included adenosine triphosphate (ATP), total coliform, *E. coli*, and total organic carbon (TOC). Continued disinfection performance was monitored using quarterly MS2 challenge tests.

1.7.4.2 Results

MS2 disinfection by the PearlAqua was modeled using the first application of combined variable modeling to a UV LED reactor, providing a basis for comparison of bench validation results to demonstration-scale quarterly virus challenge tests. Quarterly MS2 challenge testing disinfection was well-predicted by the bench testing validation model upon installation at the small system and throughout the year during periods of high UVT, but not during May and August when UVT was lower and turbidity was higher. During these times, disinfection performance was actually higher than predicted, presumably due to photosensitization or confounding of UVT measurements by light scattering. These data and this approach can be used to compare, validate, and test other emerging types of UV sources (including LEDs) and reactors in the rapidly developing UV industry. This UV LED demonstration study indicated a high degree of resilience and no detrimental disinfection effects of fouling even though the reactor was provided zero maintenance, and cost only an estimated < $25 in electricity to treat

0.5 lpm at an MS2 reduction equivalent dose of at least 40 mJ/cm^2 (LP UV) for the entire year, while losing only 27% of initial LED output power.

This year-long demonstration study confirms hypothesis 4, indicating that the LED PearlAqua reactor was inexpensive and easy to operate, while being efficacious for disinfection. This first longitudinal demonstration study of a flow-through UV LED disinfection reactor at a small system drinking water treatment plant provides evidence for the practicality of LEDs as an emerging disinfection technology, allowing faster adoption in the future.

1.8 Summary

Overall, this thesis increases understanding of how UV inflicts biomolecular damage, and how that damage is repaired, at different UV-C wavelengths. Molecular tools used here could be applied for reactor optimization, validation, and monitoring in the future. This mechanistic understanding bolsters technology developments using combinations of new and/or existing UV light sources that can be optimized for more efficient drinking water disinfection. By optimizing wavelength selection, reactor design, and operation of mercury-free UV sources, equivalent or better disinfection performance can be achieved with less electricity, thereby improving the sustainability of the UV disinfection process. Additionally, this research can inform emerging UV regulatory guidance so that when optimized wavelengths are used, lower UV doses will be required, increasing the attainability (affordability and feasibility of implementation) of this technology for small systems.

2. Spectral Ultraviolet Mechanisms of MS2 Bacteriophage and Adenovirus Disinfection

This chapter describes application of molecular tools to characterize damage to proteins and nucleic acids after irradiation of MS2 bacteriophage and adenovirus by various wavelengths across the UV-C spectrum.

This work will be prepared to submit for publication after further studies replicating results and broadening the range of UV doses in some cases:

Hull NM, Herold WH, Jeanis KM, Beck SE, and Linden KG (*in preparation,* 2018). Spectral Ultraviolet Mechanisms of MS2 Bacteriophage and Adenovirus Disinfection.

2.1 Introduction

Although advancements have been made toward understanding disinfection mechanisms by specific ultraviolet (UV) wavelengths, molecular mechanisms of disinfection are still not completely understood for viruses including MS2 bacteriophages (a nonpathogenic surrogate commonly used for UV reactor validations) and Adenoviruses (a pathogen on which UV drinking water disinfection regulations are based in the US). Understanding viral inactivation mechanisms is important to ensure that optimization, validation, and monitoring of UV disinfection based on surrogates will protect public health from pathogens. Understanding wavelength-dependent mechanisms of viral inactivation is becoming more important as UV water disinfection increasingly incorporates polychromatic (multiple wavelength) medium pressure (MP) mercury vapor lamps and emerging mercury-free wavelength-selectable sources such as light emitting diodes (LEDs) and excimer lamps (excilamps), versus traditional monochromatic (single wavelength) low pressure (LP) mercury lamps.

For both MS2 and adenovirus, genome damage is the primary driver of inactivation at 254 nm, the primary wavelength emitted by LP lamps (Beck et al., 2015, 2014a; Bosshard et al., 2013; Vazquez-Bravo et al., 2018). LP UV has also been demonstrated to cause site-specific cleavage of MS2 coat protein using mass spectrometry techniques, although the contribution to inactivation was limited (Wigginton et al., 2012a; Wigginton and Kohn, 2012). Another MS2 study of LP UV compared viral infectivity, genome damage by long range (LR) qPCR, and capsid damage by treatment with a nucleic acid binding dye (propidium monoazide or PMA) assumed to be impermeable to intact viral capsids coupled with LR-qPCR, and demonstrated more

similarity between infectivity and dye-coupled qPCR, again indicating a contribution of protein damage to loss of infectivity (McLellan et al., 2016). Other studies of MS2 and adenovirus comparing LR-qPCR and infectivity across the UV-C spectrum demonstrated good agreement at 254 nm, but increasing deviation between genome damage and infectivity at wavelengths less than 240 nm, which indicates an increasing contribution of non-genomic damage at low wavelengths (Beck et al., 2015, 2014a). For both MS2 and adenovirus, their spectral sensitivity (i.e. action spectrum) dramatically increases at wavelengths below 240 nm, with a smaller relative peak around 260 – 270 nm (Bolton, 2017). Protein damage to the viral capsid has been quantitatively linked with increased spectral sensitivity at low wavelengths for adenovirus (Beck et al., 2017a, 2014a; Eischeid et al., 2009; Eischeid and Linden, 2011; Sangsanont et al., 2014), and has been speculated to contribute to enhanced low-wavelength MS2 inactivation (Beck et al., 2015). For adenovirus, damage to the fiber proteins (which bind with high affinity to specific host cell receptors) and penton proteins (which bind with lower affinity to integrins that activate viral endocytosis) seems to play a role in disrupting the lytic cycle at low wavelengths, while damage to other constituents seems to prevent enzymatic repair at higher wavelengths near 280 nm (Beck et al., 2017a; Bosshard et al., 2013; Vazquez-Bravo et al., 2018).

Previous studies have used a variety of molecular methods to elucidate mechanisms of viral inactivation at different UV-C wavelengths. Some indirect (enzyme mediated) quantification methods that have been used include short and long range quantitative PCR amplification of genes or transcription products (including reverse transcription approaches) (Beck et al., 2015, 2014a; McLellan et al., 2016; Nizri et al., 2017; Rodríguez et al., 2013; Vazquez-Bravo et al., 2018), coupling PCR with nucleic acid binding dyes (such as PMA) that

penetrate UV-damaged capsids and render genes or transcription products unable to be amplified by PCR (McLellan et al., 2016; Sangsanont et al., 2014; Vazquez-Bravo et al., 2018), and infectivity assays coupled with PCR. Direct quantitations have used variations of mass spectrometry techniques (Bosshard et al., 2013; Qiao and Wigginton, 2016; Rule Wigginton et al., 2010; Wigginton et al., 2012a), and sodium dodecyl sulfate polyacrylamide gel electrophoresis (SDS-PAGE) coupled with gel staining and image densitometry for these and other viruses (Beck et al., 2017a; Bosshard et al., 2013; Eischeid and Linden, 2011; Tanaka et al., 2018). An endonuclease sensitive site assay (ESS) has been applied to other infectious agents (but not viruses) to indirectly quantify cyclobutane pyrimidine dimers (CPDs) using a nuclease enzyme (Eischeid and Linden, 2007; Oguma et al., 2001). However, this is the first study to directly quantify dose-dependent CPD nucleic acid lesions in either adenovirus or MS2 bacteriophage after wavelength-specific UV irradiation, using an enzyme-linked immunosorbent assay (ELISA) employing a monoclonal antibody specific to the structure of CPDs (Oxi-Select, Cell Biolabs Inc). Although one study used SDS-PAGE to study MS2 protein damage after visible light photocatalysis (Akhavan et al., 2012), this is the first study to use SDS-PAGE to quantify dose-dependent damage to MS2 coat proteins after wavelength-specific UV irradiation, enabling direct comparison of wavelength-specific protein damage between MS2 and published data for adenovirus (Beck et al., 2017a). These approaches (SDS-PAGE and CPD-ELISA) enable direct quantitation of UV induced viral damage without the use of enzymes such as polymerase or nuclease.

2.2 Methods

2.2.1 Virus Propagation and Enumeration

Adenovirus stocks provided by the EPA in Cincinnati, OH (Human adenovirus 2, ATCC VR-846) that had been propagated in A549 human lung carcinoma cells (ATCC CCL-185) were diluted 1:1 in sterile water with continuous stirring for previously described UV irradiations (Beck et al., 2017a). Adenovirus suspensions were irradiated as described previously by an LP lamp, LEDs with peak wavelengths of 261 and 278 nm, or a bandpass-filtered deuterium lamp with peak emissions of 214, 220, 227, 240, and 268 nm (Beck et al., 2017a). MS2 bacteriophage (ATCC 15597-B1) stocks were propagated and enumerated using *E. coli* F_{amp} host (ATCC 700891) as described previously (Beck et al., 2015), and were diluted ten-fold in 1X PBS with continuous stirring for UV irradiations. MS2 suspensions were irradiated as described previously (see Chapter 4) following standard protocols (Bolton and Linden, 2003; Linden and Darby, 1997) by an LP lamp, a KrCl excimer lamp, LEDs of peak (nominal) wavelengths of 258 (255), 268 (265), and 282 (285) nm, or a bandpass-filtered deuterium lamp with peak emissions of 214 or 240 nm. LEDs and the bandpass filtered deuterium lamp emission spectra had full width half maximum bandwidth of approximately 10 nm, while the LP lamp and KrCl excilamp were nearly monochromatic. Incident irradiances were multiplied by petri, divergence, water, and reflection factors to determine average irradiances. After correcting for nonlinear spectral radiometer response, average irradiances were used to calculate exposure times without any other spectral weighting. In the case of evaporation (always < 20% of 2 mL sample volume), volume lost was measured by pipette and added back using PBS for MS2 samples, and added

back using water for adenovirus samples (Beck et al., 2017a). Irradiated samples were frozen at < -70 °C until molecular analysis.

2.2.2 Molecular Assays and Data Analysis

Nucleic acids were extracted from rapidly thawed samples following kit protocols with slight modifications (DNeasy for adenovirus and RNeasy for MS2, Qiagen). For MS2 RNA extraction, 100 µL of the irradiated sample was incubated with 500 µL of Buffer RLT, spin columns were fully dried using the optional centrifuging step, and RNA was eluted in 200 µL of RNase-free water. For adenovirus DNA extraction, 100 µL of the irradiated sample, 100 µL 1X PBS, and 20 µL proteinase K were added to a centrifuge tube and mixed thoroughly by vortexing before loading spin columns, and DNA was eluted in a single step in 200 µL AE buffer. Extracted nucleic acids were quantified fluorometrically (PicoGreen for adenovirus DNA and RiboGreen for MS2 RNA, Quant-iT Invitrogen) following Quantus fluorometer (Promega) protocols for low-concentration assays. CPD nucleic acids were quantified spectrophotometrically using a 96-well plate reader (Epoch, Biotek) following ELISA kit protocols for isolated nucleic acids (Oxi-Select, Cell Biolabs Inc) without sample mass normalization, as described previously (Hull et al., 2017). To prevent evaporation during the overnight incubation of samples with the high-binding microplate, the wells were sealed with clear tape. After quantification, the CPD concentration was normalized to the total RNA or DNA concentration. Protein extraction, SDS-PAGE, SYPRO Ruby gel staining, and gel staining image densitometry were performed for MS2 samples as previously described (Beck et al., 2017a) for adenovirus samples.

2.3 Results

2.3.1 MS2 Nucleic Acid Damage

The dose dependent concentrations of total RNA, CPDs, and their ratio are shown in Figure 3 for MS2 samples exposed to a range of doses by each UV source. RNA concentrations (Figure 3a) were consistent with UV dose in all experiments, and were consistent between experiments using the LEDs and the LP lamp, but were higher in the experiment using the excimer lamp. CPD dose responses (Figure 3b) demonstrated the 265 nm LED to be the most effective at inflicting CPD nucleic acid damage. After normalizing measured CPD concentrations based on total RNA concentrations (Figure 3c), trends remained similar between dose responses for individual UV sources, with the 265 nm LED being most effective at inflicting CPD damage, the KrCl excilamp being the least effective, and the other sources being similar in efficacy.

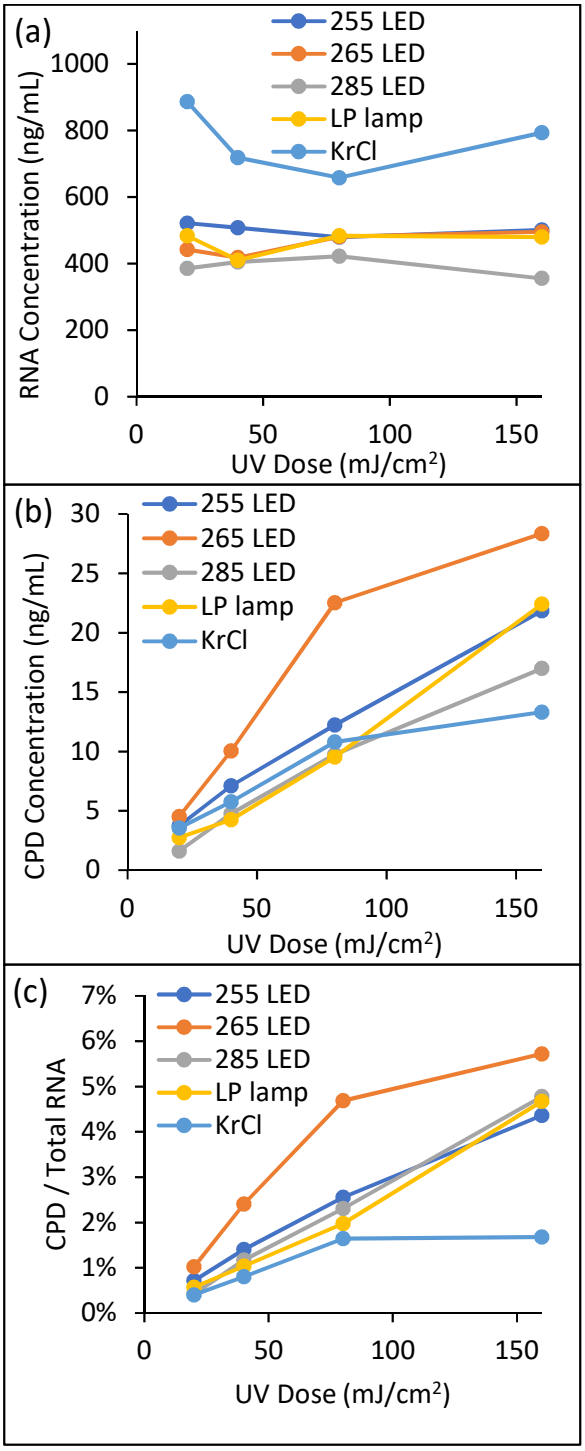

Figure 3 MS2 sample dose dependent (a) RNA concentration (measured by Ribogreen), (b) CPD concentration (measured by ELISA), and (c) the ratio of CPD to total RNA after exposure to each UV source.

2.3.2 Adenovirus Nucleic Acid Damage

The dose dependent concentrations of DNA, CPD, and their ratio for duplicate experiments are shown in Figure 4 for adenovirus samples exposed to a range of doses for several UV sources (Beck et al., 2017a). The total DNA concentration (Figure 4a) and CPD concentration (Figure 4b) differed between duplicate experiments for all dose responses. After normalizing by taking the ratio of CPD to total DNA (Figure 4c), there was no clear dose response trend of nucleic acid damage for samples exposed to doses from 100 – 400 mJ/cm^2 emitted by 260 or 280 nm LEDs, or the LP lamp. Dose responses and replicates demonstrated a high degree of variability in these samples, centered near the ratio of 100% CPD / Total DNA, indicating the need to test adenovirus at lower UV Doses to better determine CPD dose responses. There was dose dependent nucleic acid damage for samples exposed to doses up to 38 mJ/cm^2 of the 220 nm emission by the bandpass-filtered deuterium lamp. However, because the fraction of CPD to total DNA doesn't reach a high amount, higher doses need to be tested for this source to more clearly determine the dose response. Also, because of the high degree of variability in the assay, further replication is needed, ensuring consistent conditions between biological and technical replicates.

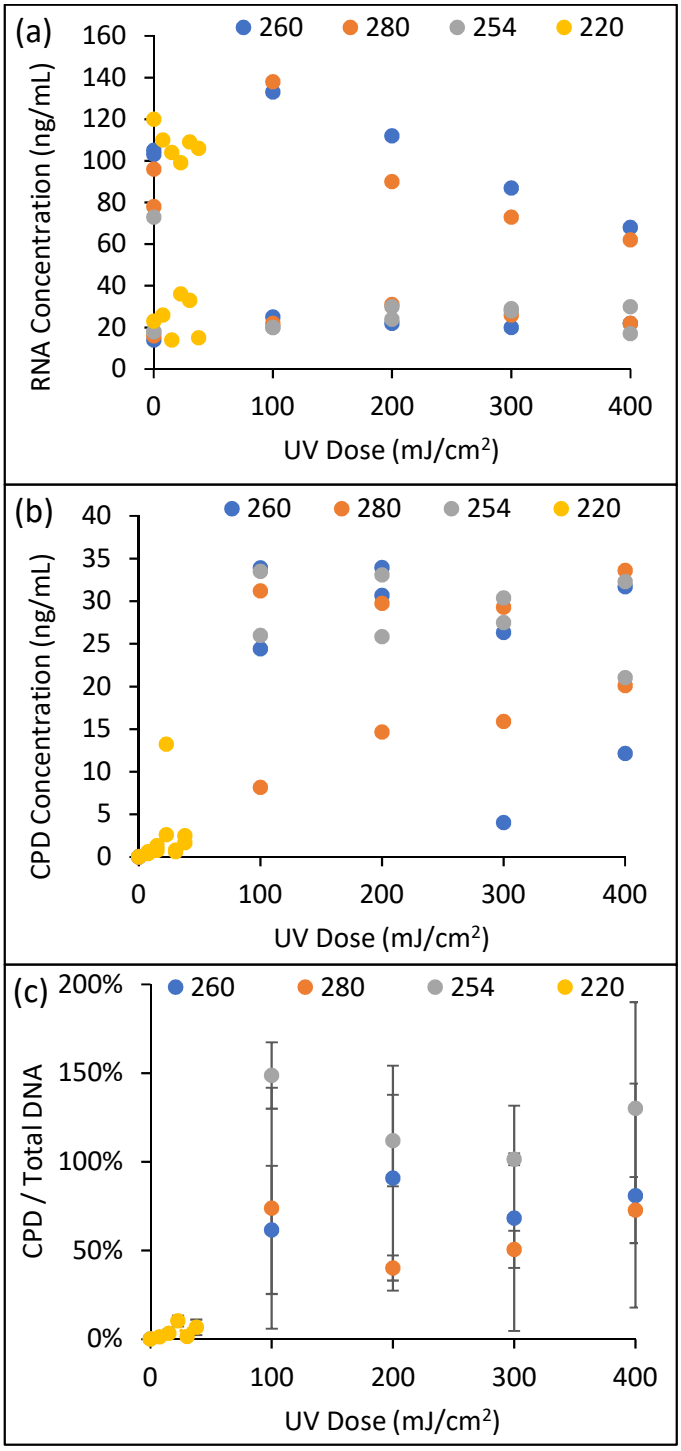

Figure 4 Adenovirus sample dose dependent (a) DNA concentration (measured by Picogreen) (b) CPD concentration (measured by ELISA) and (c) the ratio of CPD to total DNA for each UV source (260 or 280 nm LEDs, 254 nm LP UV, or bandpass filtered 220 nm) averaged between experiments with error bars showing standard error of the mean (SEM).

In a separate experiment, adenovirus samples were exposed to a UV dose of 50 mJ/cm^2 by each UV source (except for 214 nm where the dose was 28 mJ/cm^2, 220 nm where the dose was 38 mJ/cm^2, and 227 nm where the dose was 45 mJ/cm^2) to determine the spectral response of nucleic acid damage. After taking the ratio of measured CPD to Total DNA for each sample, responses for samples exposed to less than 50 mJ/cm^2 were dose-corrected with the assumption of linear kinetics. Figure 5 shows results of this ratio for each sample relative to the result at 254 nm (averaged between duplicate experiments), indicating peaks in relative nucleic acid damage at wavelengths near 220 nm and near 265 nm. The high degree of variability in this assay again points to the need for increased replication in these results.

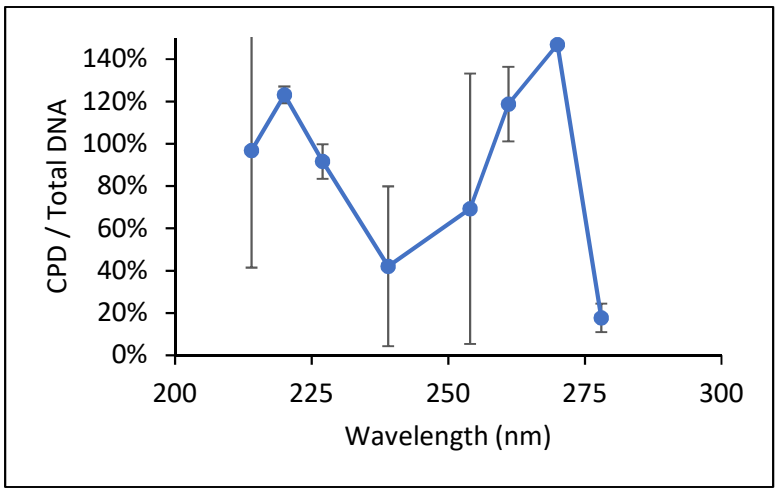

Figure 5 Adenovirus ratio of CPD to total DNA after exposure to a single dose (corrected assuming linear kinetics so all doses were equal) of each UV source, averaged between experiments with error bars showing standard error of the mean (SEM).

2.3.3 MS2 Protein Damage

MS2 samples were exposed to a UV dose of 80 mJ/cm^2 by each UV source. Figure 6a shows a representative a gel depicting the response of MS2 coat protein before and after exposure. The MS2 coat protein and the internal standard (1 ng aprotinin) are shown in each lane. Image densitometry was used to normalize the relative staining intensity of the coat protein to the internal control to account for differences in protein extraction efficiency. The normalized MS2 coat protein amount in the unexposed sample was then divided by the normalized MS2 coat protein in all UV exposed samples to determine the relative amount of damage inflicted by each UV source. The amount of damage for each source was then expressed as a ratio relative to the response for LP UV, and plotted at the UV source's peak wavelength to develop the plot of relative spectral sensitivity shown in Figure 6b. For reference, the relative lamp emission spectra are plotted along with the calculated spectral sensitivity of the coat protein. Figure 6 demonstrates that the MS2 coat protein was damaged much more efficiently at wavelengths lower than 240 nm than at 254 nm, and slightly more efficiently at wavelengths above 254 nm.

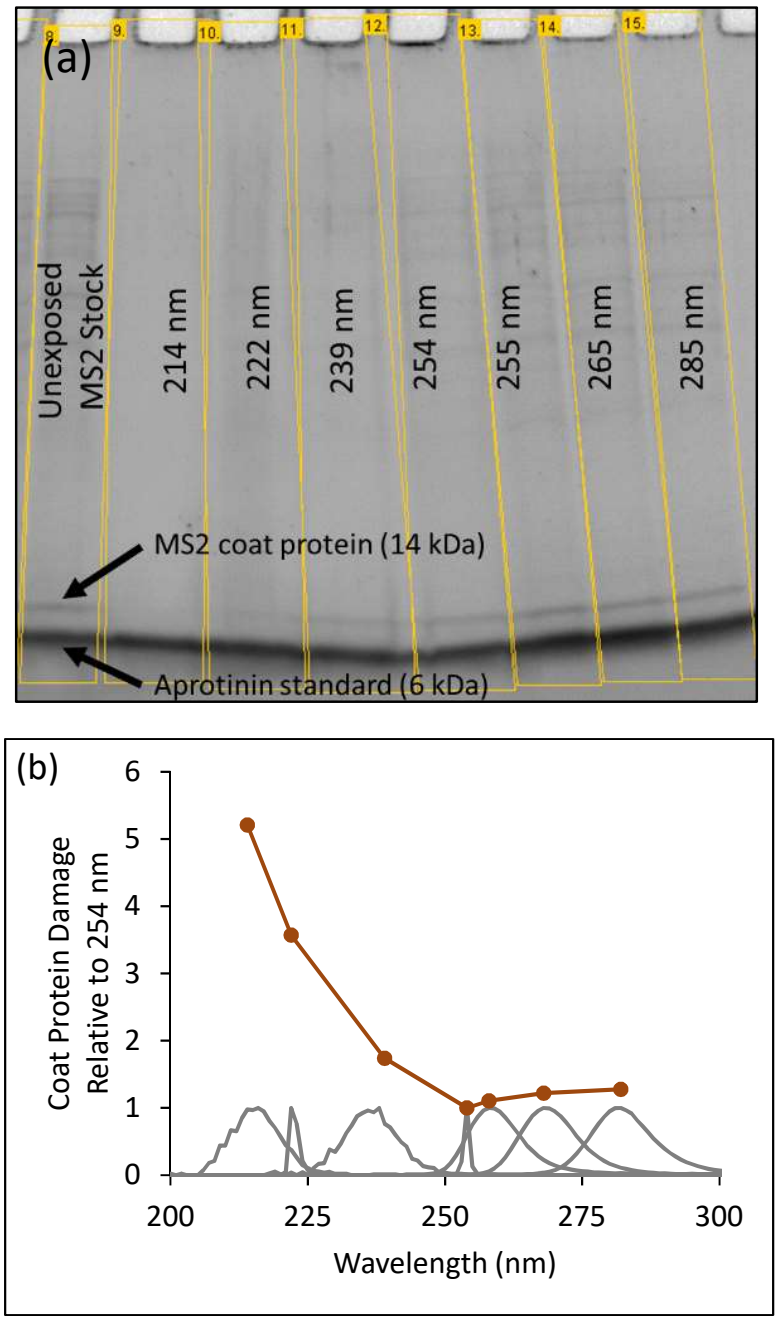

Figure 6 MS2 coat protein damage shown by (a) representative SYPRO Ruby stained SDS-PAGE gel showing coat protein response to 80 mJ/cm^2 emitted by each UV source and (b) image densitometry quantification of coat protein damage response (unexposed / exposed) relative to the LP UV response (at 254 nm) after normalizing based on the aprotinin internal control.

MS2 samples exposed to UV doses from 20 – 160 mJ/cm^2 that were analyzed for nucleic acid damage (shown in Figure 3) will also be analyzed for protein damage to develop dose responses for MS2 coat protein damage by each UV source before submitting these data for publication.

2.4 Discussion

The results presented here include novel indication of the relative contributions of directly measured protein and nucleic acid damage to MS2 inactivation. These results complement previous data demonstrating correlation between loss of genome amplification indirectly measured by LR-RTqPCR, and loss of MS2 infectivity (Beck et al., 2015). However, the direct measurements here of protein damage by SDS-PAGE and CPD lesions by ELISA indicate that loss of MS2 genome amplifiability and infectivity at low wavelengths is caused mainly by protein damage and to a lesser extent by nucleic acid damage (Figure 3 and Figure 6 for damage, (US EPA, 2017) for inactivation), rather than nucleic acid damage alone. Together, these studies indicate that protein – genome cross-linking may influence MS2 inactivation mechanisms at low UV wavelengths. Techniques that have been used to study nucleic acid binding proteins in human cells including mass spectrometry, restriction digests immunoprecipitation, microarrays, and/or RNA sequencing (Darnell, 2010; Gott et al., 1991; Kuo and Allis, 1999; Kurdistani and Grunstein, 2003; Tretyakova et al., 2015; Ule et al., 2005; Welsh and Cantor, 1984) could be used to further elucidate protein interactions with the MS2 genome at low UV-C wavelengths.

These MS2 results concur with recent advancements using molecular approaches to understand spectral mechanisms of adenovirus inactivation (Beck et al., 2017a, 2014a; Vazquez-Bravo et al., 2018), where both protein damage and nucleic acid damage contribute to inactivation at low wavelengths, but genome damage is primarily responsible for inactivation at higher wavelengths. Protein damage likely affects virus internalization by host cells that disrupts the lytic cycle for both viruses. Although not measured here due to detection limits, damage to the single-copy MS2 maturation protein (MP) may have contributed to inactivation caused by protein damage. The MP binds to bacterial pili and is essential for delivery of the infective viral genome into the host cell during pilus retraction (Dai et al., 2017; Dent et al., 2013). Our results showing limited protein damage to MS2 at 254 nm concur with one study of LP UV which demonstrated little MS2 protein damage or effect on association to host cell (Rattanakul and Oguma, 2017). Although one previous study showed significant adenovirus protein damage at low wavelengths (Beck et al., 2017a), another study of adenovirus showed that neither high nor low wavelengths prevented association of adenovirus with host cells (Vazquez-Bravo et al., 2018). However, the wash used in the association study may not have removed loosely attached virions (Ryu et al., 2015), and methods couldn't discriminate whether both host-cell binding sites necessary to initiate adenovirus endocytosis had been bound.

Although the ELISA used here to measure CPDs wasn't designed for RNA, these results demonstrate that dose-dependent CPD lesions can be measured using the CPD antibody in both RNA (Figure 3) and DNA (Figure 4 and Figure 5). Although the antibody used here is proprietary, the most common anti-CPD antibody (clone TDM-2) was established by mouse immunization with UV-irradiated DNA antisera containing heterogenous photoproducts (Mori et al., 1991).

Stable binding of this antibody has been shown for all dipyrimidines in single DNA strands of at least 8 bases (Kobayashi et al., 2001), where at least one of the 5’ or 3’ negatively charged nucleotide phosphates interacts electrostatically with the positively charged antibody binding site (Komatsu et al., 1997; Torizawa et al., 2000). Because the antibody interactions are both steric and electrostatic and are not completely understood, it is plausible that the CPD antibody antigen-binding site can accommodate both the additional oxygen molecule on the RNA pentose sugar, and the slight differences between uracil and thymine bases. Additionally, the novel demonstration of clear and measurable dose response using the proprietary monoclonal CPD antibody in MS2 RNA demonstrates that CPD damage can be detected and possibly quantified in RNA. Further study is needed to elucidate the affinity and epitope specificity of this assay when comparing DNA and RNA. One major caveat to these ELISA results is that the positive control used for the standard and calculating CPD concentration is not truly quantitative. The manufacturer' standard concentration is the original concentration of total DNA that was irradiated extensively to generate an undetermined concentration of CPDs. Positive control CPD standards corresponding to a known mass or number of dimers need to be developed for this assay to become truly quantitative. For example, one study used a high UV dose to dimerize all possible sites in a well characterized plasmid for the positive control (Sinha et al., 2001). However, complete dimerization needs to be verified for a truly quantitative standard.

One study of LP UV irradiated free MS2 RNA oligonucleotides found more lesions by mass spectrometry than by RT-qPCR, and found more photohydrates than CPDs while noting that the quantitation was less sensitive to CPDs (Qiao and Wigginton, 2016). Together, these

results indicate that a combination of molecular methods including direct measurements (e.g mass spectrometry, ELISA) and indirect measurements (based on PCR) may be necessary for a comprehensive and quantitative understanding of the molecular mechanisms of viral UV disinfection. For example, proteomics approaches applied to adenovirus exposed to sunlight and LP UV (Bosshard et al., 2013) could be enhanced by analyzing all size fractions rather than just the expected molecular weights, including proteins with UV-induced irreversible bonds that prevent SDS-PAGE migration (Beck et al., 2017), which could inform specific types and locations of damage to viral proteins of both adenovirus and MS2. Using these combined with other molecular approaches to understand damage to both proteins and nucleic acids will help overcome obstacles of traditional culture-based methods, such as long incubation times and confounding effects of host cell repair (Cashdollar et al., 2016; Ryu et al., 2015).

Although mechanisms for MS2 and adenovirus are similar to each other, they may not be similar to other pathogenic or surrogate viruses (Sigstam et al., 2013; Simonet and Gantzer, 2006; Wigginton et al., 2012b; Wigginton and Kohn, 2012). However, approaches using CPD antibodies have been applied to measure sunlight inactivation of total indigenous communities in natural waters (Blyth et al., 2013; Stephanie et al., 2011), to measure UV-C inactivation of various bacteria in lab water (Stephanie et al., 2011), and as an immunofluorescent assay for UV irradiated airborne bacteria (Peccia and Hernandez, 2002) that could be amenable to future online flow cytometry applications (Hammes et al., 2008), enabling rapid quantitative assessment of total nucleic acid damage. Quantification of nucleic acid damage to entire populations by 16S rRNA gene qPCR was also recently demonstrated to be effective for on-site UV reactor validation testing (Nizri et al., 2017). However, these approaches may quantify

damage to noninfectious agents (Sherchan et al., 2014), whereas coupling with short incubations and measuring transcription (Vazquez-Bravo et al., 2018) may better measure infectivity.

Emerging regulatory and validation approaches are moving toward crediting UV disinfection systems for high and low wavelength contributions (Adams, 2016). These approaches will replace the use of overly conservative validation factors that decrease the sustainability of UV disinfection (Jones et al., 2018), which will prevent overdosing while maintaining public health protection. However, wavelength targeted optimization of UV disinfection requires fundamental understanding of wavelength specific mechanistic damage to pathogens and surrogates. The data presented here demonstrated that the primary mechanisms of disinfection for surrogate MS2 bacteriophage and pathogenic adenovirus are similar across the UV-C spectrum. The direct quantitation methods (CPD ELISA and SDS-PAGE) have promise for wavelength-targeted disinfection optimization studies at the bench, and for reactor validation and monitoring in the field.

2.5 Conclusions

These direct measurements of molecular damage (protein damage measured by SDS-PAGE and nucleic acid damage measured by ELISA for CPD) inform spectral UV-C inactivation mechanisms of MS2 bacteriophage and adenovirus. These data taken in context of existing literature indicate that MS2 is a compatible surrogate for adenovirus based on molecular damage across the UV-C spectrum (primarily protein damage at wavelengths below 240 nm and primarily nucleic acid damage at higher wavelengths). For MS2, protein damage at low

wavelengths may be dominated by protein-RNA crosslinking. Direct molecular measurements of inactivation targets are promising ways to optimize, validate and monitor UV disinfection.

3. Algal DNA Repair Kinetics Support Culture-Based Enumeration for Validation of UV Ballast Water Treatment Systems

This chapter describes application of an ELISA molecular assay to assess LP UV dose dependent DNA damage (formation of cyclobutane pyrimidine dimers) and repair kinetics in the marine alga *Tetraselmis suecica*. Because DNA repair is an enzymatic process that is insensitive to culture conditions, these quantifications and application of this disinfection efficacy monitoring tool, coupled with a brief culturing step to account for photorepair, might be applied after further study and assay development for validating and monitoring other UV disinfection reactors in other water matrices.

This work has been published:

Hull NM, Isola MR, Petri B, Chan P, and Linden KG (2017). Algal DNA Repair Kinetics Support Culture-Based Enumeration for Validation of UV Ballast Water Treatment Systems. *ES&T Letters* 4(5):192-196.

3.1 Introduction

The International Maritime Organization (IMO) (IMO, 2004) and United States Coast Guard (USCG) (USCG, 2012) regulate discharge of ballast water used by ships to maintain balance with and without cargo. Intake and discharge of huge water volumes in divergent ports can transport pathogens or non-indigenous species (NIS). Size delineated discharge performance standards that took full effect in 2017 were set by IMO in 2004, and adopted by USCG in 2012. Ballast water treatment systems (BWTS) can be installed to mitigate NIS and pathogen transport, and comply with new regulations.

IMO type-approval can be obtained by demonstrating BWTS efficacy using various biological enumeration methods for each of the regulated criteria (IMO, 2004). Approval by USCG, however, requires enumeration of organisms in the 10 – 50 µm size fraction (which is dominated by phytoplankton (Casas-Monroy et al., 2015)) using 'vital' stains FDA and CMFDA that detect esterase enzyme activity in cells with intact membranes (MacIntyre and Cullen, 2016; Nelson et al., 2009; Steinberg et al., 2011; USCG, 2012). These stains are appropriate for oxidative disinfectants that affect metabolism and membranes, but they cannot detect DNA damage- the primary mechanism of treatment by ultraviolet (UV) light (Olsen et al., 2015). Absorption of UV by DNA induces formation of cyclobutane pyrimidine dimers (CPD) that inhibit reproduction (Weber, 2005). Just as pathogens must reproduce to cause an infection (Alberts et al., 2002), multiplication of viable cells is necessary for NIS invasion (Casas-Monroy et al., 2015; John J. Cullen and MacIntyre, 2016).

Because the UV dose required to inflict enzyme and membrane damage detectable by vital stains is much higher (up to 11X (Olsen et al., 2015)) than the dose necessary to render organisms unable to reproduce (R. O. Olsen et al., 2016), UV BWTSs have struggled to obtain USCG approval without using exorbitant doses (John J. Cullen and MacIntyre, 2016). This disconnection necessitates urgent investigation of accurate enumeration techniques. Besides FDA/CMFDA and other stains coupled with microscopy or flow cytometry (Adams et al., 2014; MacIntyre and Cullen, 2016; R. Olsen et al., 2016; Olsen et al., 2015; R. O. Olsen et al., 2016; Steinberg et al., 2011; Tao et al., 2010), other biological methods such as microscopic examination of morphology and motility (First and Drake, 2014; R. O. Olsen et al., 2016), active fluorescent measurements for photosynthetic state (Bradie et al., 2017; Drake et al., 2014), and ATP measurements for metabolic activity (First and Drake, 2014; van Slooten et al., 2015), have been suggested for enumerating phytoplankton, but can differ by taxon and/or disinfection mechanism. Additionally, these methods may underestimate concentrations when applied to UV-treated discharge by neglecting possible growth of cells with damaged DNA after photorepair of CPD by the photolyase enzyme (Bohrerova and Linden, 2007; Casas-Monroy et al., 2015; Grob and Pollet, 2016; Liebich et al., 2012; Sancar, 1994; Weber, 2005).

Culture-based methods, however, are consistent with all treatment mechanisms, and should provide a conservative assessment by allowing repair during incubation (John J Cullen and MacIntyre, 2016; John J. Cullen and MacIntyre, 2016; First and Drake, 2014; Nelson et al., 2009; Romero-Martínez et al., 2016; Stehouwer et al., 2015). A serial dilution culture method known as most probable number (MPN) has been proposed to enable accurate enumeration of viable 10 – 50 µm phytoplankton in discharge water for various BWTS technologies (John J

Cullen and MacIntyre, 2016; John J. Cullen and MacIntyre, 2016). In 2015 the USCG rejected MPN (USCG, 2012), deeming it less protective by measuring viability (ability to reproduce) instead of vitality (ability to live) (Knox, 2016), and citing uncertainties about false-negatives (non-detection of viable cells) and potential repair after UV treatment (Knox, 2015). Neither stains nor MPN provide a complete assessment of living status, as both measure some but not all properties of life, and recent work shows neither method to be more susceptible to false-negatives (Cullen and MacIntyre, 2017; John J Cullen and MacIntyre, 2016; John J. Cullen and MacIntyre, 2016; MacIntyre and Cullen, 2016). However, MPN should be equally protective for preventing NIS invasion, because neither non-viable nor non-vital organisms can successfully colonize an environment (John J. Cullen and MacIntyre, 2016). The contribution of viable cells that repair but may not resuscitate is poorly understood for any enumeration method (Li et al., 2014; Pinto et al., 2015; Ramamurthy et al., 2014). However, culture-based methods that enumerate both undamaged and repairable cells should be more accurate than existing methods of BWTS validation. To molecularly test the hypothesis that culturing avoids underestimating viable cell concentration by including DNA repair, *Tetraselmis suecica* (a phytoplankton species commonly used for BWTS studies (Olsen et al., 2015; R. O. Olsen et al., 2016)) were treated with UV, and DNA damage was measured over incubation time after UV treatment. Repair was compared for harsh (seawater only) and favorable (seawater with additional nutrients) culture conditions, over a range of light levels to simulate environmental discharge.

3.2 Materials and Methods

3.2.1 Algae Cultivation

Tetraselmis suecica (CCMP 904) marine phytoplankton were cultured in 0.2 µm filter-sterilized artificial seawater (Crystal Sea) supplemented with 'nutrients' (Guillard's f/2 Marine Water Enrichment Media, Sigma Aldrich) under visible light emitting diodes (LEDs) emitting Photosynthetically Active Radiation (PAR) intensity of 100 µmol m^{-2} s^{-1} (LightScout Quantum light meter with PAR sensor, Spectrum Technologies, Inc.). The relative spectral output (Maya USB 2000, Ocean Optics) of LEDs is shown in Figure 7. For UV experiments, cells were cultured to a target concentration of ~60,000 cells/mL. UV absorbance at 254 nm (A_{254}) and pulse amplitude modulated (PAM) fluorometry F_v measurements (Hach BW680) were used to estimate concentrations based on previous correlations with cell counts (Coulter Multisizer 4). Cells grown to this density had a PAM F_v/F_m ratio of 0.65 (indicating good health) and A_{254} = 0.1 cm^{-1} in seawater with nutrients.

3.2.2 UV Irradiation and DNA Repair Incubations

For collimated low pressure (LP) UV exposures, incident irradiance (IL1700 radiometer) was corrected for petri (PF), water (WF), divergence (DF), and reflection factors (RF=0.9750) to determine average irradiance, which was used to calculate exposure time to deliver a chosen dose to a well-mixed sample (Bolton and Linden, 2003). Though BWTS utilize both LP and medium pressure (MP) UV lamps (which can additionally damage proteins (Eischeid et al.,

2009)), LP was used here to pinpoint DNA damage. To determine *T. suecica's* DNA damage dose response to LP UV, algae samples (A_{254} = 0.1013 cm^{-1}) were exposed to a range of doses from 0 – 400 mJ/cm^2. An incident irradiance of 0.294 mW/cm^2, resulted in an average irradiance of 0.139 mW/cm^2 after corrections (WF = 0.59, DF = 0.89, PF = 0.92). Analysis of DNA extracted from these samples immediately after UV irradiation indicated that a LP UV dose of 300 mJ/cm^2 induced sufficient DNA damage to assess repair in subsequent visible light incubations, without complete algal inactivation.

For UV exposure and repair experiments, algae were harvested on 0.5 µm nylon net filters (Millipore) by gravity filtration and resuspended in artificial seawater without nutrients. Absorbance was used to match cell density between the UV dose-response and repair experiments. Because nutrients added 0.02 cm^{-1} absorbance, the target A_{254} in seawater without nutrients for UV exposures was 0.08 cm^{-1} (actual A_{254} = 0.0803 cm^{-1}). An incident irradiance of 0.224 mW/cm^2 resulted in an average irradiance of 0.127 mW/cm^2 after corrections (WF = 0.68, DF = 0.91, PF = 0.94). Samples were collected before and after UV irradiation for DNA analysis and MPN enumeration.

After splitting the remaining UV-irradiated sample and supplementing with equal volumes of either artificial seawater or nutrients (for harsh and favorable incubation conditions, respectively), 50 mL aliquots were distributed into polypropylene tubes for repair incubations under fluorescent lamps emitting in the active region (350 - 450 nm) of photolyase (Bohrerova and Linden, 2007; Sancar, 1994; Weber, 2005). Different light intensities were achieved by varying the number of fluorescent lamps and distance between samples and lamps. The relative spectral outputs of the fluorescent and LP UV lamps are shown in Figure 7. The 50 mL samples

were incubated for 0.5, 3, 6, 24, or 48 hours under fluorescent lamp intensities of 25, 50, 100 or 200 µmol m^{-2} s^{-1}, and frozen rapidly at -80°C after the specified incubation time.

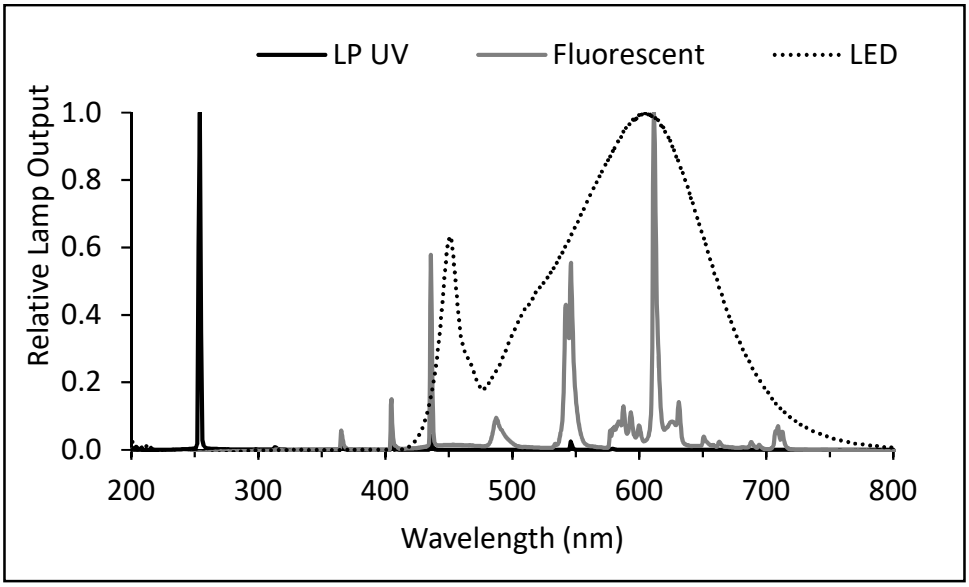

Figure 7 Relative lamp output of light sources used for UV irradiation (LP UV), algae cultivation (LED), and MPN and repair incubation (Fluorescent).

3.2.3 MPN Enumeration

Untreated and UV-treated algae samples were enumerated in duplicate by MPN (John J Cullen and MacIntyre, 2016; John J. Cullen and MacIntyre, 2016). For each sample, 5 replicate subsamples of serial 10-fold dilutions were incubated in media with nutrients under 100 µmol m^{-2} s^{-1} fluorescent lamps. Algal growth was measured by fluorescence (Promega Quantas fluorometer; red channel) after 7, 14, and 21 days of incubation. Subsample fluorescence was

scored positive for growth when increase between consecutive measurements exceeded 4 x standard deviation of 5 replicate media blanks. Positive scores were used to calculate MPN (Curiale, 2004). Consecutive fluorescence measurements of positive subsamples were used to calculate exponential growth rates (n = 7 subsamples).

3.2.4 DNA Analyses

Frozen samples were thawed rapidly and 10 mL duplicates were aliquoted and centrifuged at 4,696 x *g* for 30 min to pellet algae. After discarding supernatant, the pellet was suspended in 200 µL 1X PBS, and DNA was extracted by Qiagen DNeasy blood and tissue kit (Simonelli et al., 2009), with an elution volume of 100 µL. DNA was quantified by Picogreen (Invitrogen) on a Quantus fluorometer (Promega), and by absorbance (Nanodrop 1000). CPD-DNA was quantified spectrophotometrically (Epoch, BioTek) using pyrimidine dimer-specific antibodies (OxiSelect UV-Induced DNA Damage ELISA Kit, Cell Biolabs, Inc) without mass normalization.

3.3 Results and Discussion

The dose-dependent CPD-DNA damage concentration in LP UV treated algae samples is shown in Figure 8. Total DNA measured by picogreen (3.0 $\pm$ 0.5 ng/µL) did not vary with dose, and was near the optimal ELISA assay loading value of 4 ng/µL, negating need for mass normalization. At 300 mJ/cm^2, CPD-DNA comprised 0.24 % of the total DNA. Shielding by the

high lipid content of these algae could have contributed to slight shouldering at the lowest doses.

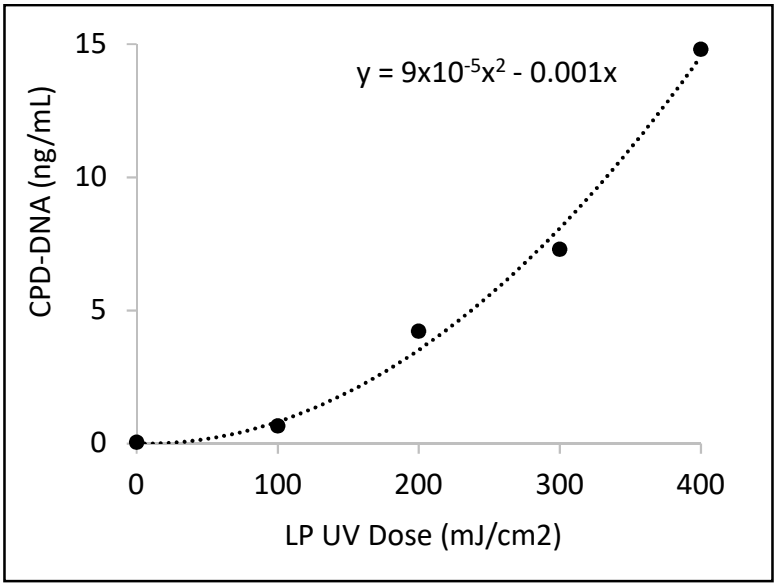

Figure 8 CPD-DNA damage concentration in UV-treated algae samples, and fitted dose-response equation (R^2=0.99).

For the repair study, total DNA concentration was measured by both Nanodrop absorbance and Picogreen fluorescence for all samples to ensure accuracy of comparisons between longitudinal samples for CPD-DNA data, by verifying constant total DNA and equal ELISA mass loading. DNA was quantified by both methods because the effect of UV treatment and DNA damage on these quantification mechanisms is not known. Untreated control and UV-treated sample DNA concentrations (n = 2 for each) did not differ by nanodrop (t-test p = 0.39) or picogreen (t-test p = 0.08), indicating that DNA structural changes did not affect quantification for either method. By the more specific picogreen assay, neither nutrients

(ANOVA p = 0.54, n = 20 each), time (ANOVA p = 0.40, n = 8 each), nor light (ANOVA p = 0.21, n = 10 each) affected DNA concentration (average = 1.7 $\pm$ 0.6 ng/µL), validating ELISA results and comparisons between samples. The concentrations of viable cells determined by MPN in untreated and UV-treated samples were 29,000 and 0.20 cells/mL respectively, resulting in 5.2 log reduction by 300 mJ/cm^2 LP UV, and an apparent UV resistance of 58 mJ/cm^2 per log. This concurs with recent culture-based studies where no growth was detected either 21 days after irradiating ~10^4 cells/mL *T. suecica* with 400 mJ/cm^2 MP UV (R. O. Olsen et al., 2016), or 7 days after irradiating ~10^3 cells/mL of another *Tetraselmis* species with 500 mJ/cm^2 LP UV (First and Drake, 2014). Based on untreated MPN and assuming genome mass = 0.7 pg (Simonelli et al., 2009), DNA extraction efficiency was 85 %.

No CPD-DNA was detected in the repair study for the untreated algae sample. To demonstrate DNA repair kinetics in 300 mJ/cm^2 LP UV treated samples, relative CPD-DNA ($\boldsymbol{R_{CPD}}$) was calculated for each time point and condition as the ratio of CPD-DNA in the repair-incubated sample vs. CPD-DNA in the time zero UV treated sample. Figure 9 shows the average relative CPD-DNA concentrations over time in UV-treated samples incubated a) in seawater with and without nutrients, and b) at each light level. As shown by overlapping standard deviations, neither nutrient condition nor light level affected relative CPD-DNA concentrations.

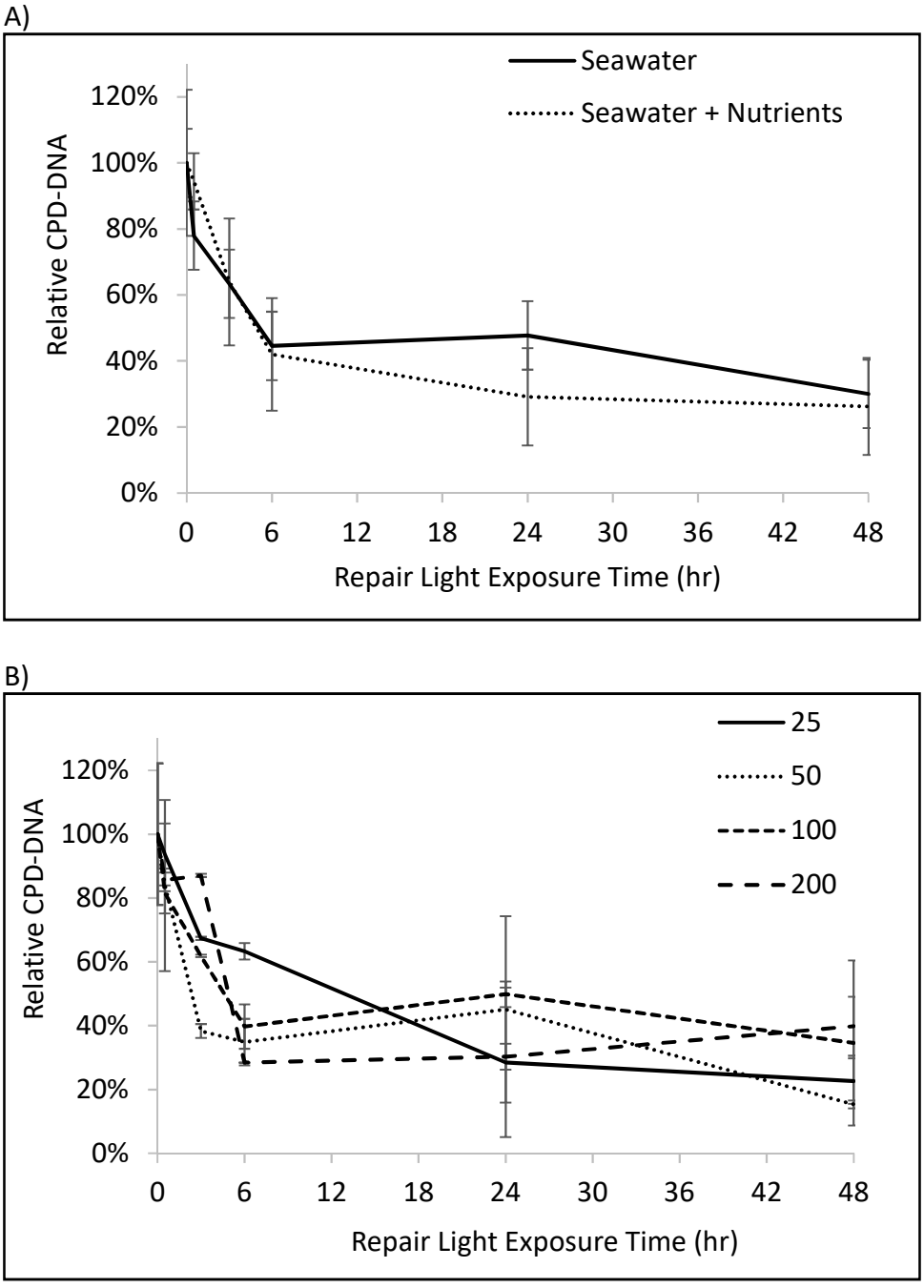

Figure 9 Average CPD-DNA damage concentration in UV-treated relative to unexposed algae samples by A) nutrient condition, or B) fluorescent lamp PAR light intensity (µmol m^{-2} s^{-1}). After averaging duplicate samples, standard deviations shown by error bars were calculated for A) all light levels or B) both nutrient conditions.

Accuracy of culture-based enumeration requires detection of all viable cells, including those that are damaged and have an initial lag time to repair and regain ability to reproduce. This requires monitoring long enough for a subsample with a single viable cell to grow to the detection limit. For exponentially growing cells, at a given time (t, hr), the number of cells (N_t) growing in a subsample can be expressed as function of the initial cell number (N_0), growth rate (k, hr^{-1}), and lag time for a damaged cell to repair (l, hr), as shown in Equation 1.

Equation 1 Algae growth kinetics

$$\boldsymbol{N_t = N_0 e^{k(t-l)}}$$

Based on untreated algae fluorescence data (where $l = 0$), growth rates ranged from $k = 0.028 - 0.042\ hr^{-1}$, in concurrence with another *Tetraselmis* species with doubling times of 24 – 48 hr (Lu et al., 2017). At the slowest growth rate, it would take 82 hr (3.4 days) for each subsequent 10–fold diluted subsample to reach the detection limit.

The same calculation can be applied to UV-treated cells to determine the additional incubation time required for accurate detection of damaged cells. Lag times for individual cells can vary after UV treatment because some cells are more damaged than others, some cells can reproduce before complete DNA repair, and some cells cannot repair. Algal CPD-DNA repair kinetic data were modeled to determine maximum lag time in UV-treated samples. The relative amount of CPD-DNA (R_{CPD}) versus incubation time (t, hr) for UV-treated algae was modeled (RMSE = 0.23) by exponential decay (Equation 2).

Equation 2 Relative CPD-DNA kinetics

$R_{CPD} = 0.33 + 0.62e^{-0.26}$

The asymptote of this model represents the minimum expected R_{CPD} (33%, with 95% confidence interval = 25 – 41 %), or the maximum capacity for CPD-DNA repair. Based on this expected limit of DNA repair capacity, 87% of repairable CPD-DNA inflicted by 300 mJ/cm^2 LP UV was repaired in the first 6 hr of incubation, and repair was essentially complete within 24 hr. So, a conservative estimate of maximum lag time for UV-treated cells is $l = 24\ hr$. A similar lag was reported for complete restoration of photosynthetic activity in *T. suecica* 24 hr after UVB exposure (Kristoffersen et al., 2016). This lag time would increase the time t required to ensure no further detection of growth in subsequent subsample dilutions to 106 hr (4.4 days). Within untreated and UV treated samples, the most dilute subsamples that scored positive did so by day 14, and no subsamples of greater dilution showed growth in the following 7 days. Thus, 14 days were sufficient to detect growth of the most dilute subsamples containing viable cells, and the additional 7 days verified this. All viable cells (both undamaged and repairable), were detected by day 14, confirming that cell repair and growth were conservatively modeled. These repair and growth models are supported by studies of other algae, where growth rates after UV treatment were equal to control samples after an initial lag (Romero-Martínez et al., 2016; Tao et al., 2010).

By the principle of dose reciprocity (Bunsen and Roscoe, 1855), equal doses of light delivered in different combinations of time and intensity cause equal effects. Algal CPD-DNA repair did not differ with repair light intensity, indicating that repair occurred more rapidly or

was affected less significantly than could be detected. Alternatively, lack of dose-reciprocity suggests that R_{CPD} kinetics were driven primarily by enzymatic interactions between photolyase and CPD-DNA, where light was not the limiting factor (Sancar, 1994; Sinha and Häder, 2002; Weber, 2005). Photolyase enzymatic reactions are fast (<1 ns) and efficient (quantum yield ≈ 1 (Rastogi et al., 2010; Sinha and Häder, 2002)), causing photorepair to be much more rapid than dark repair mechanisms (Romero-Martínez et al., 2016). Additionally, because nutrients had no effect on R_{CPD} kinetics, these data are consistent with repair rates being determined by enzymatic reaction rates, rather than biological growth rates. This indicates that photorepair would be unaffected by environmental conditions (light, nutrients), or taxon-specific conditions (growth rate/phase).

Because photorepair of UV damage occurs rapidly within incubations, culture-based enumeration of treated samples is accurate, fair to UV and other BWTS, and environmentally protective. This information supports recent efforts (Bradie et al., 2017; Drake et al., 2014; First and Drake, 2014, 2013; Steinberg et al., 2012; Wright et al., 2015) to assess enumeration techniques that could be appropriate for UV and other BWTS, enabling faster approval and adoption within the US to comply with increased regulatory stringency.

4. Synergy of MS2 Disinfection by Sequential Exposure to Tailored UV Wavelengths

This chapter describes synergy in MS2 disinfection attained by sequential exposure to UV sources of varying wavelengths. In particular, synergy was achieved when exposing samples to UV-C LEDs after exposure to either LP or KrCl excimer lamps. After normalizing disinfection based on electrical requirements and wavelength specific UV absorbance, results demonstrated the current competitiveness of mercury-free, wavelength tailored disinfection using these emerging UV sources compared to existing MP UV technology.

This work has been published:

Hull NM and Linden KG (2018). Synergy of MS2 Disinfection by Sequential Exposure to Tailored UV Wavelengths. *Water Research* 143:292-300.

4.1 Introduction

Conventional ultraviolet (UV) water disinfection technology utilizes either monochromatic (~254 nm) low pressure (LP) or polychromatic medium pressure (MP) mercury vapor UV lamp sources. While federal regulations in the United States require a LP UV dose of 186 mJ/cm^2 for 4-log virus inactivation based on pathogenic adenoviruses (US EPA, 2006b, 2006a), MP can achieve the same inactivation at less than half the dose (Eischeid et al., 2011; Eischeid and Linden, 2011; Linden et al., 2007; Shin et al., 2015). The high LP UV dose requirement coupled with the Groundwater Rule statement (US EPA, 2006c) that it is not possible to validate UV systems for such a high dose, has handicapped the use of UV for some disinfection applications. However, the demonstration of increased efficiency for polychromatic MP UV indicates the possibility to optimize UV disinfection based on wavelength. Additionally, recent research (Adams, 2016) on innovative validation practices for MP reactors has led to drafted federal recommendations enabling alternative approaches that account for polychromatic UV advantages, especially at low wavelengths (US EPA, 2017).

Recent advances in UV light emitting diodes (LEDs) and excimer lamps (excilamps) now offer the potential to gain efficiency over MP by utilizing wavelength tailored disinfection systems. Wavelengths are selectable for both of these emerging technologies by changing the semiconductor composition for LEDs, or by changing the excited dimer molecule for excilamps (Chen et al., 2017b; Oppenländer, 2007). These technologies have improved electrical and cost- efficiency compared to early models, contain no hazardous mercury, have long lifetimes, suffer no damage from repeated on/off cycles, reach full power nearly instantaneously, and can

be implemented in diverse designs due to their small size and low power requirements (Chen et al., 2017b; Hirayama et al., 2015; Ibrahim et al., 2013; Muramoto et al., 2014; Oppenländer, 2007; Pagan and O, 2015; Song et al., 2016).

Past studies of simultaneous irradiations by multiple UV-C LED wavelengths demonstrated no synergy (Beck et al., 2017b) or negative impacts due to waste heat (Oguma et al., 2013), indicating the need for research on the effects of sequential exposures that may allow more flexible designs. The possible synergy from combining excimer lamps, UV LEDs, and/or conventional LP lamps in a sequential exposure tailored wavelength disinfection system has barely been investigated. One study demonstrated greater *E. coli* inactivation in a flow through reactor with sequential exposure to KrCl excimer followed by LP lamps versus the same reactor operating each source alone (Ramsay et al., 2000). However, UV doses were not determined and detection limits were inadequate to fully assess synergy. Another study examined *E. coli* inactivation and genome damage from sequential exposures to various UV wavelengths, using bandpass filters on an MP lamp (Poepping et al., 2014). No studies have determined effects of sequential exposures on viral disinfection.

Because UV disinfection depends on the spectral sensitivity of the target microorganism rather than source of photons, the disinfection efficacy of LEDs or excilamps for any agent is equal to conventional mercury lamp UV disinfection for a given wavelength and dose combination. A recent comprehensive review of disinfection literature for UV sources relevant to this study is updated and graphically summarized in Figure 10. Figure 10 demonstrates that bacteria and protozoa are easily inactivated at low UV doses, while viruses require higher doses for inactivation. Figure 10 also demonstrates that lower doses are required by polychromatic

MP for equivalent disinfection in all classes of infectious agents. No study has measured viral disinfection by KrCl excilamps.

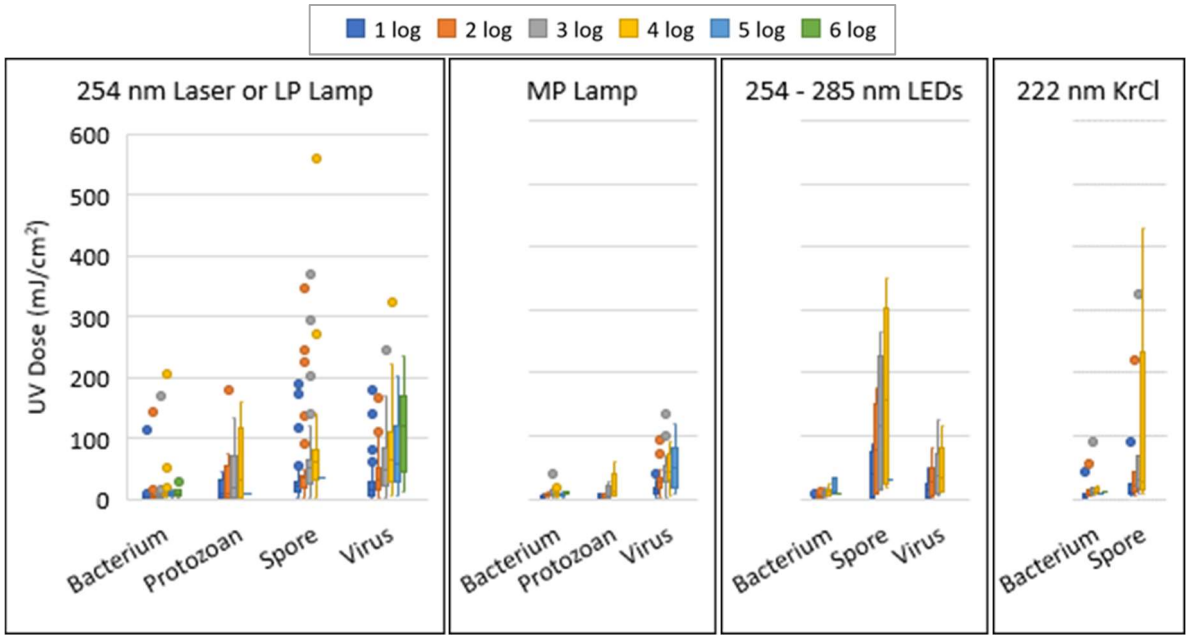

Figure 10 Summary of UV doses reported in literature for log_{10} reductions of bacteria, protozoa, viruses, and spores by 254nm laser or LP lamp, MP lamp, UV-C LEDs, and KrCl excilamps (Beck et al., 2017b; Chevremont et al., 2012b; Malayeri et al., 2017; Song et al., 2016)**.**

MS2 bacteriophage is often used as a surrogate for pathogenic virus disinfection due to its ease, reproducibility, and safety of cultivation. The spectral sensitivity of both MS2 (the surrogate) and adenovirus (the regulated pathogen) display marked increase in sensitivity at wavelengths below 240 nm and a relative peak in sensitivity at wavelengths between 260 and 280 nm, as shown in Figure 11 where their action spectra have been scaled by the LP UV Dose required to achieve one log reduction. At wavelengths below 240 nm, adenovirus is more

susceptible to UV disinfection than MS2, making MS2 a conservative surrogate for low-wavelength disinfection studies. These scaled action spectra also demonstrate that protozoan pathogens such as *Cryptosporidium* and bacterial pathogens such as *Salmonella typhimurium* are more easily inactivated than viruses at all wavelengths across the UV spectrum. Thus, viruses in general and MS2 specifically serve as conservative estimators of UV disinfection across the UV-C spectrum, enabling wavelength tailored engineering optimizations based on virus disinfection. Most importantly, Figure 11 shows that disinfection can be optimized by selecting UV sources emitting wavelengths where infectious agents are most easily inactivated, where D_L is lowest.

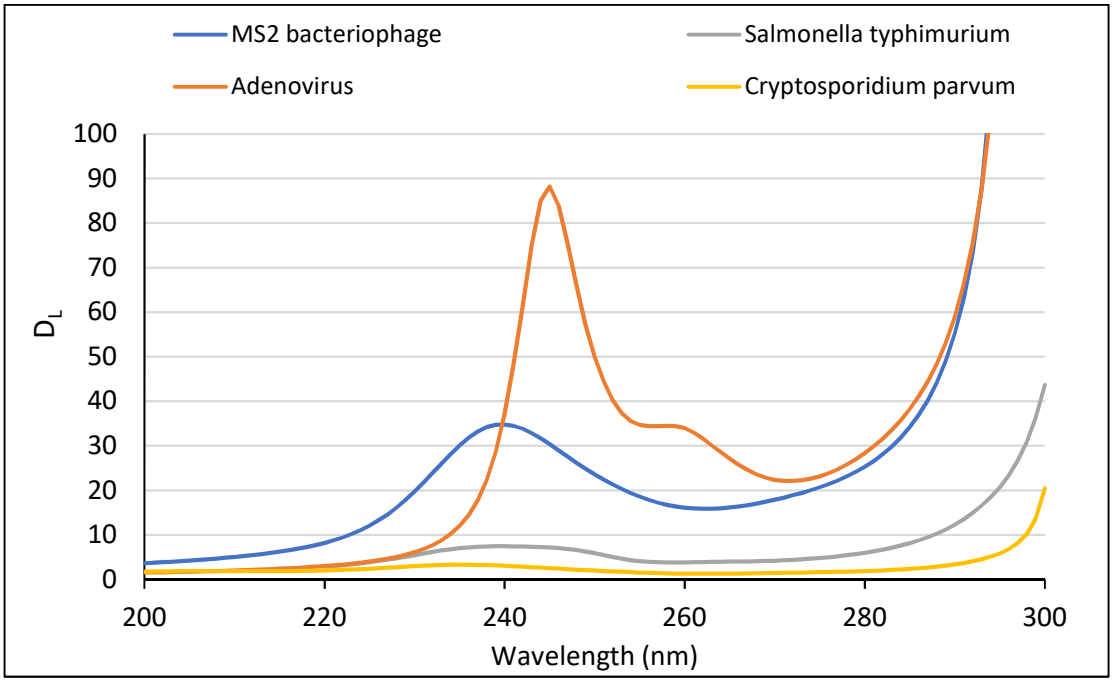

Figure 11 Scaled spectral sensitivity for virus (MS2 bacteriophage and adenovirus), protozoa (*Cryptosporidium*), and bacteria (*Salmonella typhimurium*) relative to the 254 nm D_L, the LP UV Dose (mJ/cm^2) required to achieve one log reduction based on linear fit to literature averages (Figure 10) between 1 and 4 log reduction (Beck et al., 2014b; Bolton, 2017; Malayeri et al., 2017; WRF, 2015)**.**

This study sought to fill these knowledge gaps and take advantage of emerging mercury-free wavelength tailored UV sources, recent advances in quartz sleeves and sensors, and drafted validation approaches to maximize the disinfecting power and resulting disinfection credit for every germicidal photon. This study provides novel viral disinfection dose response from exposure to a KrCl excimer lamp. This study also investigated potential synergies of viral disinfection from sequential exposure to multiple UV sources. Finally, data were modeled to determine if and how disinfection performance from sequential exposures could be predicted to inform wavelength tailored optimized UV disinfection strategies.

4.2 Materials and Methods

4.2.1 UV Exposures

UV LEDs emitting at nominal peak wavelengths of 255, 265, and 285 nm were used to target maximum nucleic acid absorbance near 260 nm due to their heterocyclic rings (Harm, 1980) and the secondary peak of protein absorbance due to amino acids (and minimally due to disulfide bonds) near 280 nm (Anthis and Clore, 2013). A benchtop UV LED system emitting these wavelengths was supplied by Aquisense (Earlanger, KY). A KrCl excimer lamp emitting at 222 nm was used to target near-maximum protein absorbance due to peptide bonds at 205 nm (Anthis and Clore, 2013), and was supplied by USHIO (Cypress, CA). These novel, non-mercury UV sources were tested individually and in sequence with each other and a conventional LP mercury lamp to determine the optimum wavelength tailored disinfection strategy using these sources. Normalized emission spectra for UV each source tested in this study are shown in Figure 12.

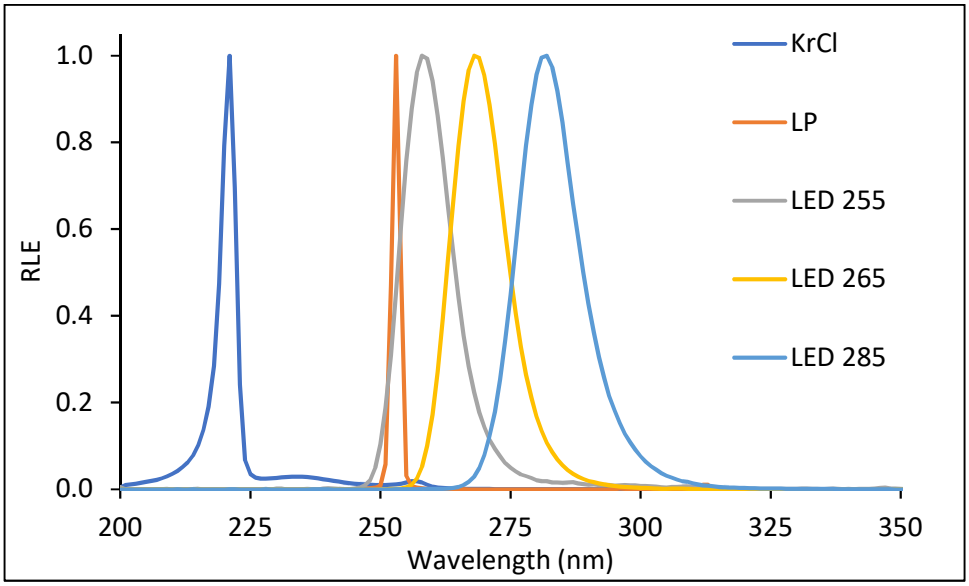

Figure 12 Relative lamp emission (RLE) for the KrCl excilamp (KrCl) with peak wavelength of 222 nm, low-pressure lamp (LP) with peak wavelength of 254 nm, and each LED with nominal (peak) wavelengths of 255 (258), 265 (268), and 285 (282) nm.

UV irradiations were performed according to standard protocols where UV fluence calculations included adjustments of measured incident irradiance (ILT-1700 radiometer) for non-uniformity across sample surface, polychromatic sample absorbance (Cary 100 UV-Vis Spectrophotometer), divergence of light through the sample, reflection factor at peak wavelength, NIST-traceable radiometer response, and polychromatic lamp emission (USB Maya or Maya Pro, Ocean Optics) to determine sample exposure times (Bolton and Linden, 2003; Linden and Darby, 1997). No additional weighting factors (such as germicidal) were used to adjust exposure times. For single UV source dose responses, the exposure time for each sample was calculated using the total UV Dose. For sequential UV source dose responses, the exposure time for each sample for each source was calculated using half the total UV dose. This

experimental design is illustrated in the Graphical Abstract. Three biologically independent samples were irradiated and enumerated for each UV source or combination of sources.

4.2.2 Biological Assays

The ability to disinfect was measured via MS2 bacteriophage infectivity. MS2 bacteriophage (ATCC 15597-B1) were propagated and enumerated using *E. coli* F_{amp} host (ATCC 700891) using the EPA 1602 single layer agar method (USEPA, 2001), modified as a spot plating assay when viral titer was expected to be $>10^2$ PFU/mL (Beck et al., 2009). MS2 $\log_{10}$ reduction was calculated as the $\log_{10}$ ratio of PFU/mL before versus after UV irradiation. A minimum of 3 or 10 replicates were plated and counted for each dilution of each sample for pour plates (sample volume 0.1 or 1 mL) and spot plates (sample volume 10 µl), respectively. Frozen MS2 stocks of 10^{11} PFU/mL were diluted in 1X PBS with continuous stirring between $5x10^6$ and $1x10^7$ PFU/mL for UV irradiations.

4.2.3 Model and Energy Assessments

Disinfection efficacy was normalized to fluence (UV Dose), and energy use (Electrical Energy Per Order or E_{EN}), enabling comparisons between UV source combinations. Second order polynomial regressions with zero intercept were fitted to all observed MS2 $\log_{10}$ reduction vales at all UV doses, for each single UV source or sequential combination of sources (by lm() in R v. 3.4.3 using RStudio v. 1.0.136) (US EPA, 2017, 2006a). To compare measured MS2 $\log_{10}$ reductions in sequential exposures to single source UV exposures, the modeled dose

responses for single UV sources were used to calculate predicted sequential dose responses by various methods. Equation 3 and Equation 4 represent modeled dose responses for individual UV sources 1 and 2, where $f(x)$ = MS2 $\log_{10}$ reduction, x = UV Dose in mJ/cm^2, and $a - d$ are model coefficients. For all methods, x_{tot} = total UV Dose in sequential exposure using sources 1 and 2, where the percent contributed by each source was half or $p = 50\%$. Predicted dose responses $f(x_{tot})$ were calculated using each of the following methods for 0 < x_{tot} < 50 mJ/cm^2. A diagram clarifying these computations of sequential dose responses by individual dose responses is shown in Appendix C Figure 26.

Equation 3 Dose response 1: $\boldsymbol{f_1(x)}$

$$\boldsymbol{f_1(x) = ax + bx^2}$$

Equation 4 Dose response 2: $\boldsymbol{f_2(x)}$

$$\boldsymbol{f_2(x) = cx + dx^2}$$

For the additive method f_+, predicted sequential dose responses were calculated by Equation 5.

Equation 5 Additive method: $\boldsymbol{f_+(x_{tot})}$

$$f_+(x_{tot}) = f_1(p * x_{tot}) + f_2(p * x_{tot})$$

For the percentage method $f_{\%}$, predicted sequential dose responses were calculated by Equation 6.

Equation 6 Percentage method: $\boldsymbol{f_{\%}(x_{tot})}$

$$f_{\%}(x_{tot}) = p * f_1(x_{tot}) + p * f_2(x_{tot})$$

For the method f_X based on combining dose response curves based on the x axis (equivalent UV Dose), predicted sequential dose responses were calculated by Equation 7.

Equation 7 Equivalent dose method: $\boldsymbol{f_X(x_{tot})}$

$$f_X(x_{tot}) = f_1(p * x_{tot}) + f_2(x_{tot}) - f_2(p * x_{tot})$$

For the method f_Y based on combining dose response curves based on the y axis (equivalent MS2 $\log_{10}$ reduction), predicted sequential dose responses were calculated by Equation 8.

Equation 8 Equivalent disinfection method: $\boldsymbol{f_Y(x_{tot})}$

$$f_Y(x_{tot}) = f_2(x_e + p * x_{tot})$$

For Equation 8, assuming the order of exposure was UV source 1 followed by UV source 2, x_e is the UV Dose where $f_2(x_e)$ results in equal MS2 $\log_{10}$ reduction to $f_1(p * x_{tot})$, which was calculated by Equation 9.

Equation 9 Equivalent dose: x_e

$$x_e = \frac{-d+\sqrt{d^2+4*f_1(p*x_{tot})*c}}{2*c}$$

Electrical energy per order (E_{EN}), the UV Dose in mJ/cm^2 required to achieve a given (N) $\log_{10}$ reduction of MS2, was calculated as described previously (Beck et al., 2017b; Rattanakul and Oguma, 2018) using the formula for nonlinear dose response kinetics shown in Equation 10. For sequential exposures, values of $C \times WF$ were averaged for the two UV sources, because each contributed half the total dose.

Equation 10 Electrical Energy per Order: E_{EN}

$$E_{EN} = \frac{A \times D_N}{3.6\times10^6 \times V \times C \times WF}$$

4.3 Results

4.3.1 Single UV Exposures

The dose responses for single exposures of MS2 to each UV source are shown in Figure 13a. The second-order dose responses significantly differed, as indicated by lack of overlap in 95% confidence intervals. Model coefficients and their standard error are shown in Appendix C Table 3. For a given UV Dose (or fluence), the order of effectiveness of the UV sources tested for MS2 inactivation was KrCl excimer lamp > 255 nm LED > 265 nm LED > LP UV > 285 nm LED.

As indicated in Figure 13b, average of germicidal factors for these dose responses calculated at 1, 2, and 3 MS2 $\log_{10}$ reduction corroborate the published action spectrum of MS2 weighted by each lamp emission. Additionally, the dose responses for MS2 exposures to LP fell within the 95% confidence intervals recommended by US EPA (US EPA, 2006a) for UV reactor validations (not shown).

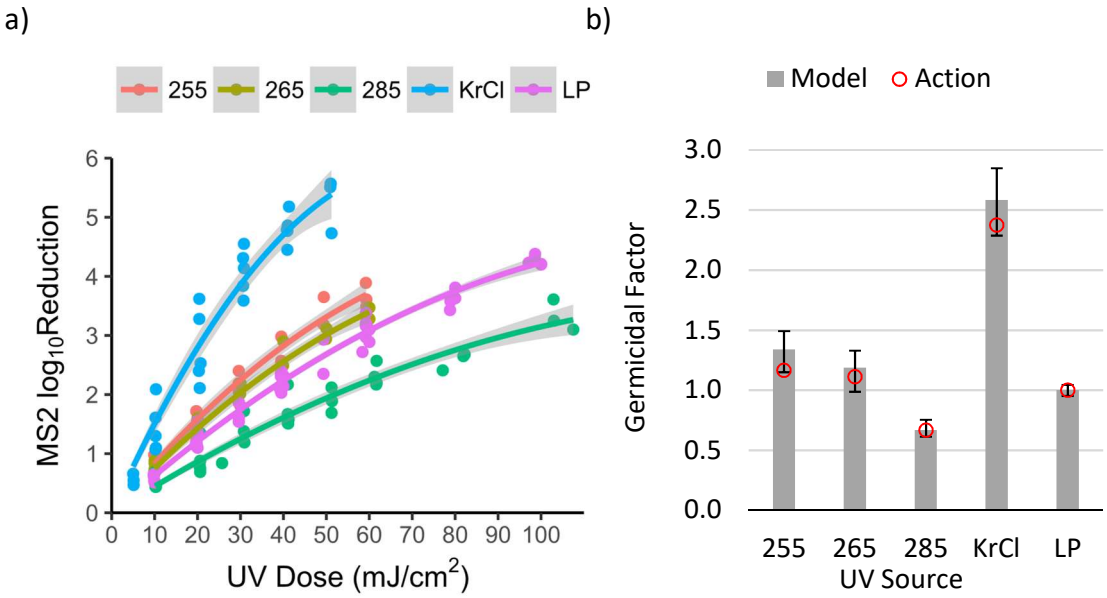

Figure 13 a) MS2 $\log_{10}$ reduction dose responses and zero-intercept second order polynomial models with 95% confidence intervals for individual UV sources. b) Average germicidal factors calculated from dose response models (Appendix C Table 3) or published MS2 action spectrum (Bolton, 2017) **weighted by relative lamp emission (Figure 12).**

4.3.2 Sequential UV Exposures

The dose responses for sequential exposures of MS2 to the excimer and LP lamps, where half the dose was contributed by each source, are shown in Figure 14. Model

coefficients and their standard error for these sequential dose responses are shown in Appendix C Table 4. The dose responses for sequential exposures of the excilamp and LP lamp in forward and reverse order were indistinguishable, as shown by their overlapping 95% confidence intervals throughout the entire tested range from 0 to 50 mJ/cm^2.

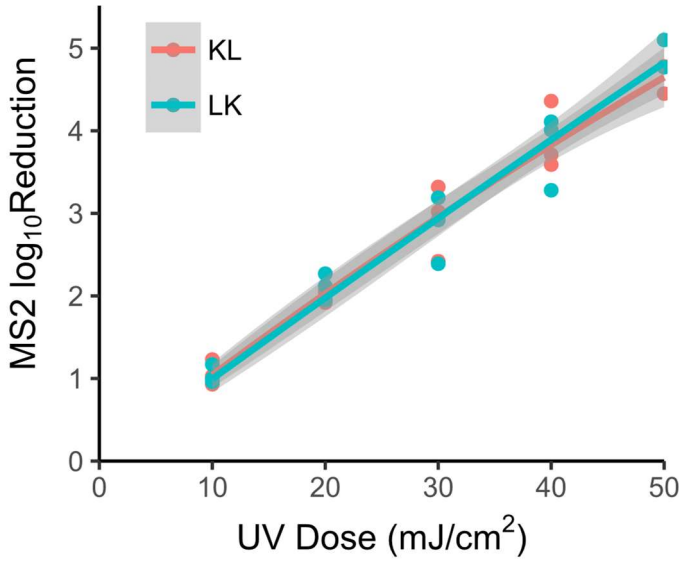

Figure 14 MS2 $\log_{10}$ reduction dose responses and zero-intercept second order polynomial models with 95% confidence intervals for sequential UV exposures of excimer (K) and LP (L) lamps. KL indicates the sample was exposed first to half the dose from the excimer lamp and then to half the dose from the LP lamp, and LK indicates the exposure order was reversed. The x-axis represents the total UV Dose (Fluence), where half was contributed by each source.

The dose responses for sequential exposures of MS2 to the excilamp tested with the LEDs, and to the LP lamp tested with the LEDs, are shown in Figure 15. Model coefficients and their standard error for sequential dose responses are shown in Appendix C Table 4. For sequential exposures of the excilamp and LEDs, MS2 was more efficiently inactivated for a given dose when exposed first to the excilamp than when exposed first to any of the LEDs. The 95%

confidence intervals for zero-intercept second order polynomials did not overlap for forward and reverse sequential exposures of the excilamp and LEDs, indicating statistical significance of the advantage of exposure to the excilamp before rather than after LEDs. For sequential exposures of the LP lamp and LEDs, MS2 was similarly more efficiently inactivated for a given dose when exposed first to the LP lamp than when exposed first to any of the LEDs. Again, models and confidence intervals for forward and reverse sequential exposures of LP and LEDs indicated statistical significance of the advantage of exposure to the LP lamp before rather than after LEDs.

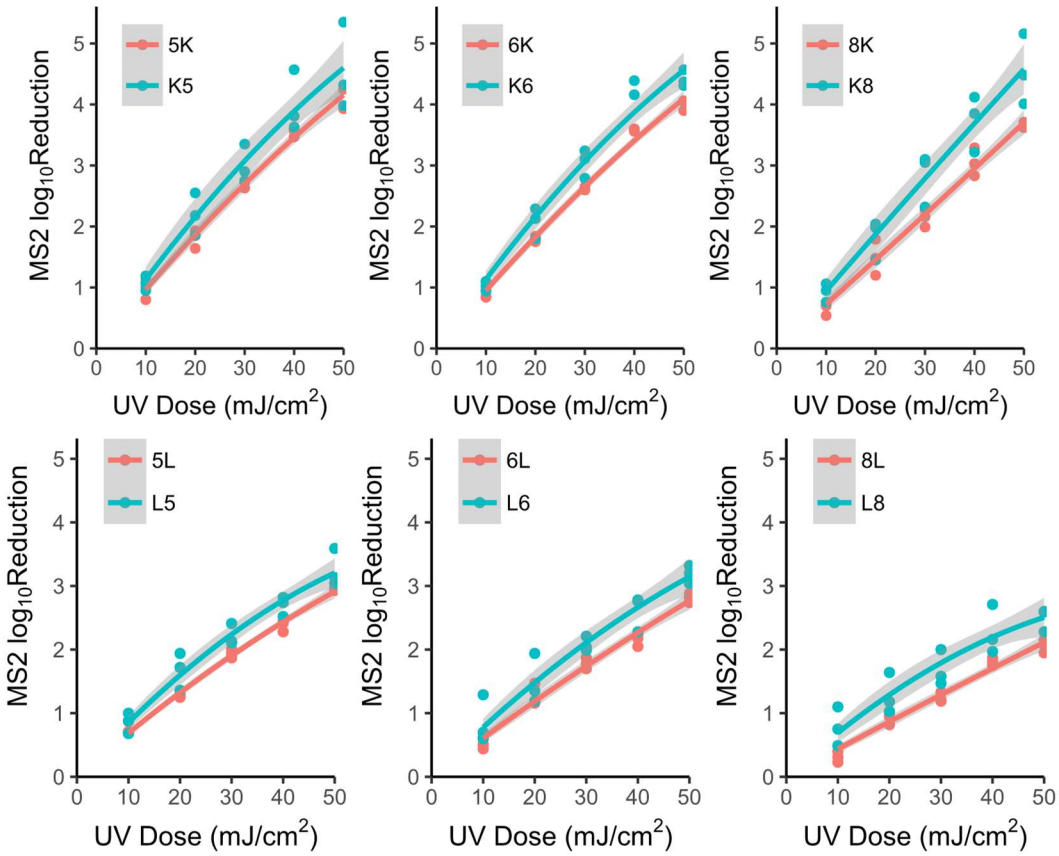

Figure 15 MS2 $\log_{10}$ reduction dose responses and zero-intercept second order polynomial models with 95% confidence intervals for sequential UV exposures. Top row, excimer lamp (K) was tested with LEDs, Bottom row, LP lamp (L) was tested with LEDs. 5= 255 nm LED, 6 = 265 nm LED, 8 = 285 nm LED. For example, 5K means the sample was exposed first to half the dose from the 255 nm LED and then to half the dose from the excimer lamp, and K5 indicates the exposure order was reversed. The x-axis represents the total UV Dose (Fluence), where half was contributed by each source.

Modeled dose responses of sequential exposures from Figure 14 and Figure 15 are plotted for visual comparison in Appendix C Figure 27 with individual dose responses from Figure 13. As expected, the MS2 dose responses for sequential exposures fall between dose responses for exposure to individual UV sources. However as noted from Figure 15, sequential exposures of the LEDs with either the excimer or LP lamps in forward and reverse sequence

resulted in dose responses that were different from each other, where greater MS2 inactivation was achieved for a given UV dose when first exposed to either LP or excimer lamps before LEDs. Dose responses for 5L, 6L, and L8 were very similar to dose responses for LP alone, while L5, L6, and 8L were very similar to dose responses of respective LEDs alone.

4.3.3 Predicting Sequential UV Exposure Dose Responses

Because of the differences in sequential dose responses based on order of exposure and the need to design and optimize wavelength-tailored systems without testing every possible sequential exposure combination, dose responses for sequential exposures were predicted by several calculations (Equations 3 – 10 for methods f_+, $f_{\%}$, f_X, and f_Y) using single UV source dose responses (Figure 13 and Appendix C Table 3) to determine if and how sequential exposure dose responses could be predicted.

Plots comparing modeled (zero intercept second order polynomial fitted to measured values) versus predicted (by f_+, $f_{\%}$, f_X, and f_Y) dose responses from sequential exposures of the excimer and LP lamps are shown in Appendix C Figure 28. RMSE residuals, slope, and R^2 comparing models (fit to observed sequential dose responses) to predictions (f_+, $f_{\%}$, f_X, and f_Y calculated using individual UV Source dose response models) are shown in Table 2 and Appendix C Table 5 - Table 7. The consistent overprediction by f_+ and underprediction by $f_{\%}$ could be used as a conservative envelope for predictive modeling of forward and reverse sequential exposures of LP and excimer lamps. The modeled and predicted dose responses combining the excimer or LP lamps with LEDs are plotted in Appendix C Figure 29 - Figure 32, and compared by RMSE, residuals, slope and R^2 in Table 2 and Appendix C Table 5 - Table 7. All

methods underpredicted LED-last dose responses with the LP lamp. All methods overpredicted MS2 log reduction for LED-first exposures. The f_+ overpredicted and $f_{\%}$ underpredicted LED-last dose responses with the excilamp, again forming a conservative predictive envelope.

Table 2 RMSE for sequential exposure dose responses comparing modeled (zero intercept second order polynomial fitted to measured values) versus predicted (f_+, $f_{\%}$, f_X, and f_Y calculated using individual UV Source dose responses) MS2 $\log_{10}$ reduction.

UV Sources	f_+	$f_{\%}$	f_X	f_Y
LK	0.12	0.32	0.57	0.20
KL	0.13	0.26	0.05	0.23
L5	0.10	0.20	0.25	0.20
L6	0.07	0.20	0.24	0.21
L8	0.16	0.23	0.25	0.24
K5	0.35	0.10	0.11	0.15
K6	0.25	0.17	0.04	0.23
K8	0.07	0.39	0.13	0.39
5L	0.26	0.08	0.13	0.09
6L	0.27	0.12	0.15	0.13
8L	0.27	0.18	0.16	0.19
5K	0.68	0.28	0.18	0.37
6K	0.60	0.23	0.17	0.32
8K	0.55	0.27	0.27	0.40

4.3.4 Electrical Energy Requirements

The required electrical energy per order (E_{EN}) to achieve a given (N) MS2 $\log_{10}$ reduction is shown for $1 < N < 3$ for individual UV sources in Figure 16a, and for sequential UV sources in Figure 16b. Data are shown for multiple log reductions because of nonlinear inactivation kinetics. Bars represent the average E_{EN} and error bars extend to current best-case (min E_{EN})

and worst-case (max E_{EN}) scenarios. The max and min E_{EN} were calculated using the min and max water factors (WF) tested in this study, and min and max wall plug efficiencies (C) reported in the literature for each UV source, which are listed in Appendix C Table 8. For ease of comparison, Appendix C Figure 33 shows single exposure and sequential exposure E_{EN} for each pairwise combination of sources. These data demonstrate that for single exposures (Figure 6a), the LP ($E_{E1, min}$ = 0.029 and $E_{E1, max}$ = 0.037 kWh/m^3) and excimer lamps ($E_{E1, min}$ = 0.029 and $E_{E1, max}$ = 0.095 kWh/m^3) are currently competitive in energy requirements for disinfection, while LEDs require roughly an order of magnitude more energy for equivalent disinfection.

Results from well-controlled bench studies can be directly compared to other studies, such as one reporting E_{EO} (electrical energy per order of magnitude reduction based on linear inactivation kinetics) for MS2 exposure to MP UV (Beck et al., 2017b). For current worst-case scenarios of sequential exposures, E_{E1} for LK, KL, L5 and L6 are already below the reported (Beck et al., 2017b) MS2 E_{EO} for MP of 0.06 kWh/m^3, and 5L and L8 were close contenders with E_{E1} = 0.066 and 0.067 respectively. For current best-case scenarios of sequential exposures, all but 8L and 8K were more efficient than MP (but were close with E_{E1}=0.065 and 0.074 kWh/m^3 respectively, indicating the current feasibility of more efficient wavelength-specific targeted disinfection using these emerging UV sources alone or with conventional LP UV. Applying the same calculation for individual sources to various infectious agents using their scaled action spectra (Figure 11) and relative lamp emission (Figure 12) demonstrates in Figure 16c that the predicted electrical energy required for adenovirus disinfection by the excimer lamp is on average lower than the LP lamp, although the error bars representing the range of electrical efficiencies and water absorbance overlap. For bacteria and protozoa disinfection (*Salmonella*

typhimurium and *Cryptosporidium*), the LP lamp is predicted to be the most electrically efficient. The low doses required to inactivate bacteria and protozoa make the electrical requirements for LEDs similar to those for LP and excimer lamps to inactivate viruses.

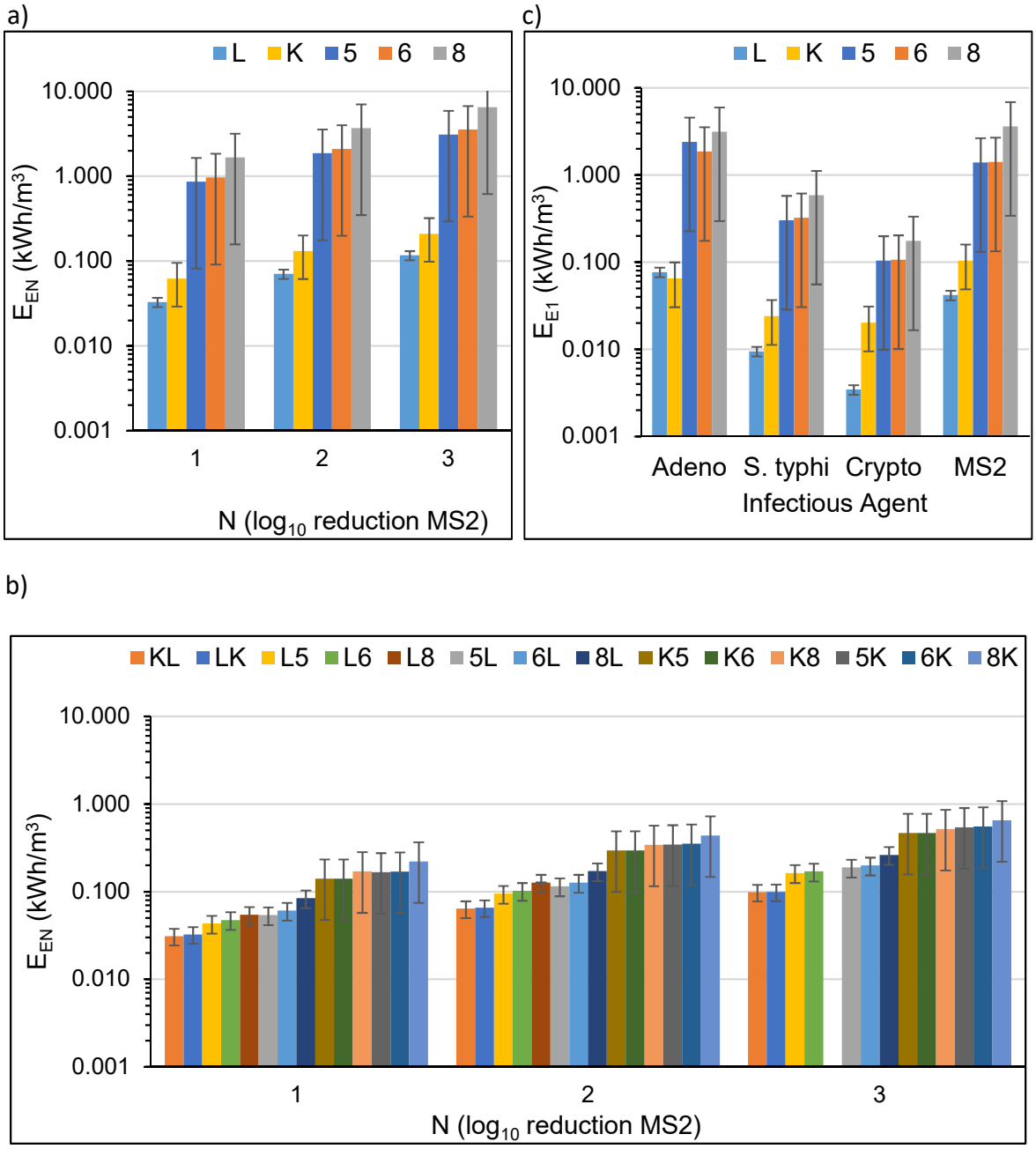

Figure 16 Electrical energy required (E_{EN}) to achieve a given (N) MS2 log_{10} reduction based on modeled dose responses (Figure 13, Appendix C Table 3) for a) individual UV exposures of MS2 and b) sequential UV exposures of MS2. For c) E_{E1} was calculated for individual exposures of Adenovirus, *Salmonella typhimurium*, and *Cryptosporidium* using scaled action spectra (Figure 11) and relative lamp emission (Figure 12). Error bars extend from the average to the minimum and maximum E_{EN} based on tested WFs and range of wall plug efficiencies reported in the literature (Appendix C Table 8). Note L8 E_{E3} could not be calculated due to dose response model curvature.

4.4 Discussion

4.4.1 KrCl Excilamps and UV-C LEDs for Tailored Wavelength Disinfection

Although dose responses for MS2 have been reported for exposure to other LEDs (Aoyagi et al., 2011; Bowker et al., 2011; Kim et al., 2017; Oguma et al., 2013; Zyara et al., 2017), Figure 13a presents the first published MS2 dose responses from exposures to LEDs with these emission spectra. These data also include also the first reported dose response for MS2 bacteriophage (or any virus) exposed to a KrCl excimer lamp. For both the LEDs and the excimer lamp, there was good agreement between germicidal factors calculated using modeled dose responses and germicidal factors calculated using the published action spectrum weighted by lamp emission (Figure 13b), indicating corroboration with previous work that provides confidence in results from sequential exposures. This agreement indicates that precisely defined action spectra can be used in conjunction with lamp emission spectra to accurately predict relative disinfection efficacy for emerging UV sources, enabling easier design and optimization of tailored wavelength disinfection reactors. The same approach can be used in conjunction with published LP dose response data to predict UV dose responses for infectious agents exposed to emerging tailored-wavelength UV sources (Figure 10 and Figure 11). These data can in turn be used to calculate electrical energy requirements to achieve pathogenic disinfection targets (Figure 16c), which can direct technology advancement and water treatment technology decisions.

As an example, these data (Figure 16c) show that excilamps are currently competitive with LP UV for adenovirus disinfection in terms of electrical requirements. These relative E_{EN}

predictions for adenovirus are comparable to a previous study (Beck et al., 2017b) comparing adenovirus disinfection efficacy by LEDs, LP, and MP UV which demonstrated that LP and MP were nearly equal in efficiency, while the older LEDs required nearly 100x more energy. Although KrCl excilamps are currently not yet commercially available for water disinfection, these promising results indicate the need for more research and development of this technology, especially in applications for viral disinfection. Further study is needed to determine life cycle impacts of excilamps for water treatment.

Additionally, because bacteria (i.e., *S. typhi*) and protozoa (i.e., *Cryptosporidium*) are inactivated by UV at such low doses, LEDs could be used for bacterial and protozoan disinfection at similar electrical requirements to those currently required for viral disinfection by LP and excilamps (Figure 16c). Further study is required to fully consider tradeoffs between the flexibility in reactor design offered by LEDs, the greater electricity requirements of UV LEDs until their electrical efficiency rivals visible light LEDs, and negative impacts of conventional UV sources which contain toxic mercury (Chen et al., 2017b; Muramoto et al., 2014; Shatalov et al., 2017).

4.4.2 Imminent Potential for Partnering KrCl Excimer and LP Lamps

Forward and reverse exposures of KrCl excimer and LP lamps were nearly indistinguishable both on fluence and electrical bases (Figure 14 and Figure 16). By combining these lamps in sequence, viral disinfection can be enhanced over conventional LP UV technology at the same total original dose. This could have implications for extending reactor lifetimes or allowing greater redundancy and resiliency by operating them at lower power to

achieve the same level of disinfection. Additionally, the sequential application of these lamps is amenable to diverse treatment train configurations, using two smaller reactors installed in series versus one large LP UV reactor. KrCl excilamps could be added to achieve credits for viral disinfection by utilities who currently use LP UV for protozoan disinfection credits, to enable them an easy retrofit installing KrCl excilamps either upstream or downstream of their current UV disinfection. Although not studied here because MS2 is a ssRNA virus which cannot be repaired by the photolyase enzyme, another possible benefit of incorporating excilamps with existing LP UV is the lower potential for photorepair and photoreactivation (Clauß et al., 2005; Oguma et al., 2002) due to protein damage at low wavelengths (Beck et al., 2017a) and emission of much less photoreactivating light than conventional MP. The targeted nature of emission with these wavelength tailored sources may also decrease the potential for formation of nitrogenous disinfection byproducts (DBPs) compared to MPUV (Kolkman et al., 2015). Also, excilamps have lifetimes similar to existing mercury lamps (Zhang and Boyd, 2000), and their efficiency is likely to increase with further technology development. However, the tradeoffs with potential low wavelength water quality impacts when using the excimer lamp require further consideration. Although the calculations of electrical energy requirements (Figure 16) account for water absorbance, impacts from non-target absorbance and results in other water matrices require further study.

4.4.3 Combinations of LEDs with KrCl Excimer or LP Lamps

On a fluence basis, exposure to the excimer or LP lamps before exposure to LEDs resulted in greater MS2 inactivation for a given dose than by exposure to LEDs first (Figure 15).

The reason for this difference is unclear, but could possibly be due to the nearly monochromatic emission of excimer and LP lamps (FWHM = 3.3 and 1.9 nm respectively) versus polychromatic LEDs (FWHM = 11.1, 12.2, and 13.5 for 255, 265, and 285 nm LEDs). The difference is unlikely to be due to differences in incident irradiance in bench experiments; all but the 255 nm LED were similar (~0.2 mW/cm^2), while the 255 nm LED was 10-fold less. Another explanation for the combination of the excilamp with the LEDs could be reversal of photocleavage (reversal of DNA damage). One study using MP with bandpass filters for 228 and 280 nm peak wavelengths used qPCR to detect photocleavage when *E. coli* exposure to 280 nm was followed by 228 nm, but found none when the order of exposure was reversed (Poepping et al., 2014). This mechanism may depend on UV wavelength and/or and nucleic acid sequence, based on charge transfer promoting reversal of photolesions (Bucher et al., 2016; Szabla et al., 2018). Alternatively, the difference could be due to differences in electrical operation; both excilamps and mercury vapor lamps run on alternating current (AC), while LEDs run on direct current (DC). The effect of AC essentially makes the excimer and LP lamps deliver photons as a pulsed source with very high frequency. Pulsing LEDs has been shown to increase microbial inactivation efficiencies in liquids (Tran et al., 2014; Wengraitis et al., 2013) and biofilms (Li et al., 2010). Future research could implement LEDs in pulsed mode in sequential exposures with other LEDs, and optimize pulsing duty rate of both LEDs and excilamps, to improve their efficiency since neither are negatively affected by on-off cycles and both reach full power nearly instantaneously.

Regardless of differences in order of exposure, the best-case scenarios for maximum wall plug efficiency and water transmittance for all sequential exposures were more efficient

than current MP (Beck et al., 2017b) for MS2 inactivation (Figure 16b), signaling the current feasibility of wavelength tailored disinfection using emerging UV sources (LEDs and excimer lamps) combined together or with conventional LP lamps. Due to the higher wall plug efficiency and lower water absorbance effects on wavelengths relevant for LP, on an electrical basis the LP before and after LEDs were more efficient than the excilamp before and after LEDs. Again, photorepair should be considered when comparing different sequential applications of UV sources. Recently 280 nm LEDs were shown to limit photorepair compared to LP UV, 265 nm LEDs, or simultaneous exposure to both LEDs, which was attributed to damage of photolyase enzyme at the higher wavelength where protein absorbance is greater (Li et al., 2017b). Additionally, time-based efficiency of batch and flow-through UV LED reactors is greatest with higher wavelength LEDs even if their fluence-based efficiencies are lower, due to higher output power (Oguma et al., 2013). In this study, emission measured at the same distance from three 285 nm LEDs was more than twice as powerful as emission by three 265 nm LEDs, and more than 12 times as powerful as emission by six 255 nm LEDs. As a result, higher flowrates can be treated or fewer LEDs can be used for more powerful emitters while achieving the same disinfection, which must be balanced with electrical efficiency. Another consideration for targeted wavelength disinfection is damage to multiple biomolecule types. For instance, MS2 RNA is more sensitive to damage at low UV-C wavelengths than high wavelengths, while adenovirus DNA is damaged consistently across the UV-C spectrum but adenovirus proteins are more sensitive to damage at low wavelengths than high wavelengths (Beck et al., 2017a, 2015, 2014a). More work is required to elucidate wavelength-specific and

sequential exposure mechanisms of MS2 protein damage, and wavelength-specific biomolecular damage to other pathogens, that may enhance disinfection.

4.4.4 Prediction and Practicalities of Sequential UV Disinfection

The different methods of dose response prediction can practical insight to designing wavelength tailored sequential UV systems (Table 1, Appendix C Table 4, and Appendix C Figure 27 - Figure 32). Based on previous methods of assessing synergy using $f_{\%}$ (Beck et al., 2017b; Li et al., 2017b), both orders of sequential exposures of LP and excimer lamps resulted in disinfection synergy. Sequential exposures of LP followed by LEDs were also best predicted by the additive method, but were underpredicted by all methods, suggesting a definite synergy. Sequential exposures of the excimer lamp followed by LEDs were overpredicted by $f_{+}$and underpredicted by $f_{\%}$. Sequential exposures of LEDs before either excimer or LP lamps overpredicted, indicating the potentially detrimental effect of this sequential disinfection strategy. Mechanistic reasons why exposure to LEDs after LP or excimer lamps resulted in less efficient disinfection of MS2 require further study.

The ability to predict dose responses of KrCl excimer and LP lamps by adding their dose responses by the f_{+} method (Table 2 and Appendix C Figure 28) concurs with studies that have shown theoretically the additive disinfection of full-scale UV reactors in series (Lawryshyn and Hofmann, 2015; Young and Lawryshyn, 2017). The ability to predict sequential exposures of LEDs after excimer lamps using the envelope of f_{+} and $f_{\%}$ indicates potential to design wavelength tailored systems for optimized disinfection based on fluence and electricity use without having to test all possible combinations at the bench. For sequential application of

LEDs after LP, the additive method alone could be used as a conservative predictor for disinfection optimization. These predictive approaches can be used to design disinfection reactors to achieve specific disinfection targets within constraints such as electrical power, cost, and space.

4.5 Conclusions

This research demonstrates current feasibility of KrCl excimer lamps for water disinfection, because their ability to target low wavelengths where viruses have greatest spectral sensitivity and their reasonable wall plug efficiencies make them competitive with current LP technology. Additionally, the current feasibility of wavelength targeted disinfection that is equally or more efficient than conventional MP UV lamps was demonstrated using sequential exposure to excilamps, LEDs, and conventional LP UV lamps. Individual dose responses were well predicted using published action spectra, but sequential dose responses indicated synergy on both fluence and electrical bases from exposure to the LP or excilamps before exposure to polychromatic LEDs. The most electrically efficient wavelength targeted sequential strategy was forward or reverse exposure to excilamps and LP lamps, indicating realistic possibility of retrofitting existing LP systems with excimer lamps to increase disinfection (especially for viruses) while maintaining the same level of electrical efficiency, or decrease electricity use while maintaining the same level of disinfection. The feasibility of sequential application of these emerging UV sources for water disinfection coupled with advancements in quartz sleeves, sensors, and validation recommendations will allow utilities to minimize their energy use while maximizing multi-barrier public health protection.

5. Validation and Small System Demonstration Study of the First Commercial UV-C LED Water Disinfection Reactor

This chapter describes bench validation and year-long demonstration testing at a local small drinking water treatment system of a novel UV-C LED disinfection system. This work demonstrated viral and bacterial disinfection efficacy and resilience of the system, providing proof of concept for application of UV-C LED for municipal applications.

This work is almost ready to submit for publication:

Hull NM, Herold WH, and Linden KG (*in preparation,* 2018). Validation and Small System Demonstration Study of the First Commercial UV-C LED Water Disinfection Reactor**.**

5.1 Introduction

The disparity in the ratio of municipal drinking water system size to population served contributes to smaller systems accruing a disproportionate number of violations, especially health-based violations. As summarized in Figure 17, most municipal drinking water systems in the US range in size from very small to medium (97% of systems serve fewer than 3,300 people each), but most people with municipal water are served by larger systems (80%). More accessible, sustainable technologies and strategies of disinfection could prevent some of these health-based violations in order to protect the people served by the majority of systems.

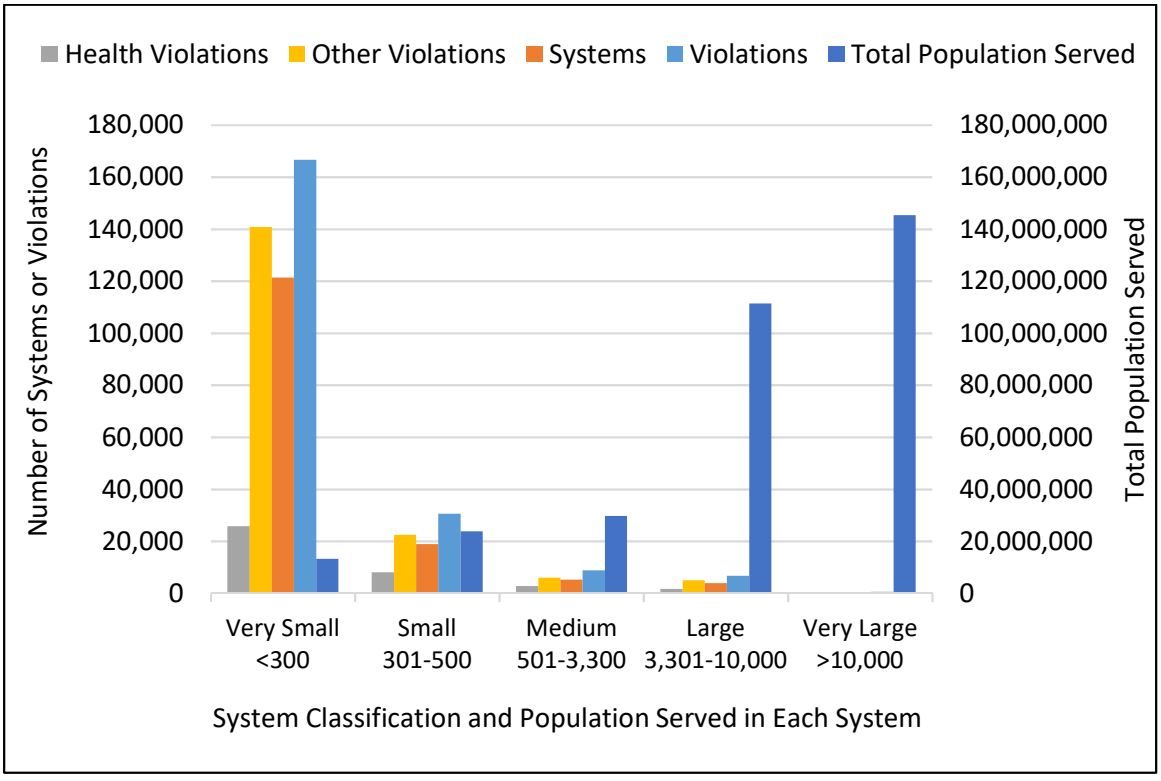

Figure 17 US municipal drinking water system characteristics and violations in 2017 (downloaded February 2, 2018 and summarized from echo.epa.gov).

Disinfection by ultraviolet (UV) light could be an advantageous option for small system water treatment. UV disinfection requires no chemical additions, causes no taste/odor issues, has no harmful effect from overdosing, does not apply selective pressure for chemical resistance, and has little to no effect on disinfection byproduct (DBP) formation (Chatterley et al., 2010; Guo et al., 2013; Reckhow et al., 2010). UV is effective against bacteria and viruses and is commonly used for drinking water treatment in the US and Europe (US EPA, 2006a). UV also inactivates chlorine-resistant protozoa (i.e. Giardia and Cryptosporidium) at very low doses (Clancy et al., 1998; Linden et al., 2002). Regulatory guidance for UV disinfection of viruses in the United States (US) is currently based on adenovirus inactivation by traditional low pressure (LP) mercury lamps with narrow emission spectra at 254 nm (US EPA, 2006a). Because adenoviruses exhibit resistance to this wavelength, the UV dose required to achieve 4-log virus inactivation is high enough to be cost-prohibitive for some small systems. However, most infectious agents vary in their sensitivity to different UV wavelengths (WRF, 2015). Adenovirus, for example, is more susceptible to multi-wavelength (polychromatic) medium pressure (MP) UV disinfection (Eischeid et al., 2011). This varying wavelength sensitivity offers an opportunity to optimize wavelength specific UV disinfection using emerging UV sources.

Light emitting diodes (LEDs) are non-mercury sources of polychromatic UV with promise as a sustainable solution for drinking water disinfection in small communities. LEDs can be designed to emit specific wavelengths by changing the energy band gap (based on material composition) of the semiconductor in the diode (Ibrahim et al., 2013). Manufacturers and researchers have produced LEDs capable of emitting wavelengths across the UV-C spectrum as low as 220 nm, although the lower wavelength LEDs are less powerful and efficient, have much

shorter lifespans, and are much more expensive to produce (Lawal et al., 2018). UV LEDs could be more sustainable than traditional UV lamps because they do not contain toxic mercury, have lower power requirements, are more compact, and are becoming more efficient as materials science advances (Song et al., 2016). Additionally, LEDs are capable of nearly instantaneous power-up, do not suffer from unlimited cycling, have long lifespans, are small in size, and have higher power density than conventional mercury UV lamps (Nelson et al., 2013). Because disinfection does not depend on the UV lamp type, these sources disinfect bacteria, protozoa, and viruses just as well as traditional mercury UV lamps for a given dose and wavelength (WRF, 2015). The proven efficacy of LEDs of varying wavelengths against bacteria, viruses, and protozoa in bench-scale and flow-through studies has been recently reviewed (Song et al., 2016).

The PearlAqua shown in Figure 18a is the world's first commercially available UV LED product designed for water disinfection (Aquisense, Erlanger, KY). The PearlAqua was designed using LEDs emitting a nominal (actual) peak wavelength of 285 (282) nm, with a bandwidth at full-width half maximum of 13.5 nm, as shown in Figure 18b. Although published action spectra indicate that these wavelengths aren't as effective for disinfection on a fluence basis (Bolton, 2017), higher wavelength UV LEDs are currently less expensive, more powerful, and more electrically efficient than lower wavelengths. Reflectivity, hydraulics, and thermal management were also carefully considered when designing the PearlAqua to maximize electrical and disinfection efficiency. Additionally, UV transmittance (UVT) tends to be greater as wavelength increases, which increases the probability of photon absorption by disinfection targets compared to 254 nm. The objectives of this research were to validate PearlAqua disinfection

performance across a range of flowrates and UV transmittances, and to operate the first long-term demonstration of an LED disinfection reactor in a small drinking water system to study parameters relevant to sustainability, robustness, and disinfection performance over time.

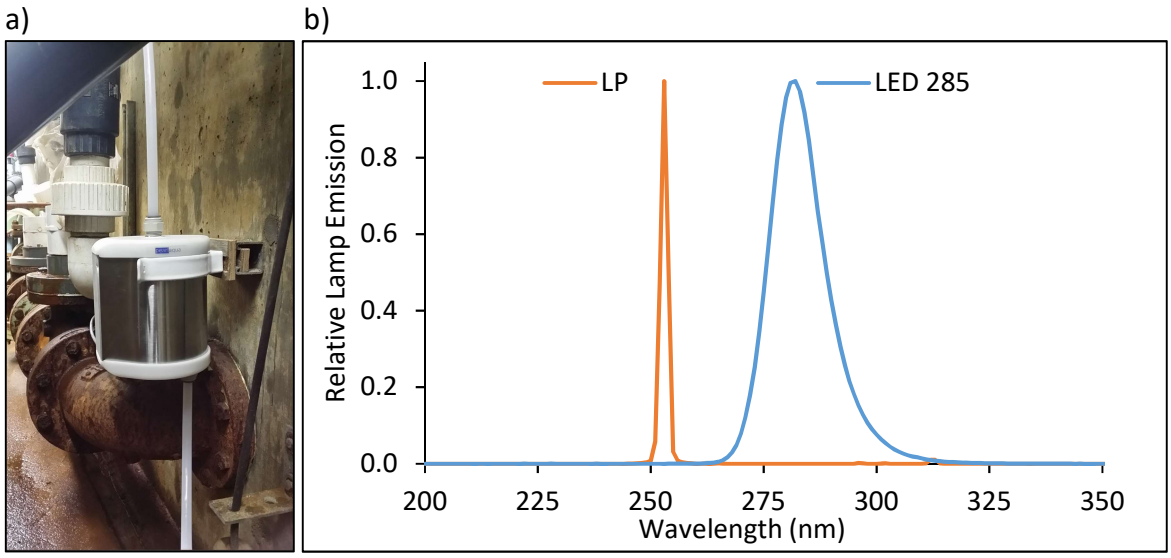

Figure 18 (a) PearlAqua installed at the Jamestown, CO drinking water treatment plant demonstration study site after sand filtration. (b) Lamp emission spectra of LEDs in the PearlAqua UVinaire compared to a traditional low pressure (LP) lamp.

5.2 Methods

5.2.1 PearlAqua 25G Characteristics (Aquisense Technologies, 2016)

The PearlAqua model 25G is an NSF 61 and IP65 certified UV-C LED water disinfection system with a maximum operating pressure of 100 psi and a pressure drop at max flow (12 liters per minute or lpm) of 1.3 psi. It is rated for operating in water temperatures ranging from

0 – 50 °C, connects with ½" (outer diameter FNPT) fittings, weighs 3.3 lbs, and measures roughly 6 x 6 x 6 cm for the entire system. The PearlAqua operates in upflow where water passes through an internal diffuser before irradiation, can be mounted with a spring-loaded bracket, and is powered by a single cable from the UVinaire LED module to a standard outlet (120V and 60 Hz), as shown in Figure 18a. The UVinaire houses the internal electronics, fan, heat sink, and array of LEDs that irradiate through a quartz window to the PearlAqua interior. The outside of the UVinaire has two visible LED indicator lights coded for various electronic warnings to indicate status of the system and LEDs. The UVinaire has an internal 4-20mA current loop that can be used to measure lamp life remaining or for remote monitoring and operation. The UVinaire runs on 12 V DC, with 2.5 A max current and 26 W nominal power consumption.

5.2.2 Bench Validation and Post-Demonstration Assessment

Before and after the year-long demonstration study, the PearlAqua was challenge tested with MS2 bacteriophage (ATCC 15597-B1) in dechlorinated (GAC-treated) tap water across a range of flowrates and UV absorbances/transmittances (UVA / UVT) that were modified using lignin sulfonate (LSA). UVT was calculated based on measured UV absorbance (cm^{-1}) (UV-Vis Cary 100, Agilent) using Equation 11.

Equation 11 UV Transmittance

$$UVT = 100\% \times 10^{-UVA}$$

MS2 infectivity before and after treatment was enumerated using *E. coli* F_{amp} host (ATCC 700891) by the EPA 1602 single layer agar method (USEPA, 2001), modified as a spot plating assay when viral titer was expected to be >10^2 PFU/mL (Beck et al., 2009). MS2 $\log_{10}$ inactivation was calculated as the $\log_{10}$ ratio of PFU/mL before versus after UV irradiation. A minimum of 3 or 10 replicates were plated and counted for each dilution of each sample for pour plates (sample volume 0.1 or 1 mL) and spot plates (sample volume 10 µl), respectively. Based on MS2 $\log_{10}$ inactivation ($logI$) in the flow-through reactor, the reduction equivalent dose (RED) was back-calculated from collimated beam MS2 dose responses to either 285 nm LEDs or an LP lamp. For collimated beam studies (Bolton and Linden, 2003; Linden and Darby, 1997), thawed MS2 stocks of 10^{11} PFU/mL were diluted to between 5x10^6 and 1x10^7 PFU/mL in 1X PBS, GAC-treated tap water to remove chlorine (with or without LSA), or filter effluent from the water treatment plant with continuous stirring for UV irradiations. RED or $logI$ values were modeled using a combined variable approach (Wright et al., 2011), shown in Equation 12, to determine empirical coefficients ($a - e$) using nls() in R v. 3.4.3 using RStudio v. 1.1.383.

Equation 12 Combined Variable Model

$$RED\ or\ logI = 10^a \times UVA^b \times \left(\frac{S/S_0}{Q}\right)^{c+d\times UVA+e\times UVA^2}$$

For Equation 12, UVA is UV absorbance at 254 nm, 285 nm, 282 nm, or the UV absorbance weighted by the LED relative lamp emission (RLE). S/S_0 is the ratio of measured UV intensity (S) over UV intensity for new lamps (S_0), and Q is flowrate (lpm). For initial bench validation testing of the new PearlAqua, S/S_0 was assumed to be 1.

5.2.3 Demonstration Study

The field site for the demonstration study was the drinking water treatment plant in the small mountain town (population ~300 and elevation ~7,000 ft) of Jamestown, CO. Surface water directly from James Creek or from a shallow infiltration gallery is sand filtered before chlorination and distribution of ~10 to 55 thousand gallons per day depending on seasonal demand. The PearlAqua was installed in the slow sand filter effluent, and treated ~ 190 gallons per day (operating at 0.5 lpm). The water treated by the PearlAqua was returned to the head of the plant.

Daily over the course of 1 year, starting at the end of January 2017, UVT and turbidity were measured in UV reactor influent (i.e., the sand filter effluent), while temperature and pH were measured in chlorinated effluent, as shown in the water treatment plant schematic and sampling key in Figure 19. Bi-weekly samples were collected in the treatment plant influent, slow sand filter effluent, existing chlorine disinfection effluent, and UV LED disinfection effluent. Analytes for bi-weekly samples included adenosine triphosphate (ATP), total coliform and E. coli (TC/EC), and total and dissolved organic carbon (TOC/DOC). Upon installation and approximately once every three months (quarterly), the disinfection performance of the UV reactor was monitored by MS2 challenge testing and compared to bench validation testing completed before installation. Additionally, total dissolved solids (TDS), Alkalinity, Hardness, Nitrate/Nitrite, inorganics (including Br), and DBPs were measured periodically. Cost of electricity use was calculated based on manufacturer information for the PearlAqua and utility

billing rates in Longmont, CO. LED output intensity measurements taken before and after the demonstration were provided by Aquisense.

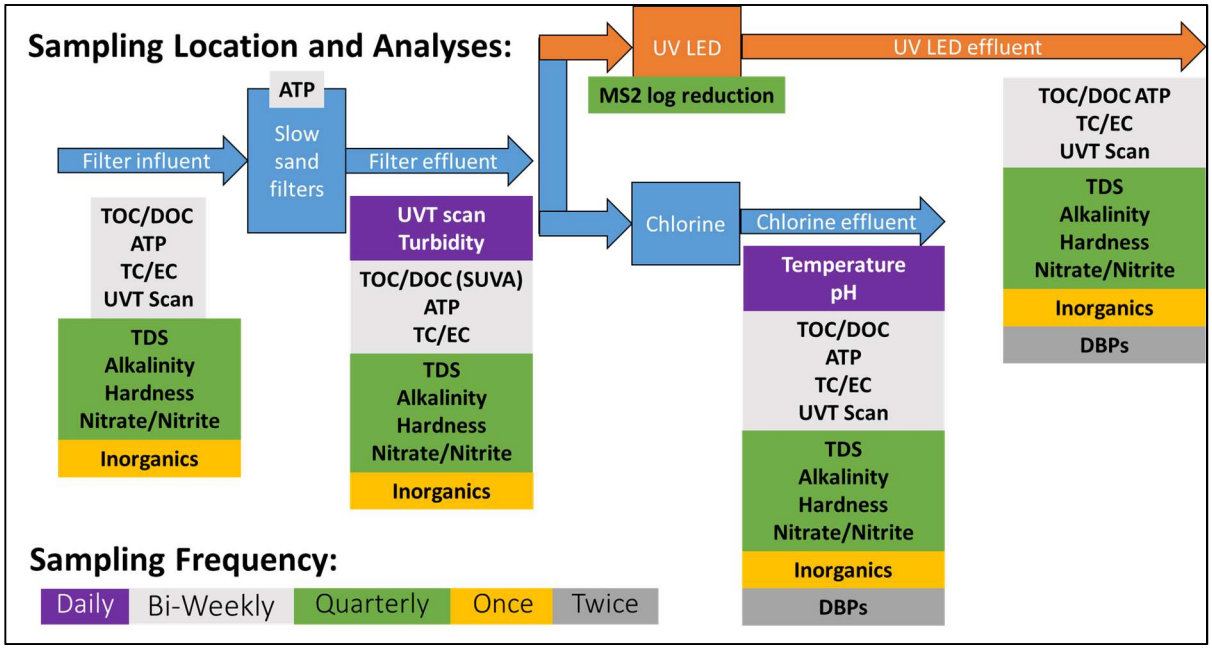

Figure 19 Schematic of existing treatment and demonstration study UV LED disinfection, showing color-coded sampling locations and schedule for the demonstration study.

Turbidity, pH, water temperature, and chlorine residual were measured by water treatment plant operators using standard methods and calibrated probes, and data were compiled from monthly operating reports to the state. TOC and DOC (after 0.45 um nylon membrane filtration, VWR) were measured using a Sievers M5310 C. Nitrate and nitrite were measured using Hach low-range kits (TNT 835 and 839). Alkalinity was measured by sulfuric acid titration of bromocresol green/methyl red (Hach). For disinfection byproducts (DBPs), total trihalomethanes (TTHMs) and haloacetonitriles (HANs) were measured by EPA Method 551.1

and haloacetic acids (HAAs) were measured by EPA Method 552.2 on an Agilent 6890 GCμECD to assess yield under uniform formation conditions (Summers et al., 1996). Inorganics measured by indicatively coupled plasma optical emission spectrometry (ICP-OES, Laboratory of Environmental and Geological Sciences at University of Colorado Boulder) of acidified samples (to pH < 2 with nitric acid) were used to calculate hardness. UVA was scanned from 200 – 800 nm and used to calculate UVT by Equation 11. Total Coliform and *E. coli* were quantified by 0.45 μm membrane filtration (HA S-Pak, Sigma Aldrich) using Chromocult media (Merck KGaA) by EPA Method 1604/ISO 9308-1. ATP was quantified by Luminultra QGA kit protocols. Stream flow data was downloaded for Left Hand Creek (USGS 06724970) after the confluence with James Creek from USGS (waterdata.usgs.gov). Temperature and precipitation data were downloaded for the nearest weather station with complete historical data (GHCN: USW00094075) from NOAA (gis.ncdc.noaa.gov/maps/ncei/cdo/daily).

For quarterly challenge testing, as for validation testing, MS2 was spiked into filter effluent so that $\log_{10}$ inactivation and RED could be determined. MS2 inactivation predicted from the bench validation model was plotted versus measured inactivation for each quarterly challenge test and for bench validation testing. Slopes and 95% confidence intervals of quarterly challenge test data were compared to the validation data to determine if there were changes in disinfection performance of the PearlAqua over time.

5.3 Results

5.3.1 Bench Validation

The PearlAqua was challenged with MS2 bacteriophage across a range of flowrates from 0.1 to 0.6 liters per minute (lpm) and UVTs ranging from nearly 100% to almost as low as 70% (RLE weighted UVT) as shown in Figure 20. The PearlAqua achieved 1 – 6 $\log_{10}$ inactivation of MS2 over these conditions. Based on these validation test data, preliminary screening of the planned reactor influent water quality at the local small system, and a targeted LP UV MS2 reduction equivalent dose (RED) of 40 mJ/cm^2 (approximately 2 $\log_{10}$ reduction) commonly used in UV disinfection, the reactor was installed on the slow sand filter effluent of the small system drinking water treatment plant with a flowrate of 0.5 lpm. Dose responses from collimated beam studies that were used to calculate reduction equivalent doses (REDs) for exposures to LP UV and 285 nm LEDs are shown in the Appendix D Figure 34. These dose responses indicate that, when standard collimated beam procedures were used to account for sample depth, water absorbance, and other factors (Bolton and Linden, 2003), neither water matrix (PBS or dechlorinated tap water) nor LSA used to modify UV transmittance affected the LP UV dose response, as shown by overlapping 95% confidence intervals. These dose responses for LP UV fall within established (US EPA, 2006a) limits for MS2 validation testing (not shown).

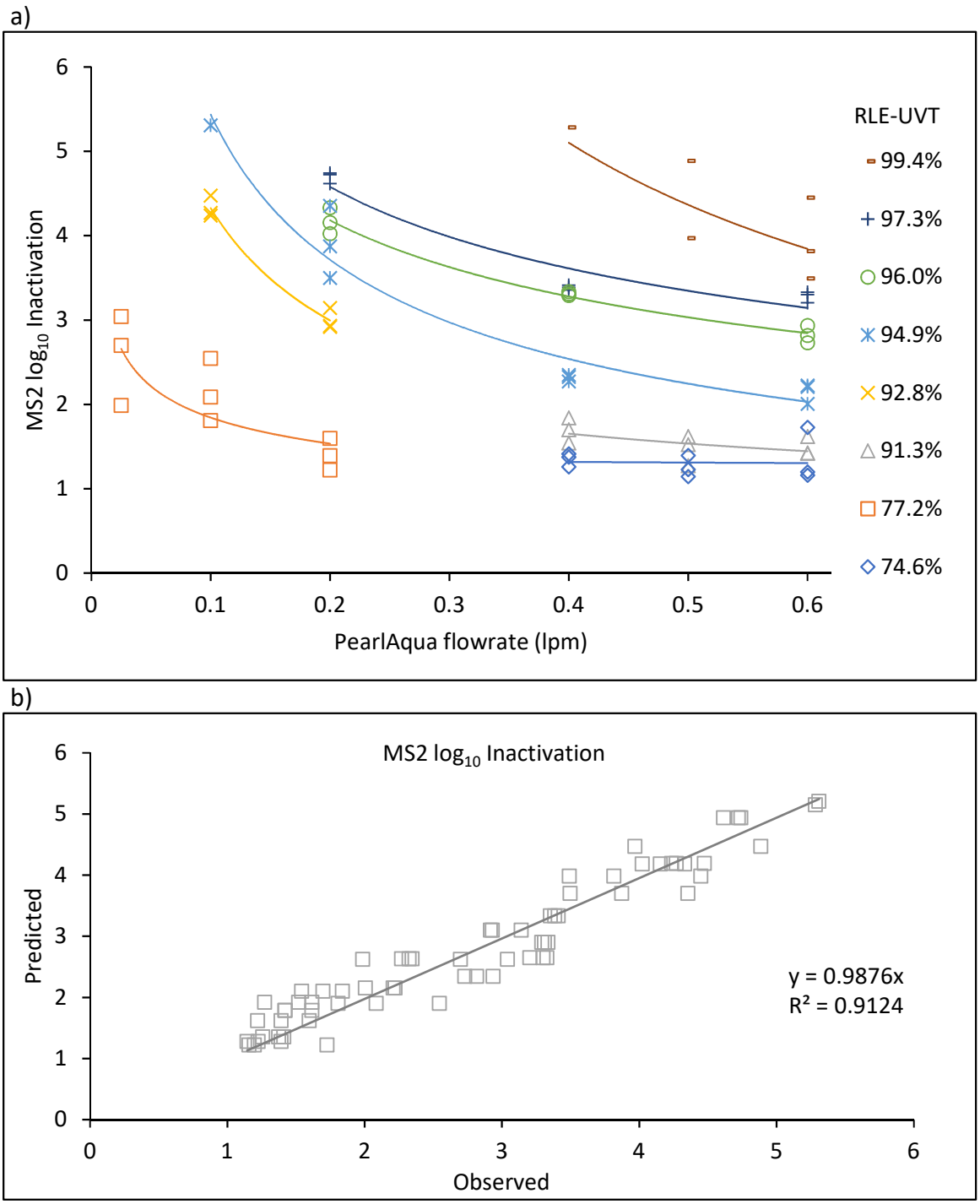

Figure 20 (a) PearlAqua bench validation MS2 challenge testing log inactivation data fit with power functions at each UVT, and (b) final validation combined variable model (Equation 12) predicting MS2 logI as a function of UVT-RLE and flowrate, with statistically significant model coefficients ($p<0.05$) a = -0.1952, b = -0.25607, c = 0.65497, d = -7.99858, and e = 37.65489.

Bench validation results for MS2 challenge testing across these UVTs and flowrates were modeled using a combined variable approach (Equation 2). Models were assessed for best fit by predicting RED (calculated based on either LP UV or 285 nm LED dose responses shown in Appendix D Figure 34) or MS2 log inactivation (log I). Models were also assessed for best-fit predictions based on absorbance at different relevant wavelengths; 254 nm, 285 nm, 282 nm, and the relative lamp emission (RLE) weighted absorbance. As shown in Appendix D Figure 35, models using RED calculated for the 285 nm LED were hindered by dose response curvature that resulted in inability to calculate REDs for flow-through samples with high log inactivation. Models were better fit when directly predicting log inactivation rather than RED for both LP and 285 nm LED dose responses. The best (slope closest to 1 and highest R^2) models were those that predicted log inactivation using UVA at the peak wavelength of the LED (282 nm) and the RLE-weighted UVA. Although the slope was higher for the peak wavelength absorbance model, the R^2 was higher for the RLE absorbance model; however, these differences were very slight (0.000004 for slope and 0.000013 for R^2). The model predicting log inactivation as a function of the RLE absorbance and flowrate was chosen as the final validation model shown in Figure 20.

5.3.2 Demonstration Study Conditions

For UV disinfection, the most important water quality characteristic related to performance is UVT. In this mountain system, temporal variations in snowmelt and precipitation (in the form of snow and rain) that increased stream flow were most closely related to temporal changes in UVT (as shown in Figure 21). The lowest UVT occurred in the Spring at the inflection point where daily air temperature started to increase, which would

coincide with the beginning of snowmelt. Turbidity was also closely related to changes in UVT, but was more closely associated with air temperature. UVT at 285 nm was always higher than at 254 nm. UVT at the nominal peak wavelength (285 nm) was always higher than at the actual peak wavelength (282 nm). The UVT weighted by relative lamp emission (RLE) of the LEDs was between UVT at 282 and 285 nm, as expected.

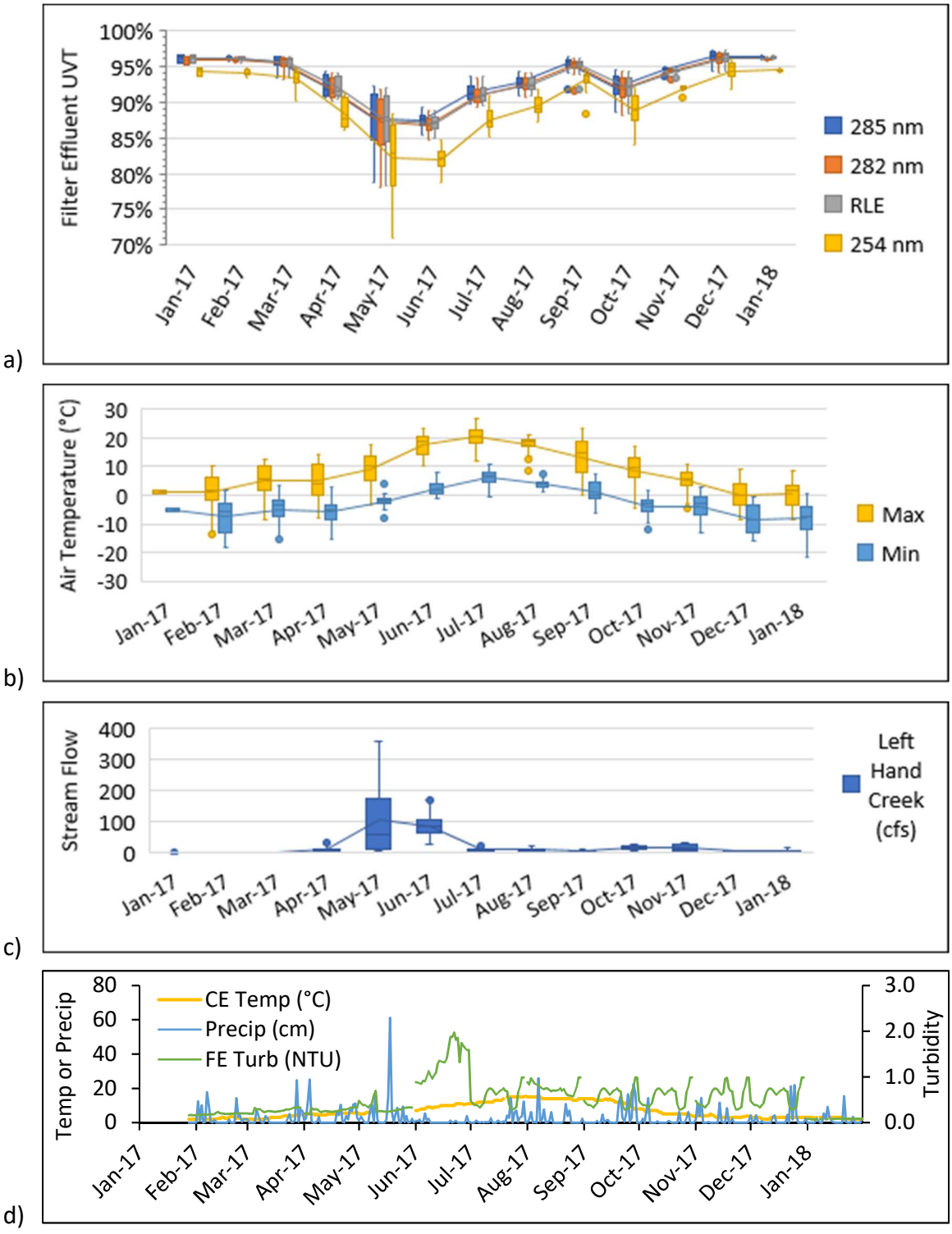

Figure 21 Variations in UVT and environmental conditions over the year-long demonstration study. (a) UVT at various wavelengths or the relative lamp emission (RLE) weighted UVT. (b) Summary of daily air temperature near Jamestown, CO. (c) Summary of real-time stream flow in Left Hand Creek just downstream of the confluence with James Creek near Jamestown, CO. (d) Jamestown drinking water treatment plant chlorine effluent water temperature and turbidity, and precipitation for the nearest weather station.

Disinfection performance was analyzed in terms of ATP (microbial activity), and by common bacterial indicators, Total Coliform and *E. coli*, as shown in Figure 22. The ATP concentration in bi-weekly samples exhibited two peaks in filter influent that coincided with the peak stream flow for the first peak in the Spring, and peak water temperature for the second peak in the Fall. UV LED effluent ATP was slightly less than in the filter effluent, while chlorine disinfection nearly eliminated ATP. The first snowmelt- and stream flow-driven peak in ATP resulted in greater ATP in the filter and UV LED effluent. Total Coliform were detected at highest concentrations in filter influent when water temperatures were warmest in the Fall. Total Coliform in filter effluent followed a similar temporal pattern, with a much lower concentration (average = 5 CFU/mL throughout the entire year). Total Coliform were detected only sporadically in UV LED and chlorinated effluent (6 and 5 times respectively at $\leq$ 2 CFU/mL). *E. coli* were detected at low levels in filter influent and at lower concentrations in filter effluent, but never in UV LED or chlorine effluent, indicating effective disinfection by both processes of this fecal indicator.

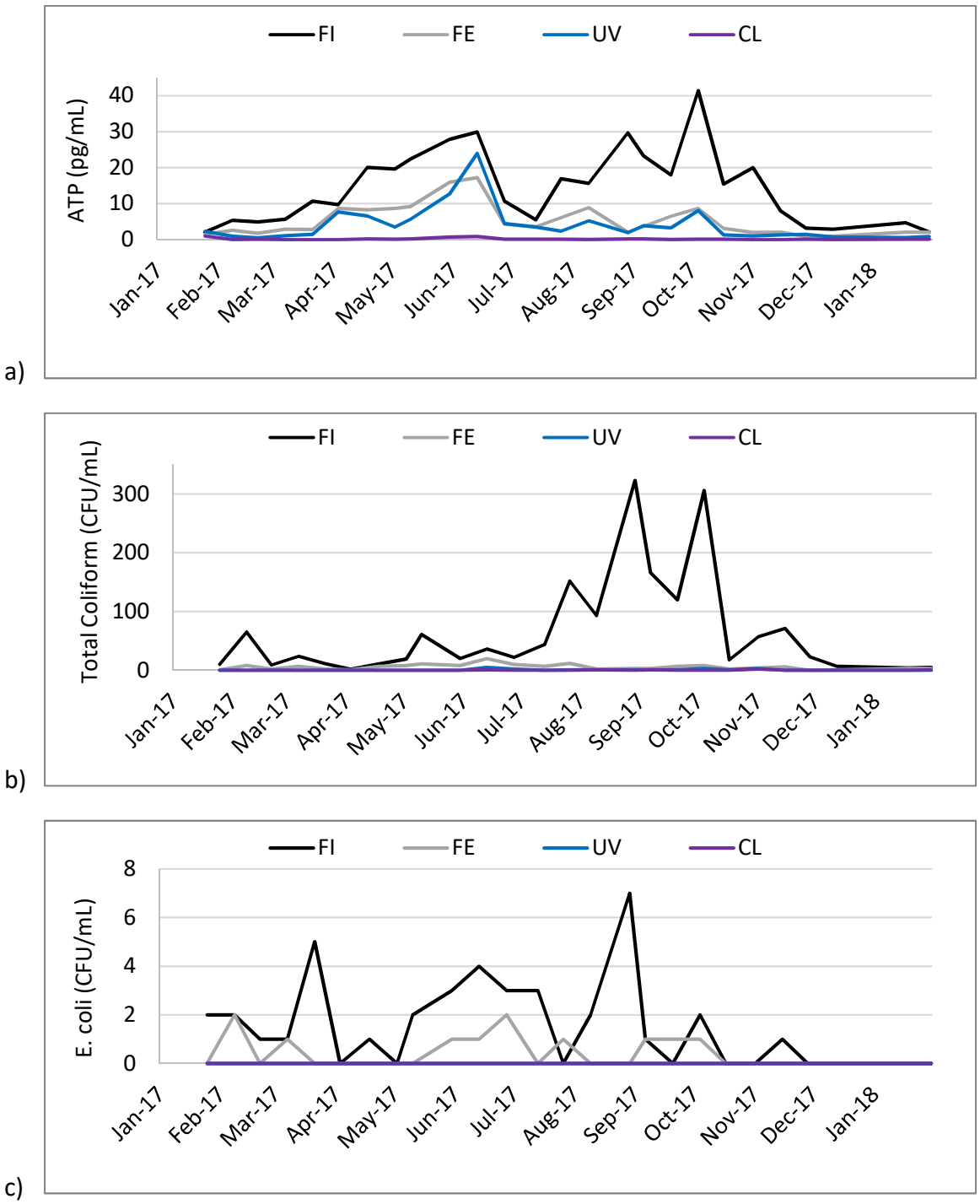

Figure 22 Microbiological measurements of (a) adenosine triphosphate, or ATP (b) Total Coliform, and (c) *E. coli* in filter influent (FI), filter effluent (FE), UV LED effluent (UV), or chlorinated effluent (CL).

The pH and chlorine residual in chlorine effluent over the course of the year were stable at 7.4 +/- 0.3 and 1.4 +/- 0.3 mg/L, respectively (mean +/- standard deviation). In January, hardness in the filter influent (21.9 mg/L as $CaCO_3$) was lower than other samples collected throughout the treatment process (27.8 +/- 0.4 mg/L as $CaCO_3$). Iron was below detection (0.013 ppm) in all January samples. Total Alkalinity averaged across samples collected in influent and, after various stages of treatment, was lowest in May when stream flow was highest (4.75 +/- 1.50 mg/L as $CaCO_3$) compared to January 2017, August 2017, November 2017, and January 2018 (15.75 +/- 0.5, 14.00 +/- 0.00, 18 +/- 3.37, and 26.250+/- 2.87 respectively). Low alkalinity and hardness indicate low mineral fouling potential of the UV LED reactor for this application. Metal concentrations were higher in the UV effluent (1.4 ppm total, especially Cu and Al, Ba) than filter effluent (0.3 ppm total) and chlorine effluent (0.2 ppm total). Data for these and other inorganics are summarized in Supplementary Table S1. All inorganics concentrations in all samples were below Maximum Contaminant Levels (MCLs) in the US EPA National Primary Drinking Water Regulations (US EPA, 2009), and all concentrations except copper in the UV LED effluent were below MCLs for National Secondary Drinking Water Regulations regarding nuisance chemicals. Because inorganics were only measured throughout the treatment plant and in the UV LED effluent upon installation for the demonstration study, temporal effects on inorganics are unknown.

Bromine and Iodine were below detection (1.24 and 0.6 ppb respectively) in all samples in January, except for Br in chlorine effluent (13.8 ppb), indicating low potential for brominated and iodinated DBP formation in this water. Nitrate and nitrite were always below detection in quarterly samples (<0.2 mg/L nitrate and < 0.015 mg/L nitrite), indicating low potential for

nitrogenous DBP formation in this water. DBP samples collected in January and May from filter effluent and UV effluent simulated a comparison of chlorination alone versus LED + chlorination respectively, where each resulted in chlorine residual of 1mg/L after 24 hours under uniform formation conditions (Summers et al., 1996). As shown in Figure 23, DBPs were lower in both the UV effluent and filter influent in January than in May, coinciding with TOC being much lower in January (~1 mg/L) versus May (~4 mg/L). TOC and DOC concentrations were highest in June, and were consistent throughout the treatment process, except for sporadic differences in some chlorine effluent samples. UV LED treatment had little to no effect on DBP formation potential in either January or May. In May, HAA5 and TTHMs were slightly above MCLs (60 and 80 ppb respectively) for both UV LED disinfection and chlorination (US EPA, 2009).

a)

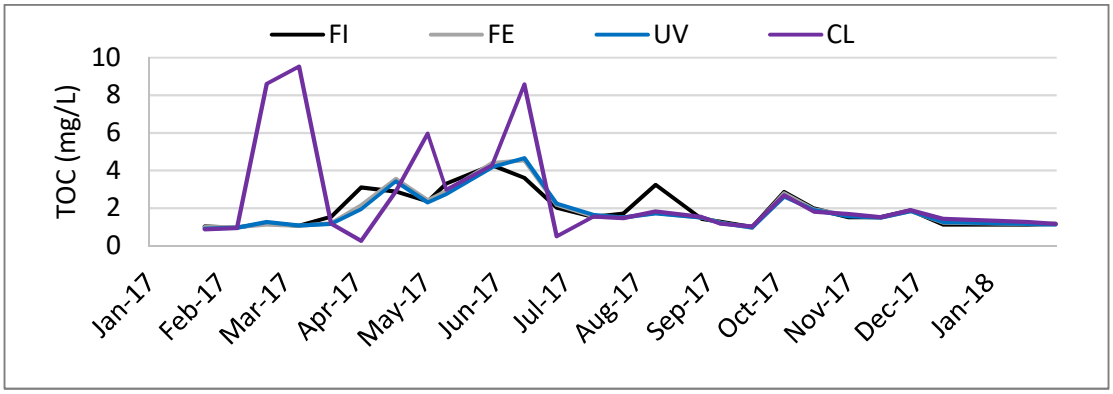

b)

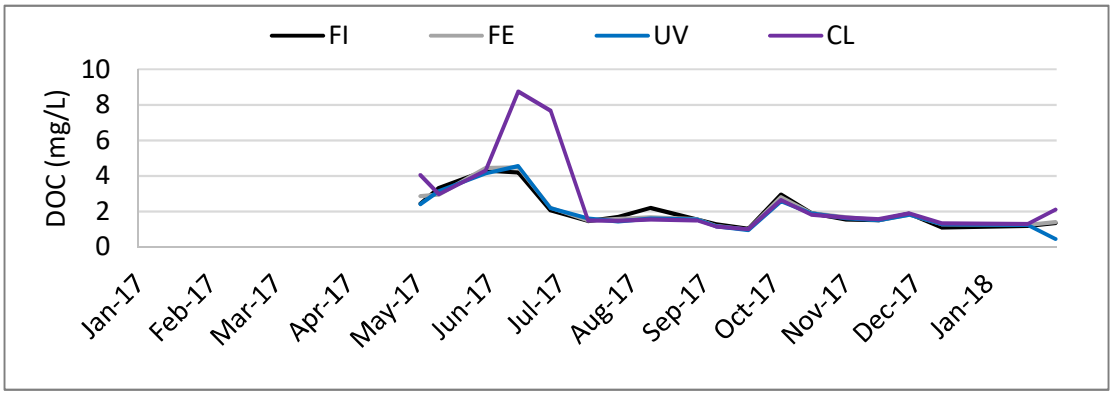

c)

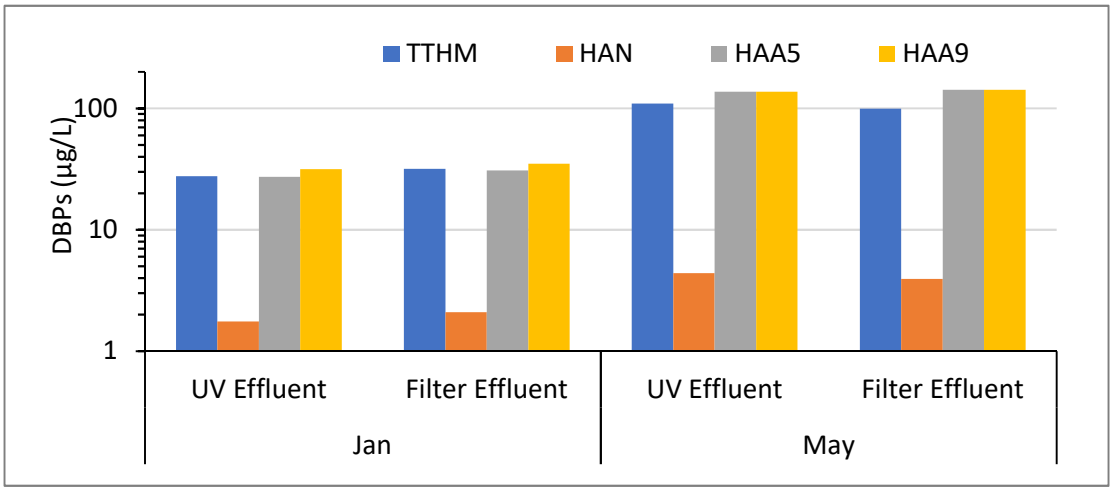

Figure 23 (a) Total and (b) dissolved organic carbon and (c) disinfection byproducts measured under uniform formation conditions in in filter influent (FI), filter effluent (FE), UV LED effluent (UV), or chlorinated effluent (CL).

5.3.3 Demonstration MS2 Disinfection Performance

The PearlAqua UV LED disinfection reactor was installed in the slow sand filter effluent in the small drinking water treatment system in the mountain town of Jamestown, CO. As shown in Figure 24, similar log inactivation of MS2 was achieved throughout the year at each flowrate, with lower inactivation observed at lower UVTs as expected. As shown in Appendix D Figure 36b, predictions of MS2 disinfection performance upon installation in January 2017 - calculated using the bench validation model (Figure 20b) - aligned, indicating no adverse, beneficial, or confounding MS2 disinfection effects of the matrix water at the demonstration site upon installation. Quarterly MS2 challenge testing in May and August (Appendix D Figure 36c-d) demonstrated slightly greater MS2 disinfection than predicted by the validation model, possibly due to photosensitization by organic matter (note that DOC was highest in these months), virus adsorption to the reactor or biofilm during warmer months when biofilm may have been most abundant, or light scattering rather than true absorbance. Collimated beam studies in filter effluent compared to collimated beam studies in PBS, using both the 285 nm LED and LP UV, are shown in Appendix D Figure 37. Slopes comparing PBS to filter effluent dose responses were greater than 1 in May and August for the 285 nm LED, and correlation was lowest (indicated by lower R^2). These studies indicate possible slight effects of photosensitization due to organic matter absorption by the 285 nm LED but not due to LP UV. This could be due to different types of organic matter reacting differently with the higher polychromatic wavelengths emitted by the LED. MS2 has been shown to be affected by organic matter sensitization under natural sunlight irradiation (wavelengths > 320 nm) (Rosado-Lausell

et al., 2013), and LP has been shown to produce photo-oxidants in the presence of dissolved organic matter at high UV fluences (Lester et al., 2013), but future studies should examine wavelength specific UV-C photosensitization of MS2 in the presence of various types of organic matter. Quarterly MS2 challenge testing in November 2017 and January 2018 (Appendix D Figure 36e-f) once again aligned well with the original validation. As demonstrated in Appendix D Figure 37 and Figure 36, only the May and August quarterly challenge testing differed significantly from the slope +/- 95% confidence interval of observed versus predicted values from the original validation testing model. The January 2018 testing confidence intervals were just slightly non-overlapping, and seem to be driven by one data point with high MS2 log inactivation, since all other predictions overlap with those predicted by the validation model.

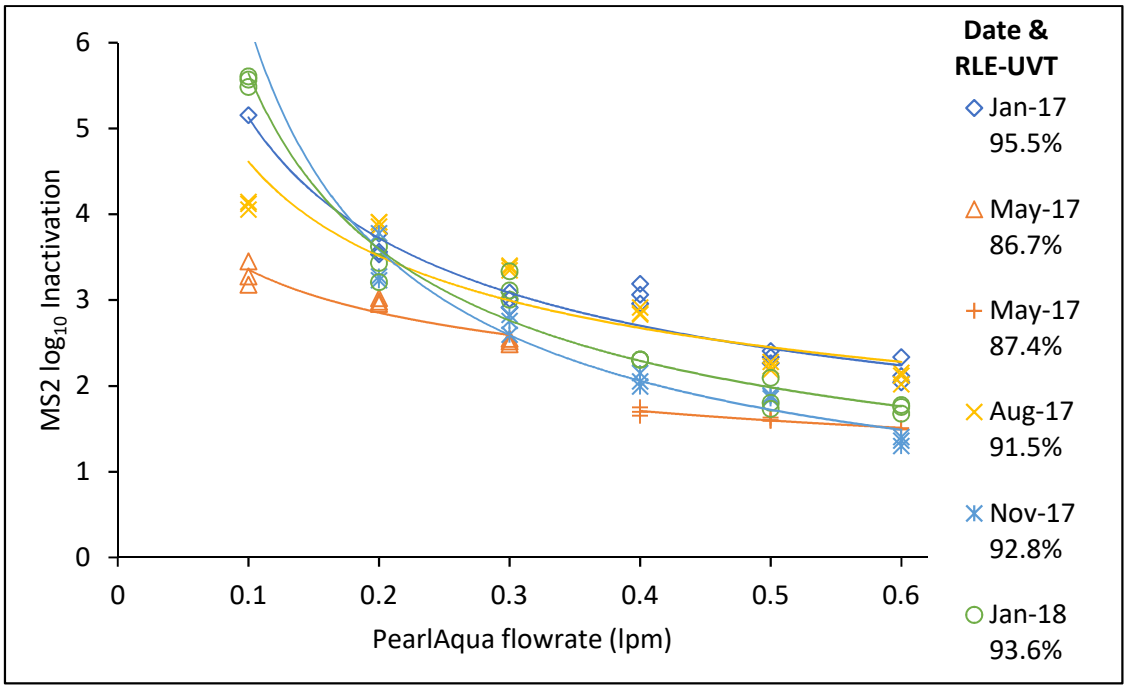

Figure 24 PearlAqua quarterly MS2 challenge testing log inactivation measured at each flowrate for each quarterly challenge test (note that two different UVTs were tested in May).

5.3.4 Post-Demonstration MS2 Disinfection Assessment

After concluding the year-long demonstration study, the reactor was uninstalled from the Jamestown water treatment plant and brought back to the lab for challenge testing to compare to the initial validation. As shown in Figure 25, MS2 inactivation at similar flowrates and UVTs were lower than the initial bench validation. This was expected due to LED aging. To quantify this effect, lamp output and life remaining were measured before and after the demonstration study, and showed a 27% decrease in output (i.e., 73% power remaining). This indicates that after one year of continuous operation (with no power failures due to the on-site generator at the drinking water treatment plant) plus additional lab testing for a total of approximately 9,000 operating hours, the LEDs were near the end of their life (generally considered to be 70% of initial output). The original validation model was a poor predictor for observed MS2 inactivation across the range of flowrates and UVTs tested, even after accounting for the difference in output by changing S/So to 0.73 (as indicated by slope being much different than 1 and R^2 being very low). Fitting a new model to post-demonstration MS2 disinfection data and including S/So = 0.73 improved goodness of fit. In the new model, the e coefficient was not statistically significant. Differences could have arisen due to testing a wider range of UVTs and flowrates in the post-demonstration evaluation, resulting in lower overall inactivation, as shown in Figure 25b, where the range of the post-demonstration covers from 0.2 to 5 log inactivation while the original validation covered from 1 to more than 5 log inactivation.

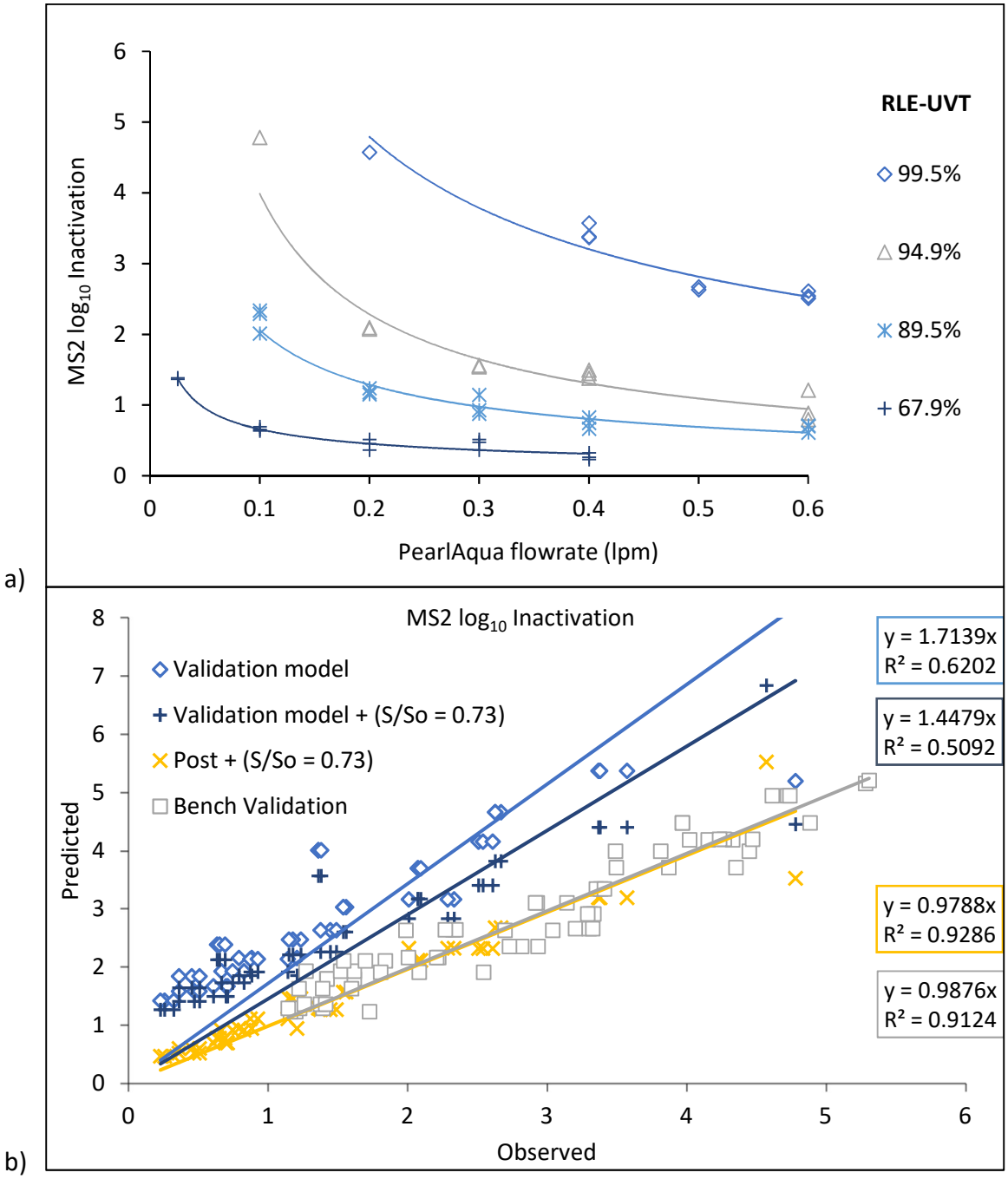

Figure 25 PearlAqua post-demonstration MS2 challenge testing log inactivation (a) measured at each flowrate and UVT and (b) and plotted versus combined variable model predictions that were calculated using coefficients from the bench validation (Equation 12 Validation model), the bench validation with substitution of S/So = 0.73 (Validation model + S/So = 0.73), calculated using a new model fit to only post-demonstration data (Post + S/So = 0.73), and compared to data from the original bench validation.

5.4 Discussion

The MS2 disinfection performance of the first commercially available flow-through UV LED reactor, the PearlAqua (Aquisense), was measured using a validation approach at various flowrates and UV transmittances (UVTs). Viral disinfection by the PearlAqua was modeled using the first application of combined variable modeling to a UV LED reactor, providing a basis for comparison of bench validation results to demonstration-scale quarterly virus challenge tests (Wright et al., 2011). For the bench validation, MS2 disinfection (log I) was best modeled when using influent water absorbance weighted by the relative LED lamp emission (RLE), although model fit was similar when using peak wavelength absorbance. Peak wavelength absorbance may be easier to monitor in the field as UV disinfection progresses toward targeted wavelength polychromatic sources, but RLE weighting may be more appropriate for water matrices with high variability in wavelength specific UV absorbance. Quarterly MS2 challenge testing disinfection was well predicted by the bench testing validation model during periods of high UVT, but not during May and August when UVT was lower and turbidity was higher. Integrating sphere measurements might be needed to further elucidate effects of scattering versus absorbance during the periods of lower UVT and higher turbidity that may have caused MS2 log inactivation to differ from predictions by the original bench validation model. Additionally, a new model had to be fit to the post-demonstration testing, which covered a wider range of UVTs. Together, these results support the need and regulatory recommendations (US EPA, 2006a) for validating reactors across a wide range of expected water qualities and flowrates in order to develop a more comprehensive model that characterizes reactor performance in all

situations. Comprehensive validations, combined with drafted regulatory guidance crediting all wavelengths (Adams, 2016), will help the industry move away from overly conservative validation factors that result in overdosing and decrease the feasibility of implementing UV disinfection for small systems (Jones et al., 2018).

These data and this approach can be used to compare, validate, and test other emerging types of UV sources (including LEDs) and reactors in the rapidly developing UV industry. Demonstration testing of the UV LED reactor in a local small drinking water treatment system (Jamestown, CO) indicated resilience and no detrimental disinfection effects of fouling, with zero maintenance, and cost an estimated < $25 in electricity to run for the entire year at 0.5 lpm, while losing only 27% of initial LED output power. Even in the face of challenging changes in water quality and lack of maintenance, bacterial and viral disinfection effectiveness were maintained. Concentration of Total Coliform and *E. coli* (TC/EC) and total organic carbon (TOC) in the PearlAqua effluent were similar to existing chlorine treatment, but ATP concentrations were higher in UV than chlorinated effluent, demonstrating in concurrence with previous studies (First and Drake, 2014; Kong et al., 2016), although UV does not immediately reduce cellular ATP activity, water was effectively disinfected as shown by indicator organisms. A previous study found better UV disinfection dose-response agreement between the ratio of free and intracellular ATP (Penru et al., 2013), while another study of UV disinfection improved concurrence after incorporating a brief (4 hr) culturing step prior to ATP assay (Cho and Yoon, 2007). Future study is needed to elucidate the approach and applicability of ATP for rapid monitoring UV LED disinfection performance.

Although this demonstration study operated at a flowrate of 0.5 lpm, the hydraulic capacity of the PearlAqua is ~4,500 thousand gallons per day (12 lpm). This flow approaches the scale of current demand at Jamestown, where demand is approximately 2.2 to 12.2 times greater than the hydraulic capacity of the PearlAqua. Future study is needed to assess and optimize disinfection performance at flowrates approaching hydraulic capacity, to enable scale-up considerations. Likely, more LEDs with greater output power configured in series or parallel will be needed to meet both hydraulic capacity and disinfection requirements.

This first longitudinal demonstration investigation of a flow-through UV LED disinfection reactor at a drinking water treatment plant provides evidence for the practicality of LEDs as an emerging disinfection technology, allowing faster adoption in the future. UV LEDs could be particularly useful to help utilities with low mineral source waters to minimize fouling potential and maximize disinfection and public health protection while minimizing chlorine use and therefore disinfection byproduct formation potential. Additionally, this research informs new approaches to UV disinfection technology validation and regulatory compliance, so that when optimized wavelengths and combined variable modeling are used, lower UV doses will be required, increasing the affordability and feasibility of implementation of this technology for small systems.

6. Conclusions and Future Directions

The research presented here increases mechanistic understanding of how different UV wavelengths damage nucleic acids and proteins in viruses, which are most resistant to UV disinfection. The research also demonstrated kinetics of DNA repair using a novel ELISA approach for a marine alga. This biomolecular data was the foundation for wavelength selection to demonstrate synergy in application of tailored wavelengths for viral disinfection optimization. Considering these wavelength specific molecular mechanisms and optimizations, in addition to other engineering practicalities of reactor design and field implementation, a novel UV-C LED system emitting carefully chosen wavelengths was run continuously for one year in a demonstration study at a local small system to investigate the feasibility and potential for improved sustainability of wavelength specific, mercury-free UV disinfection. Together, these studies demonstrate that when new and/or existing UV light sources are optimized based on wavelength specific evidence, more efficient water disinfection can be achieved to protect public health.

6.1 Hypothesis 1 (Molecular Damage)

The study in Chapter 2, considered in context of the literature, demonstrated that protein damage (measured by SDS-PAGE) is the primary driver of virus inactivation at low wavelengths for both the pathogenic adenovirus and the surrogate MS2 bacteriophage. This similarity in inactivation mechanism is likely because both viruses rely on protein capsid integrity to attach to and infect their host. In this study, ELISA was also used to investigate the

wavelength specific contribution of DNA dimer formation to adenovirus and MS2 inactivation. Together these results indicated that, at low wavelengths, protein damage (including putative protein – RNA cross linking for MS2) is the dominant molecular mechanism of inactivation at low UV-C wavelengths, while nucleic acid damage dominates at higher UV-C wavelengths. These mechanistic studies' demonstration that the viral surrogate MS2 has similar molecular response to the target pathogen adenovirus contributes confidence to UV disinfection validations and studies of novel wavelength combinations using this viral surrogate. This is important for the design and validation of tailored wavelength reactors that will be equally or more effective at lower doses than conventional mercury lamps. Mechanistic understanding of surrogate and pathogen inactivation contributes to more informed regulatory decision-making when accounting for the entire UV-C region of spectral sensitivity, and allowing validations using only MS2.

In the future of UV technology optimization, direct measurement assays such as these may help inform development of improved molecular monitoring tools. Future research should focus on determining how to make the CPD ELISA technique truly quantitative, and how to translate it into an instantaneous monitoring tool that could be used with emerging systems like online flow cytometry. Additional tools are also needed for analysis of protein damage, which is especially relevant at low wavelengths, to get a complete mechanistic picture of wavelength specific disinfection. Future studies coupling SDS PAGE with mass spectrometry to measure peptides of all molecular weights, rather than just at the expected molecular weight of proteins in mature virions, will enable even more descriptive quantitation of fragmentation and different types of molecular protein damage. Additionally, an assay could be designed using

antibodies to the MS2 coat protein (which are commercially available) to assess protein damage. A dual-endpoint assay combining MS2 coat protein and CPD antibodies could be simultaneously analyzed by online monitoring for direct and immediate molecular measurement of the effects of UV damage. Development of tools like these will provide a more comprehensive assessment of both protein and nucleic acid damage for the common surrogate MS2, which will make UV validations and monitoring faster and easier, and possibly less expensive by avoiding costly shipping and culturing processes.

6.2 Hypothesis 2 (Molecular Repair)

The study in Chapter 3 quantified UV dose dependent DNA damage (CPD formation) in a marine alga relevant to ballast water disinfection systems. Additionally, the study quantified kinetics of CPD repair in various conditions simulating environmental discharge. These data inform molecular testing techniques that could be coupled with culture to be conservative for environmental protection. The same principles of DNA damage and repair after UV disinfection may also translate from marine-relevant phytoplankton (algae) to drinking water and wastewater-relevant constituents including bacteria, viruses, archaea, and eukaryotes. These data demonstrate the need for tools that fairly quantitate UV disinfection efficacy so that systems can be designed without overdosing that cripples the sustainability of UV disinfection, while also conservatively accounting for repair and regrowth that could negatively impact public and environmental health. This study can inform monitoring strategies, indicating that including a brief culture step may be necessary for conservative enumeration of UV inactivation efficacy when applying molecular tools.

Future research should look at kinetics of DNA damage and repair in other water matrices, and in other organisms and viruses (when cultured with host cells) to ensure that molecular tools used to quantify UV disinfection efficacy are accurate and fair for relevant infectious agents. Repair mechanisms after exposure to low UV wavelengths, such as those emitted by the KrCl excilamp which are known to damage proteins responsible for photorepair, should also be studied to better inform wavelength-tailored disinfection optimization strategies. Additionally, using molecular tools will enable more accessible validations and monitoring, helping systems such as ballast water treatment and small municipal systems that lack capacity for extensive testing. This will enable UV manufacturers to develop optimized, sustainable, and protective systems that are fairly evaluated.

6.3 Hypothesis 3 (Wavelength Specific Strategies)

The study in Chapter 4 demonstrates that UV disinfection efficiency can be enhanced by sequential exposures to UV sources of varying wavelengths. The results also indicate that synergy can be achieved from sequential exposures when applying the LP or KrCl excimer lamp before LEDs. These data indicate that, even at the currently early stage of development of UV-C LEDs and excilamps for water disinfection, they already represent competitive options as a tailored wavelength and mercury-free alternative to existing polychromatic MP mercury lamps. A system incorporating the KrCl excimer lamp with LED(s) would be a mercury-free way to achieve these advantages of wavelength specific UV disinfection, while alleviating some disadvantages of MP UV, including large electrical requirements, visible light production that increases fouling and photorepair, and wasteful non-germicidal photon emission. Using this

evidence, UV disinfection systems could be designed incorporating the excimer lamp to achieve viral disinfection regulatory requirements at lower doses than are currently prescribed. Because the excimer lamp has similar electrical efficiency to the LP lamp, this will reduce electrical costs while providing equal or better public health protection.

Future bench-scale research should examine the effect of simultaneous UV exposures combining LEDs with LP UV, LEDs with the excilamp, and the excilamp with LP UV to determine if any synergy is demonstrated from combining multiple UV sources. Additionally, the excilamp should be tested to determine if pulsing is advantageous for mechanistic disinfection or electrical/thermal reasons. There is immediate need for bench testing to quantify in flow-through systems the advantages of sequential exposures of LP and excimer lamps. Additionally, full-scale research should be conducted by retrofitting existing LP systems (used for protozoa disinfection credits) with excilamps (to achieve viral disinfection credits) to determine the potential costs and benefits. To fully evaluate the challenges of incorporating excilamps (which are not yet commercially available) for municipal disinfection, life cycle and system level analyses should be performed that account for factors such as requirements for electrical supply systems, typical lamp output and lifetime, operational considerations, capital and operating costs, environmental impacts, etc. Further studies of flow-through systems need to be done to confirm bench-scale synergies identified from exposure to LEDs after LP or excimer lamps. Finally, a mercury-free flow-through system should be designed and optimized that combines the KrCl excilamp (emitting at 222 nm for protein damage) with LEDs (emitting both at 255 nm for nucleic acid damage and at 285 for high output at high UVT and for protein damage).

6.4 Hypothesis 4 (UV LED Demonstration)

In Chapter 5, viral disinfection by the UV-C LED PearlAqua was modeled using the first application of the combined variable approach to a UV LED reactor, providing a basis for comparison of bench validation results to demonstration-scale results of quarterly virus challenge tests. These data and this approach can be used to compare, validate, and test other reactors in the rapidly developing UV LED industry. This demonstration study indicated the resilience and disinfection effectiveness of the first commercially available UV LED reactor, operated continuously for nearly one year with zero maintenance, with an estimated electrical cost of less than $25 to disinfect water flowing at 0.5 lpm, at an MS2 bacteriophage reduction equivalent dose (RED) by LP UV of at least 40 mJ/cm^2. Longitudinal evaluation of the flow-through UV LED system provides data necessary for practical operation, design improvements, and scale-up, allowing faster adoption in the future.

The data from the demonstration study should be analyzed in a life cycle analysis framework to determine whether the many differences in UV-LED disinfection versus LP UV disinfection make LEDs a more holistically sustainable technology for small systems. Future work related to implementing LED reactors in the field should consider scale-up to meet flow demands of municipal systems. A large question will be whether it is more beneficial to use many LEDs in one or two large reactors, or to use a few LEDs in multiple reactors. Additionally, designs may need to be modified for applications in lower UVT water, such as wastewater and reclaimed water, where UV is an attractive disinfection alternative to the chemical- and footprint-intensive processes of chlorination and dechlorination. Studies should also compare

organic matter photosensitization between polychromatic LEDs and LP UV. Finally, effects of polychromatic sources like LEDs and excilamps on microbial communities (including antibiotic resistance genes and potential for horizontal gene transfer after irradiation) should also be evaluated and compared to traditional UV sources and chlorine disinfection.

6.5 Summary

This research ultimately aimed to direct future development and implementation of more sustainable, cost-effective, and energy efficient disinfection systems using mercury-free UV technology, through better insight and understanding of biomolecular fundamentals. Tools used here to measure molecular damage could also be adapted in the future to improve quantitation of UV disinfection efficacy at the bench and in the field. Year-long small system demonstration testing of a UV-C LED system showed mercury-free UV drinking water disinfection to be effective and resilient. With further optimization, wavelength-tailored, mercury-free UV disinfection will soon be implemented for inactivation of regulated and resistant pathogens in systems of all scales.

REFERENCES

Adams, J., 2016. Innovative Approach to Validation of Ultraviolet (UV) Reactors for Disinfection in Drinking Water Systems, in: Civil Engineering Conference in the Asian Region. Waikiki, Oahu, Hawaii.

Adams, J., Briski, E., Ram, J., Bailey, S., 2014. Evaluating the response of freshwater organisms to vital staining. Manag. Biol. Invasions 5, 197–208. doi:10.3391/mbi.2014.5.3.02

Akhavan, O., Choobtashani, M., Ghaderi, E., 2012. Protein Degradation and RNA Efflux of Viruses Photocatalyzed by Graphene–Tungsten Oxide Composite Under Visible Light Irradiation. J. Phys. Chem. C 116, 9653–9659. doi:10.1021/jp301707m

Aksozek, A., McClellan, K., Howard, K., Niederkorn, J.Y., Alizadeh, H., 2002. Resistance of Acanthamoeba castellanii cysts to physical, chemical, and radiological conditions. J. Parasitol. 88, 621–3. doi:10.1645/0022-3395(2002)088[0621:ROACCT]2.0.CO;2

Alberts, B., Johnson, A., Lewis, J., Raff, M., Roberts, K., Walter, P., 2002. Molecular biology of the cell, 4th ed. Garland Science, New York.

Anthis, N.J., Clore, G.M., 2013. Sequence-specific determination of protein and peptide concentrations by absorbance at 205 nm. Protein Sci. 22, 851–8. doi:10.1002/pro.2253

Aoyagi, Y., Takeuchi, M., Yoshida, K., Kurouchi, M., Yasui, N., Kamiko, N., Araki, T., Nanishi, Y., 2011. Inactivation of Bacterial Viruses in Water Using Deep Ultraviolet Semiconductor Light-Emitting Diode. J. Environ. Eng. 137, 1215–1218. doi:10.1061/(ASCE)EE.1943-7870.0000442

Aquisense Technologies, 2016. PearlAqua UV-C LED Water Disinfection System Operation and Maintenance Manual.

Avdeev, S.M., Orlovskii, V.M., Panarin, V.A., Pechenitsin, D.S., Skakun, V.S., Sosnin, È.A., Tarasenko, V.F., 2017. Efficient UV and VUV Radiation Sources – Excilamps and Photoreactors on Their Basis. Russ. Phys. J. 60, 1298–1302. doi:10.1007/s11182-017-1211-7

Beck, N.K., Callahan, K., Nappier, S.P.P., Kim, H., Sobsey, M.D.D., Meschke, J.S.S., 2009. Development of a spot-titer culture assay for quantifying bacteria and viral indicators. J. Rapid Methods Autom. Microbiol. 17, 455–464. doi:10.1111/j.1745-4581.2009.00182.x

Beck, S.E., 2018. UV LED Disinfection 101. IUVA News 20.

Beck, S.E., Hull, N.M., Poepping, C., Linden, K., 2017a. Wavelength-Dependent Damage to

Adenoviral Proteins Across the Germicidal UV Spectrum, Environmental Science and Technology. doi:10.1021/acs.est.7b04602

Beck, S.E., Rodriguez, R.A., Hawkins, M.A., Hargy, T.M., Larason, T.C., Linden, K.G., 2015. Comparison of UV-Induced Inactivation and RNA Damage in MS2 Phage Across the Germicidal UV Spectrum. Appl. Environ. Microbiol. AEM.02773-15-. doi:10.1128/AEM.02773-15

Beck, S.E., Rodriguez, R.A., Linden, K.G., Hargy, T.M., Larason, T.C., Wright, H.B., 2014a. Wavelength dependent UV inactivation and DNA damage of adenovirus as measured by cell culture infectivity and long range quantitative PCR. Environ. Sci. Technol. 48, 591–8. doi:10.1021/es403850b

Beck, S.E., Ryu, H., Boczek, L.A., Cashdollar, J.L., Jeanis, K.M., Rosenblum, J.S., Lawal, O.R., Linden, K.G., 2017b. Evaluating UV-C LED disinfection performance and investigating potential dual-wavelength synergy. Water Res. 109, 207–216. doi:10.1016/j.watres.2016.11.024

Beck, S.E., Wright, H.B., Hargy, T.M., Larason, T.C., Linden, K.G., 2014b. Action spectra for validation of pathogen disinfection in medium-pressure ultraviolet (UV) systems. Water Res. 70C, 27–37. doi:10.1016/j.watres.2014.11.028

Blyth, J., Templeton, M.R., Cairns, B., 2013. An Assay for Estimating UV Disinfection Dose by Direct Quantification of DNA Damage in Indigenous Microorganisms in Drinking Water, in: Proceedings of the Water Environment Federation, Disinfection. pp. 155–158.

Bohrerova, Z., Linden, K.G., 2007. Standardizing photoreactivation: comparison of DNA photorepair rate in Escherichia coli using four different fluorescent lamps. Water Res. 41, 2832–8. doi:10.1016/j.watres.2007.03.015

Bohrerova, Z., Rosenblum, J., Linden, K.G., 2015. Importance of Recovery of E. coli in Water Following Ultraviolet Light Disinfection. J. Environ. Eng. 141, 04014094. doi:10.1061/(ASCE)EE.1943-7870.0000922

Bohrerova, Z., Shemer, H., Lantis, R., Impellitteri, C.A., Linden, K.G., 2008. Comparative disinfection efficiency of pulsed and continuous-wave UV irradiation technologies. Water Res. 42, 2975–82. doi:10.1016/j.watres.2008.04.001

Bolton, J.R., 2017. Action Spectra: A Review. IUVA News 19, 10–12.

Bolton, J.R., Linden, K.G., 2003. Standardization of Methods for Fluence (UV Dose) Determination in Bench-Scale UV Experiments. J. Environ. Eng. 129, 209–215. doi:10.1061/(ASCE)0733-9372(2003)129:3(209)

Bosshard, F., Armand, F., Hamelin, R., Kohn, T., 2013. Mechanisms of human adenovirus

inactivation by sunlight and UVC light as examined by quantitative PCR and quantitative proteomics. Appl. Environ. Microbiol. 79, 1325–32. doi:10.1128/AEM.03457-12

Bounty, S., Rodriguez, R.A., Linden, K.G., 2012. Inactivation of adenovirus using low-dose UV/H2O2 advanced oxidation. Water Res. 46, 6273–8. doi:10.1016/j.watres.2012.08.036

Bowker, C., Sain, A., Shatalov, M., Ducoste, J., 2011. Microbial UV fluence-response assessment using a novel UV-LED collimated beam system. Water Res. 45, 2011–9. doi:10.1016/j.watres.2010.12.005

Bradie, J., Broeg, K., Gianoli, C., He, J., Heitmüller, S., Curto, A. Lo, Nakata, A., Rolke, M., Schillak, L., Stehouwer, P., Vanden Byllaardt, J., Veldhuis, M., Welschmeyer, N., Younan, L., Zaake, A., Bailey, S., 2017. A shipboard comparison of analytic methods for ballast water compliance monitoring. J. Sea Res. doi:10.1016/j.seares.2017.01.006

Bucher, D.B., Kufner, C.L., Schlueter, A., Carell, T., Zinth, W., 2016. UV-Induced Charge Transfer States in DNA Promote Sequence Selective Self-Repair. J. Am. Chem. Soc. 138, 186–190. doi:10.1021/jacs.5b09753

Bunsen, R., Roscoe, H.E., 1855. Photochemische untersuchungen. Poggendorff's Ann. 96, 373–394.

Cantwell, R.E., Hofmann, R., Templeton, M.R., 2008. Interactions between humic matter and bacteria when disinfecting water with UV light. J. Appl. Microbiol. 105, 25–35. doi:10.1111/j.1365-2672.2007.03714.x

Casas-Monroy, O., Linley, R.D., Adams, J.K., Chan, F.T., Drake, D.A.R., Bailey, S.A., 2015. Relative invasion risk for plankton across marine and freshwater systems: examining efficacy of proposed international ballast water discharge standards. PLoS One 10, e0118267. doi:10.1371/journal.pone.0118267

Cashdollar, J.L., Huff, E., Ryu, H., Grimm, A.C., 2016. The influence of incubation time on adenovirus quantitation in A549 cells by most probable number. J. Virol. Methods 237, 200–203. doi:10.1016/J.JVIROMET.2016.09.002

Chatterley, C., Linden, K., C, C., K, L., 2010. Demonstration and evaluation of germicidal UV-LEDs for point-of-use water disinfection. J. Water Health 8, 479–86. doi:10.2166/wh.2010.124

Chen, J., Loeb, S., Kim, J.-H., 2017a. LED revolution: fundamentals and prospects for UV disinfection applications. Environ. Sci. Water Res. Technol. 3, 188–202. doi:10.1039/C6EW00241B

Chen, J., Loeb, S., Kim, J.-H., 2017b. LED revolution: fundamentals and prospects for UV disinfection applications. Environ. Sci. Water Res. Technol. 3, 188–202. doi:10.1039/C6EW00241B

Chen, R.Z., Craik, S.A., Bolton, J.R., 2009. Comparison of the action spectra and relative DNA absorbance spectra of microorganisms: information important for the determination of germicidal fluence (UV dose) in an ultraviolet disinfection of water. Water Res. 43, 5087–5096. doi:10.1016/j.watres.2009.08.032

Chevremont, A.-C., Farnet, A.-M., Coulomb, B., Boudenne, J.-L., 2012a. Effect of coupled UV-A and UV-C LEDs on both microbiological and chemical pollution of urban wastewaters. Sci. Total Environ. 426, 304–310. doi:10.1016/j.scitotenv.2012.03.043

Chevremont, A.-C., Farnet, A.-M., Sergent, M., Coulomb, B., Boudenne, J.-L., 2012b. Multivariate optimization of fecal bioindicator inactivation by coupling UV-A and UV-C LEDs. Desalination 285, 219–225. doi:10.1016/j.desal.2011.10.006

Cho, M., Yoon, J., 2007. The application of bioluminescence assay with culturing for evaluating quantitative disinfection performance. Water Res. 41, 741–746. doi:10.1016/J.WATRES.2006.11.031

Clancy, J., Hargy, T., Marshall, M., Dyksen, J., 1998. UV Light Inactivation of Cryptosporidium oocysts. Waterborne Pathog. 90, 92–102.

Clauß, M., Mannesmann, R., Kolch, A., 2005. Photoreactivation ofEscherichia coli andYersinia enterolytica after Irradiation with a 222 nm Excimer Lamp Compared to a 254 nm Low-pressure Mercury Lamp. Acta Hydrochim. Hydrobiol. 33, 579–584. doi:10.1002/aheh.200400600

Crook, M.J., Jefferson, B., Autin, O., MacAdam, J., Nocker, A., 2015. Comparison of ultraviolet light emitting diodes with traditional UV for greywater disinfection. J. Water Reuse Desalin. 5, 17. doi:10.2166/wrd.2014.022

Cullen, J.J., MacIntyre, H.L., 2017. The case for using the Most Probable Number (MPN) method in ballast water management system type approval testing, in: 6th IMarEST Ballast Water Technology Conference. London, UK.

Cullen, J.J., MacIntyre, H.L., 2016. On the use of the serial dilution culture method to enumerate viable phytoplankton in natural communities of plankton subjected to ballast water treatment. J. Appl. Phycol. 28, 279–298. doi:10.1007/s10811-015-0601-x

Cullen, J.J., MacIntyre, H.L., 2016. A Revised Assessment of the Most Probable Number (MPN) Method for Enumerating Viable Phytoplankton Cells in Ballast Water Discharge, in: 19th International Conference on Aquatic Invasive Species. Winnipeg, MB Canada. doi:10.13140/RG.2.1.4424.2326

Curiale, M., 2004. MPN Calculator [WWW Document]. i2Workout. URL http://www.i2workout.com/mcuriale/mpn/index.html (accessed 1.1.17).

Dai, X., Li, Z., Lai, M., Shu, S., Du, Y., Zhou, Z.H., Sun, R., 2017. In situ structures of the genome and genome-delivery apparatus in a single-stranded RNA virus. Nature 541, 112–116. doi:10.1038/nature20589

Darnell, R.B., 2010. HITS-CLIP: panoramic views of protein-RNA regulation in living cells. Wiley Interdiscip. Rev. RNA 1, 266–286. doi:10.1002/wrna.31

Dent, K.C., Thompson, R., Barker, A.M., Hiscox, J.A., Barr, J.N., Stockley, P.G., Ranson, N.A., 2013. The Asymmetric Structure of an Icosahedral Virus Bound to Its Receptor Suggests a Mechanism for Genome Release. Structure 21, 1225–1234. doi:10.1016/j.str.2013.05.012

Drake, L.A., Tamburri, M.N., First, M.R., Smith, G.J., Johengen, T.H., 2014. How many organisms are in ballast water discharge? A framework for validating and selecting compliance monitoring tools. Mar. Pollut. Bull. 86, 122–128. doi:10.1016/j.marpolbul.2014.07.034

Eischeid, A.C., Linden, K.G., 2011. Molecular indications of protein damage in adenoviruses after UV disinfection. Appl. Environ. Microbiol. 77, 1145–7. doi:10.1128/AEM.00403-10

Eischeid, A.C., Linden, K.G., 2007. Efficiency of pyrimidine dimer formation in Escherichia coli across UV wavelengths. J. Appl. Microbiol. 103, 1650–6. doi:10.1111/j.1365-2672.2007.03424.x

Eischeid, A.C., Meyer, J.N., Linden, K.G., 2009. UV disinfection of adenoviruses: molecular indications of DNA damage efficiency. Appl. Environ. Microbiol. 75, 23–8. doi:10.1128/AEM.02199-08

Eischeid, A.C., Thurston, J.A., Linden, K.G., 2011. UV Disinfection of Adenovirus: Present State of the Research and Future Directions. Crit. Rev. Environ. Sci. Technol. 41, 1375–1396. doi:10.1080/10643381003608268

First, M.R., Drake, L.A., 2014. Life after treatment: detecting living microorganisms following exposure to UV light and chlorine dioxide. J. Appl. Phycol. 26, 227–235. doi:10.1007/s10811-013-0049-9

First, M.R., Drake, L.A., 2013. Approaches for determining the effects of UV radiation on microorganisms in ballast water. Manag. Biol. Invasions 4, 87–99.

Gott, J.M., Willis, M.C., Koch, T.H., Uhlenbeck, O.C., 1991. A specific, UV-induced RNA-protein crosslink using 5-bromouridine-substituted RNA. Biochemistry 30, 6290–6295. doi:10.1021/bi00239a030

Grob, C., Pollet, B.G., 2016. Regrowth in ship's ballast water tanks: Think again! Mar. Pollut. Bull. 109, 46–48. doi:10.1016/j.marpolbul.2016.04.061

Guo, M.-T., Yuan, Q.-B., Yang, J., 2013. Microbial selectivity of UV treatment on antibiotic-

resistant heterotrophic bacteria in secondary effluents of a municipal wastewater treatment plant. Water Res. 47, 6388–94. doi:10.1016/j.watres.2013.08.012

Hammes, F., Berney, M., Wang, Y., Vital, M., Köster, O., Egli, T., 2008. Flow-cytometric total bacterial cell counts as a descriptive microbiological parameter for drinking water treatment processes. Water Res. 42, 269–277. doi:10.1016/J.WATRES.2007.07.009

Harm, 1980. Biological Effects of Ultraviolet Radiation. Camgridge University Press, Cambridge.

Hirayama, H., Fujikawa, S., Kamata, N., 2015. Recent Progress in AlGaN-Based Deep-UV LEDs. Electron. Commun. Japan 98, 1–8. doi:10.1002/ecj.11667

Hull, N.M., Isola, M.R., Petri, B., Chan, P.-S., Linden, K.G., 2017. Algal DNA repair kinetics support culture-based enumeration for validation of ultraviolet disinfection ballast water treatment systems. Environ. Sci. Technol. Lett. 4. doi:10.1021/acs.estlett.7b00076

Ibrahim, M.A.S., MacAdam, J., Autin, O., Jefferson, B., 2013. Evaluating the impact of LED bulb development on the economic viability of ultraviolet technology for disinfection. Environ. Technol. 35, 400–6. doi:10.1080/09593330.2013.829858

IMO, 2004. International Convention for the Control and Management of Ships' Ballast Water and Sediments. IMODOCS, London.

Jasenak, B., 2018. Design Considerations for Creating an Optimized UV LED System. IUVA News 20.

Jones, C.H., Shilling, E.G., Linden, K.G., Cook, S.M., 2018. Life Cycle Environmental Impacts of Disinfection Technologies Used in Small Drinking Water Systems. Environ. Sci. Technol. 52, 2998–3007. doi:10.1021/acs.est.7b04448

Kang, J.-W., Kim, S.-S., Kang, D.-H., 2018a. Inactivation dynamics of 222 nm krypton-chlorine excilamp irradiation on Gram-positive and Gram-negative foodborne pathogenic bacteria. Food Res. Int. doi:10.1016/j.foodres.2018.04.018

Kang, J.-W., Kim, S.-S., Kang, D.-H., 2018b. Inactivation dynamics of 222 nm krypton-chlorine excilamp irradiation on Gram-positive and Gram-negative foodborne pathogenic bacteria. Food Res. Int. doi:10.1016/j.foodres.2018.04.018

Kim, B., Kim, A.-J., Shin, J.-K., 2013. Effect of Sterilization by Intense Pulsed Light on Radiation-resistant Bacterium, Micrococcus roseus. Korean J. Food Sci. Technol. 45, 248–251. doi:10.9721/KJFST.2013.45.2.248

Kim, D.-K., Kim, S.-J., Kang, D.-H., 2017. Inactivation modeling of human enteric virus surrogates, MS2, Qβ, and ΦX174, in water using UVC-LEDs, a novel disinfecting system. Food Res. Int. 91, 115–123. doi:10.1016/j.foodres.2016.11.042

Knox, J., 2015. Ballast water – Living vs. viable [WWW Document]. Coast Guard Marit. Commons. URL http://mariners.coastguard.dodlive.mil/2015/12/07/1272015-ballast-water-living-vs-viable/ (accessed 3.29.17).

Knox, L.J., 2016. Coast Guard decision on use of Most Probable Number method [WWW Document]. Coast Guard Marit. Commons. URL http://mariners.coastguard.dodlive.mil/2015/12/14/12142015-coast-guard-decision-on-use-of-most-probable-number-method/ (accessed 1.1.16).

Kobayashi, N., Katsumi, S., Imoto, K., Nakagawa, A., Miyagawa, S., Furumura, M., Mori, T., 2001. Quantitation and Visualization of Ultraviolet-Induced DNA Damage Using Specific Antibodies: Application to Pigment Cell Biology. Pigment Cell Res. 14, 94–102. doi:10.1034/j.1600-0749.2001.140204.x

Kolkman, A., Martijn, B.J., Vughs, D., Baken, K.A., van Wezel, A.P., 2015. Tracing Nitrogenous Disinfection Byproducts after Medium Pressure UV Water Treatment by Stable Isotope Labeling and High Resolution Mass Spectrometry. Environ. Sci. Technol. 49, 4458–4465. doi:10.1021/es506063h

Kollu, K., Örmeci, B., 2015. Regrowth Potential of Bacteria after Ultraviolet Disinfection in the Absence of Light and Dark Repair. J. Environ. Eng. 141, 04014069. doi:10.1061/(ASCE)EE.1943-7870.0000905

Komatsu, Y., Tsujino, T., Suzuki, T., Nikaido, O., Ohtsuka, E., 1997. Antigen Structural Requirements for Recognition by a Cyclobutane Thymine Dimer-Specific Monoclonal Antibody. Nucleic Acids Res. 25, 3889–3894. doi:10.1093/nar/25.19.3889

Kong, X., Ma, J., Wen, G., Wei, Y., 2016. Considerable discrepancies among HPC, ATP, and FCM detection methods in evaluating the disinfection efficiency of Gram-positive and -negative bacterium by ultraviolet radiation and chlorination. Desalin. Water Treat. 57, 17537–17546. doi:10.1080/19443994.2015.1086693

Kristoffersen, A.S., Hamre, B., Frette, Ø., Erga, S.R., 2016. Chlorophyll a fluorescence lifetime reveals reversible UV-induced photosynthetic activity in the green algae Tetraselmis. Eur. Biophys. J. 45, 259–68. doi:10.1007/s00249-015-1092-z

Kuo, M.-H., Allis, C.D., 1999. In Vivo Cross-Linking and Immunoprecipitation for Studying Dynamic Protein:DNA Associations in a Chromatin Environment. Methods 19, 425–433. doi:10.1006/meth.1999.0879

Kurdistani, S.K., Grunstein, M., 2003. In vivo protein–protein and protein–DNA crosslinking for genomewide binding microarray. Methods 31, 90–95. doi:10.1016/S1046-2023(03)00092-6

Lamont, Y., Rzezutka, A., Anderson, J.G., MacGregor, S.J., Given, M.J., Deppe, C., Cook, N., 2007.

Pulsed UV-light inactivation of poliovirus and adenovirus. Lett. Appl. Microbiol. 45, 564–7. doi:10.1111/j.1472-765X.2007.02261.x

Lawal, O., 2012. Today's Real World Applications for UV-C LED Light Sources: Next Gen UV Disinfection Today!, in: IUVA Regional Conference, Washington DC, 12-14 Aug 2012.

Lawal, O., Cosman, J., Pagan, J., 2018. UV-C LED Devices and Systems: Current and Future State. IUVA News 20.

Lawryshyn, Y., Hofmann, R., 2015. Theoretical Evaluation of UV Reactors in Series. J. Environ. Eng. 141, 04015023. doi:10.1061/(ASCE)EE.1943-7870.0000924

Lester, Y., Sharpless, C.M., Mamane, H., Linden, K.G., 2013. Production of photo-oxidants by dissolved organic matter during UV water treatment. Environ. Sci. Technol. 47, 11726–33. doi:10.1021/es402879x

Li, G.-Q., Wang, W.-L., Huo, Z.-Y., Lu, Y., Hu, H.-Y., 2017a. Comparison of UV-LED and low pressure UV for water disinfection: Photoreactivation and dark repair of Escherichia coli. Water Res. 126, 134–143. doi:10.1016/J.WATRES.2017.09.030

Li, G.-Q., Wang, W.-L., Huo, Z.-Y., Lu, Y., Hu, H.-Y., 2017b. Comparison of UV-LED and low pressure UV for water disinfection: Photoreactivation and dark repair of Escherichia coli. Water Res. 126, 134–143. doi:10.1016/J.WATRES.2017.09.030

Li, J., Hirota, K., Yumoto, H., Matsuo, T., Miyake, Y., Ichikawa, T., 2010. Enhanced germicidal effects of pulsed UV-LED irradiation on biofilms. J. Appl. Microbiol. 109, 2183–2190. doi:10.1111/j.1365-2672.2010.04850.x

Li, L., Mendis, N., Trigui, H., Oliver, J.D., Faucher, S.P., 2014. The importance of the viable but non-culturable state in human bacterial pathogens. Front. Microbiol. 5, 258. doi:10.3389/fmicb.2014.00258

Liebich, V., Stehouwer, P.P., Veldhuis, M., 2012. Re-growth of potential invasive phytoplankton following UV-based ballast water treatment. Aquat. Invasions 7, 29–36. doi:10.3391/ai.2012.7.1.004

Linden, K.G., Darby, J.L., 1997. Estimating effective germicidal dose from medium pressure UV lamps. J. Environ. Eng. 123, 1142–1149.

Linden, K.G., Shin, G.-A., Faubert, G., Cairns, W., Sobsey, M.D., 2002. UV Disinfection of Giardia lamblia Cysts in Water. Environ. Sci. Technol. 36, 2519–22. doi:10.1021/es0113403

Linden, K.G., Shin, G.-A., Lee, J.-K., Scheible, K., Shen, C., Posy, P., 2009. Demonstrating 4-log Adenovirus Inactivation in a Medium-Pressure UV Disinfection Reactor (PDF). J. Am. Water Works Assoc. 101, 90–99.

Linden, K.G., Shin, G., Sobsey, M.D., 2001. Comparative effectiveness of UV wavelengths for the inactivation of Cryptosporidium parvum oocysts in water. Water Sci. Technol. 43, 171–4.

Linden, K.G., Thurston, J., Schaefer, R., Malley, J.P., 2007. Enhanced UV inactivation of adenoviruses under polychromatic UV lamps. Appl. Environ. Microbiol. 73, 7571–4. doi:10.1128/AEM.01587-07

Loge, F.J., Emerick, R.W., Thompson, D.E., Nelson, D.C., Darby, J.L., 1999. Factors Influencing Ultraviolet Disinfection Performance Part I: Light Penetration to Wastewater Particles on JSTOR. Water Environ. Res. 71, 377–381.

Lomaev, M.I., Sosnin, E.A., Tarasenko, V.F., 2016. Excilamps and their Applications. Chem. Eng. Technol. 39, 39–50. doi:10.1002/ceat.201500229

Lomaev, M.I., Sosnin, E.A., Tarasenko, V.F., 2012. Excilamps and their applications. Prog. Quantum Electron. 36, 51–97. doi:10.1016/j.pquantelec.2012.03.003

Lomaev, M.I., Tarasenko, V.F., Shitts, D. V., 2002. An effective high-power KrCl excimer barrier-discharge lamp. Tech. Phys. Lett. 28, 33–35. doi:10.1134/1.1448635

Lu, L., Wang, J., Yang, G., Zhu, B., Pan, K., 2017. Biomass and nutrient productivities of Tetraselmis chuii under mixotrophic culture conditions with various C:N ratios. Chinese J. Oceanol. Limnol. 35, 303–312. doi:10.1007/s00343-016-5299-3

Lui, G.Y., Roser, D., Corkish, R., Ashbolt, N., Jagals, P., Stuetz, R., 2014. Photovoltaic powered ultraviolet and visible light-emitting diodes for sustainable point-of-use disinfection of drinking waters. Sci. Total Environ. Total Environ. 493, 185–96. doi:10.1016/j.scitotenv.2014.05.104

MacIntyre, H.L., Cullen, J.J., 2016. Classification of phytoplankton cells as live or dead using the vital stains fluorescein diacetate and 5-chloromethylfluorescein diacetate. J. Phycol. 52, 572–589. doi:10.1111/jpy.12415

Malayeri, A.H., Mohensi, M., Cairns, B., Bolton, J.R., 2017. Fluence (UV Dose) Required to Achieve Incremental Log Inactivation of Bacteria, Protozoa, Viruses and Algae. IUVA News.

Mamane, H., Linden, K.G., 2006. Impact of Particle Aggregated Microbes on UV Disinfection. II: Proper Absorbance Measurement for UV Fluence. J. Environ. Eng. 132, 607–615. doi:10.1061/(ASCE)0733-9372(2006)132:6(607)

Martijn, B.J., Kruithof, J.C., Hughes, R.M., Mastan, R.A., Van Rompay, A.R., Malley, J.P., 2015. Induced Genotoxicity in Nitrate-Rich Water Treated With Medium-Pressure Ultraviolet Processes. J. Am. Water Works Assoc. 107, E301–E312. doi:10.5942/jawwa.2015.107.0079

Massier, S., Bouffartigues, E., Rincé, A., Maillot, O., Feuilloley, M.G.J., Orange, N., Chevalier, S.,

2013. Effects of a pulsed light-induced stress on Enterococcus faecalis. J. Appl. Microbiol. 114, 186–95. doi:10.1111/jam.12029

Matafonova, G., Batoev, V., 2012. Recent progress on application of UV excilamps for degradation of organic pollutants and microbial inactivation. Chemosphere 89, 637–47. doi:10.1016/j.chemosphere.2012.06.012

Matafonova, G.G., Batoev, V.B., Astakhova, S.A., Gómez, M., Christofi, N., 2008. Efficiency of KrCl excilamp (222 nm) for inactivation of bacteria in suspension. Lett. Appl. Microbiol. 47, 508–13. doi:10.1111/j.1472-765X.2008.02461.x

McKinney, C.W., Pruden, A., 2012. Ultraviolet disinfection of antibiotic resistant bacteria and their antibiotic resistance genes in water and wastewater. Environ. Sci. Technol. 46, 13393–400. doi:10.1021/es303652q

McLellan, N.L., Lee, H., Habash, M.B., 2016. Evaluation of propidium monoazide and long-amplicon qPCR as an infectivity assay for coliphage. J. Virol. Methods 238, 48–55. doi:10.1016/J.JVIROMET.2016.10.004

Mori, T., Nakane, M., Hattori, T., Matsunaga, T., Ihara, M., Nikaido, O., 1991. Simultaneous Establishment of Monoclonal Antibodies Specific for Either Cyclobutane Pyrimidine Dimer or (6-4) Photoproduct from the Same Mouse Immunizied with Ultraviolet-Irradiated DNA. Photochem. Photobiol. 54, 225–232. doi:10.1111/j.1751-1097.1991.tb02010.x

Mostafa, S., Rosario-Ortiz, F.L., 2013. Singlet oxygen formation from wastewater organic matter. Environ. Sci. Technol. 47, 8179–86. doi:10.1021/es401814s

Muramoto, Y., Kimura, M., Nouda, S., 2014. Development and future of ultraviolet light-emitting diodes: UV-LED will replace the UV lamp. Semicond. Sci. Technol. 29, 084004. doi:10.1088/0268-1242/29/8/084004

Nelson, B.N., Lemieux, E.J., Drake, L., Kulis, D., Burns, K., Anderson, D., Welshmeyer, N., Smith, S., Scianni, C., Wier, T., Riley, S., Herring, P., 2009. Phytoplankton Enumeration and Evaluation Experiments.

Nelson, K.Y., McMartin, D.W., Yost, C.K., Runtz, K.J., Ono, T., 2013. Point-of-use water disinfection using UV light-emitting diodes to reduce bacterial contamination. Environ. Sci. Pollut. Res. Int. 20, 5441–8. doi:10.1007/s11356-013-1564-6

Nizri, L., Vaizel-Ohayon, D., Ben-Amram, H., Sharaby, Y., Halpern, M., Mamane, H., 2017. Development of a molecular method for testing the effectiveness of UV systems on-site. Water Res. 127, 162–171.

Oguma, K., 2018. UV LEDs for Water Treatment: Research Overview and Perspectives. IUVA News 20.

Oguma, K., 2015. Disinfection:UV-LED as a new option?, in: IUVA Frontier 2015.

Oguma, K., Katayama, H., Mitani, H., Morita, S., Hirata, T., Ohgaki, S., 2001. Determination of pyrimidine dimers in Escherichia coli and Cryptosporidium parvum during UV light inactivation, photoreactivation, and dark repair. Appl. Environ. Microbiol. 67, 4630–7. doi:10.1128/AEM.67.10.4630-4637.2001

Oguma, K., Katayama, H., Ohgaki, S., 2002. Photoreactivation of Escherichia coli after low- or medium-pressure UV disinfection determined by an endonuclease sensitive site assay. Appl. Environ. Microbiol. 68, 6029–35. doi:10.1128/AEM.68.12.6029-6035.2002

Oguma, K., Kita, R., Sakai, H., Murakami, M., Takizawa, S., 2013. Application of UV light emitting diodes to batch and flow-through water disinfection systems. Desalination 328, 24–30. doi:10.1016/j.desal.2013.08.014

Oguma, K., Mohseni, M., 2015. UV Treatment: A Solution for Small Community Water Supplies? IUVA News 17.

Oguma, K., Rattanakul, S., Bolton, J.R., 2015. Application of UV Light-Emitting Diodes to Adenovirus in Water. J. Environ. Eng. doi:10.1061/(ASCE)EE.1943-7870.0001061

Olsen, R., Hess-Erga, O., Larsen, A., Hoffmann, F., Thuestad, G., Hoell, I., 2016. Dual staining with CFDA-AM and SYTOX Blue in flow cytometry analysis of UV-irradiated Tetraselmis suecica to evaluate vitality. Aquat. Biol. 25, 39–52. doi:10.3354/ab00662

Olsen, R.O., Hess-Erga, O.-K., Larsen, A., Thuestad, G., Tobiesen, A., Hoell, I.A., 2015. Flow cytometric applicability to evaluate UV inactivation of phytoplankton in marine water samples. Mar. Pollut. Bull. 96, 279–285. doi:10.1016/j.marpolbul.2015.05.012

Olsen, R.O., Hoffmann, F., Hess-Erga, O.-K., Larsen, A., Thuestad, G., Hoell, I.A., 2016. Ultraviolet radiation as a ballast water treatment strategy: Inactivation of phytoplankton measured with flow cytometry. Mar. Pollut. Bull. 103, 270–275. doi:10.1016/j.marpolbul.2015.12.008

Oppenländer, T., 2007. Mercury-free sources of VUV/UV radiation: application of modern excimer lamps (excilamps) for water and air treatment. J. Environ. Eng. Sci. 6, 253–264. doi:10.1139/s06-059

Oppenlander, T., Sonsin, E., 2005. Mercury-free Vacuum-(VUV) and UV Excilamps: Lamps of the Future? IUVA News 7, 16–20.

Orlowska, M., Koutchma, T., Kostrzynska, M., Tang, J., 2015. Surrogate organisms for pathogenic O157:H7 and non-O157 Escherichia coli strains for apple juice treatments by UV-C light at three monochromatic wavelengths. Food Control 47, 647–655. doi:10.1016/J.FOODCONT.2014.08.004

Pagan, J., O, L., 2015. Coming Of Age UV-C LED Technology Update [WWW Document]. Water Online. URL http://www.wateronline.com/doc/coming-of-age-uv-c-led-technology-update-0001 (accessed 11.28.15).

Pang, Y., Huang, J., Xi, J., Hu, H., Zhu, Y., 2015. Effect of ultraviolet irradiation and chlorination on ampicillin-resistant Escherichia coli and its ampicillin resistance gene. Front. Environ. Sci. Eng. doi:10.1007/s11783-015-0779-9

Passantino, L., Malley, J.J., Knudson, M., Ward, R., Kim, J., 2004. Effect of Low Turbidity and Algae on UV Disinfection Performance (PDF). J. Am. Water Works Assoc. 96, 128–137.

Peccia, J., Hernandez, M., 2002. Rapid immunoassays for detection of UV-induced cyclobutane pyrimidine dimers in whole bacterial cells. Appl. Environ. Microbiol. 68, 2542–9. doi:10.1128/AEM.68.5.2542-2549.2002

Penru, Y., Guastalli, A.R., Esplugas, S., Baig, S., 2013. Disinfection of Seawater: Application of UV and Ozone. Ozone Sci. Eng. 35, 63–70. doi:10.1080/01919512.2012.722050

Pereira, V.J., Ricardo, J., Galinha, R., Benoliel, M.J., Barreto Crespo, M.T., 2013. Occurrence and low pressure ultraviolet inactivation of yeasts in real water sources. Photochem. Photobiol. Sci. 12, 626–30. doi:10.1039/c2pp25225b

Pinto, D., Santos, M.A., Chambel, L., 2015. Thirty years of viable but nonculturable state research: Unsolved molecular mechanisms. Crit. Rev. Microbiol. 41, 61–76. doi:10.3109/1040841X.2013.794127

Poepping, C., Beck, S.E., Wright, H., Linden, K.G., 2014. Evaluation of DNA damage reversal during medium-pressure UV disinfection. Water Res. 56, 181–9. doi:10.1016/j.watres.2014.02.043

Qian, S.S., Linden, K., Donnelly, M., 2005. A Bayesian analysis of mouse infectivity data to evaluate the effectiveness of using ultraviolet light as a drinking water disinfectant. Water Res. 39, 4229–39. doi:10.1016/j.watres.2005.08.017

Qiao, Z., Wigginton, K.R., 2016. Direct and Indirect Photochemical Reactions in Viral RNA Measured with RT-qPCR and Mass Spectrometry. Environ. Sci. Technol. 50, 13371–13379. doi:10.1021/acs.est.6b04281

Quek, P.H., Hu, J., 2008. Influence of photoreactivating light intensity and incubation temperature on photoreactivation of Escherichia coli following LP and MP UV disinfection. J. Appl. Microbiol. 105, 124–33. doi:10.1111/j.1365-2672.2008.03723.x

Ramamurthy, T., Ghosh, A., Pazhani, G.P., Shinoda, S., 2014. Current Perspectives on Viable but Non-Culturable (VBNC) Pathogenic Bacteria. Front. public Heal. 2, 103. doi:10.3389/fpubh.2014.00103

Ramsay, I.A., Niedziela, J.-C., Ogden, I.D., 2000. The Synergistic Effect of Excimer and Low-Pressure Mercury Lamps on the Disinfection of Flowing Water. J. Food Prot. 63, 1529–1533.

Rastogi, R.P., Richa, Kumar, A., Tyagi, M.B., Sinha, R.P., 2010. Molecular Mechanisms of Ultraviolet Radiation-Induced DNA Damage and Repair. J. Nucleic Acids 2010. doi:10.4061/2010/592980

Rattanakul, S., Oguma, K., 2018. Inactivation kinetics and efficiencies of UV-LEDs against Pseudomonas aeruginosa, Legionella pneumophila, and surrogate microorganisms. Water Res. 130, 31–37. doi:10.1016/J.WATRES.2017.11.047

Rattanakul, S., Oguma, K., 2017. Analysis of Hydroxyl Radicals and Inactivation Mechanisms of Bacteriophage MS2 in Response to a Simultaneous Application of UV and Chlorine. Environ. Sci. Technol. 51, 455–462. doi:10.1021/acs.est.6b03394

Reckhow, D.A., Linden, K.G., Kim, J., Shemer, H., Makdissy, G., 2010. Effect of UV Treatment on DBP Formation. J. Am. Water Works Assoc. 102, 100–113.

Rodriguez, R.A., Bounty, S., Beck, S.E., Chan, C., McGuire, C., Linden, K.G., 2014. Photoreactivation of bacteriophages after UV disinfection: role of genome structure and impacts of UV source. Water Res. 55, 143–9. doi:10.1016/j.watres.2014.01.065

Rodríguez, R.A., Bounty, S., Linden, K.G., 2013. Long-range quantitative PCR for determining inactivation of adenovirus 2 by ultraviolet light. J. Appl. Microbiol. 114, 1854–65. doi:10.1111/jam.12169

Romero-Martínez, L., Moreno-Andrés, J., Acevedo-Merino, A., Nebot, E., 2016. Evaluation of ultraviolet disinfection of microalgae by growth modeling: application to ballast water treatment. J. Appl. Phycol. 28. doi:10.1007/s10811-016-0838-z

Rosado-Lausell, S.L., Wang, H., Gutiérrez, L., Romero-Maraccini, O.C., Niu, X.-Z., Gin, K.Y.H., Croué, J.-P., Nguyen, T.H., 2013. Roles of singlet oxygen and triplet excited state of dissolved organic matter formed by different organic matters in bacteriophage MS2 inactivation. Water Res. 47, 4869–4879. doi:10.1016/J.WATRES.2013.05.018

Rule Wigginton, K., Menin, L., Montoya, J.P., Kohn, T., 2010. Oxidation of Virus Proteins during UV $_{254}$ and Singlet Oxygen Mediated Inactivation. Environ. Sci. Technol. 44, 5437–5443. doi:10.1021/es100435a

Ryu, H., Cashdollar, J.L., Fout, G.S., Schrantz, K.A., Hayes, S., 2015. Applicability of integrated cell culture quantitative PCR (ICC-qPCR) for the detection of infectious adenovirus type 2 in UV disinfection studies. J. Environ. Sci. Heal. Part A 50, 777–787. doi:10.1080/10934529.2015.1019795

Sancar, A., 1994. Structure and function of DNA photolyase. Biochemistry 33, 2–9. doi:10.1021/bi00167a001

Sangsanont, J., Katayama, H., Kurisu, F., Furumai, H., 2014. Capsid-Damaging Effects of UV Irradiation as Measured by Quantitative PCR Coupled with Ethidium Monoazide Treatment. Food Environ. Virol. 6, 269–275. doi:10.1007/s12560-014-9162-4

Schaefer, R., Grapperhaus, M., Schaefer, I., Linden, K., 2007. Pulsed UV lamp performance and comparison with UV mercury lamps. J. Environ. Eng. Sci. 6, 303–310. doi:10.1139/s06-068

Schalk, S., Adam, V., Arnold, E., Brieden, K., Voronov, A., Witzke, H.-D., 2006. UV-Lamps for Disinfection and Advanced Oxidation - Lamp Types, Technologies and Applications. IUVA News 8, 32–37.

Sharpless, C.M., Linden, K.G., 2001. UV Photolysis of Nitrate: Effects of Natural Organic Matter and Dissolved Inorganic Carbon and Implications for UV Water Disinfection. Environ. Sci. Technol. 35, 2949–2955. doi:10.1021/es002043l

Shatalov, M., Jain, R., Saxena, T., Dobrinsky, A., Shur, M., 2017. Development of Deep UV LEDs and Current Problems in Material and Device Technology, in: Semiconductors and Semimetals. pp. 45–83. doi:10.1016/bs.semsem.2016.08.002

Sherchan, S.P., Snyder, S.A., Gerba, C.P., Pepper, I.L., 2014. Inactivation of MS2 coliphage by UV and hydrogen peroxide: comparison by cultural and molecular methodologies. J. Environ. Sci. Health. A. Tox. Hazard. Subst. Environ. Eng. 49, 397–403. doi:10.1080/10934529.2014.854607

Shin, G.-A., Linden, K.G., Faubert, G., 2009. Inactivation of Giardia lamblia cysts by polychromatic UV. Lett. Appl. Microbiol. 48, 790–2. doi:10.1111/j.1472-765X.2009.02597.x

Shin, G.-A., Linden, K.G., Sobsey, M.D., 2015. Low pressure ultraviolet inactivation of pathogenic enteric viruses and bacteriophages. J. Environ. Eng. Sci.

Shin, G., Linden, K.G., Faubert, G., 2010. Reactivation of Giardia lamblia cysts after exposure to polychromatic UV light. Lett. Appl. Microbiol. 51, 395–9. doi:10.1111/j.1472-765X.2010.02908.x

Shin, G.A., Linden, K.G., Arrowood, M.J., Sobsey, M.D., 2001. Low-pressure UV inactivation and DNA repair potential of Cryptosporidium parvum oocysts. Appl. Environ. Microbiol. 67, 3029–32. doi:10.1128/AEM.67.7.3029-3032.2001

Sholtes, K.A., Lowe, K., Walters, G.W., Sobsey, M.D., Linden, K.G., Casanova, L.M., 2016. Comparison of Ultraviolet Light Emitting Diodes and Low-Pressure Mercury-Arc Lamps for Disinfection of Water. Environ. Technol. 1–23. doi:10.1080/09593330.2016.1144798

Sigstam, T., Gannon, G., Cascella, M., Pecson, B.M., Wigginton, K.R., Kohn, T., 2013. Subtle differences in virus composition affect disinfection kinetics and mechanisms. Appl. Environ. Microbiol. 79, 3455–67. doi:10.1128/AEM.00663-13

Simonelli, P., Troedsson, C., Nejstgaard, J.C., Zech, K., Larsen, J.B., Frischer, M.E., 2009. Evaluation of DNA extraction and handling procedures for PCR-based copepod feeding studies. J. Plankton Res. 31, 1465–1474. doi:10.1093/plankt/fbp087

Simonet, J., Gantzer, C., 2006. Inactivation of poliovirus 1 and F-specific RNA phages and degradation of their genomes by UV irradiation at 254 nanometers. Appl. Environ. Microbiol. 72, 7671–7. doi:10.1128/AEM.01106-06

Sinha, R.P., Dautz, M., Häder, D.-P., 2001. A Simple and Efficient Method for the Quantitative Analysis of Thymine Dimers in Cyanobacteria, Phytoplankton and Macroalgae. Acta Protozool 40, 187–195.

Sinha, R.P., Häder, D.-P.D.-P.P., 2002. UV-induced DNA damage and repair: a review. Photochem. Photobiol. Sci. 1, 225–236. doi:10.1039/b201230h

Sökmen, M., Değerli, S., Aslan, A., 2008. Photocatalytic disinfection of Giardia intestinalis and Acanthamoeba castellani cysts in water. Exp. Parasitol. 119, 44–8. doi:10.1016/j.exppara.2007.12.014

Song, K., Mohseni, M., Taghipour, F., 2016. Application of ultraviolet light-emitting diodes (UV-LEDs) for water disinfection: A review. Water Res. doi:10.1016/j.watres.2016.03.003

Song, K., Taghipour, F., Mohseni, M., 2018. Microorganisms inactivation by continuous and pulsed irradiation of ultraviolet light-emitting diodes (UV-LEDs). Chem. Eng. J. 343, 362–370. doi:10.1016/J.CEJ.2018.03.020

Sosnin, E.A., Avdeev, S.M., Tarasenko, V.F., Skakun, V.S., Schitz, D. V., 2015. KrCl barrier-discharge excilamps: Energy characteristics and applications (Review). Instruments Exp. Tech. 58, 309–318. doi:10.1134/S0020441215030124

Sosnin, E.A., Oppenländer, T., Tarasenko, V.F., 2006. Applications of capacitive and barrier discharge excilamps in photoscience. J. Photochem. Photobiol. C Photochem. Rev. 7, 145–163. doi:10.1016/j.jphotochemrev.2006.12.002

Stehouwer, P.P., Buma, A., Peperzak, L., 2015. A comparison of six different ballast water treatment systems based on UV radiation, electrochlorination and chlorine dioxide. Environ. Technol. 36. doi:10.1080/09593330.2015.1021858

Steinberg, M.K., First, M.R., Lemieux, E.J., Drake, L.A., Nelson, B.N., Kulis, D.M., Anderson, D.M., Welschmeyer, N.A., Herring, P.R., 2012. Comparison of techniques used to count single-celled viable phytoplankton. J. Appl. Phycol. 24, 751–758. doi:10.1007/s10811-011-9694-z

Steinberg, M.K., Lemieux, E.J., Drake, L.A., 2011. Determining the viability of marine protists using a combination of vital, fluorescent stains. Mar. Biol. 158, 1431–1437. doi:10.1007/s00227-011-1640-8

Stephanie, K., Ursula, O., Thomas, S., 2011. Immunological detection of UV induced cyclobutane pyrimidine dimers and (6–4) photoproducts in DNA from reference bacteria and natural aquatic populations. J. Microbiol. Methods 84, 435–441. doi:10.1016/J.MIMET.2011.01.004

Summers, R.S., Hooper, S.M., Shukairy, H.M., Solarik, G., Owen, D., 1996. Assessing DBP Yield: Uniform Formation Conditions. J. Am. Water Works Assoc. 88, 80–93.

Szabla, R., Kruse, H., Stadlbauer, P., Šponer, J., Sobolewski, A.L., 2018. Sequential electron transfer governs the UV-induced self-repair of DNA photolesions. Chem. Sci. 9, 3131–3140. doi:10.1039/C8SC00024G

Taghipour, F., 2018. UV LED Technology: The Times They are A-Changin'. IUVA News 20.

Tanaka, T., Nogariya, O., Shionoiri, N., Maeda, Y., Arakaki, A., 2018. Integrated molecular analysis of the inactivation of a non-enveloped virus, feline calicivirus, by UV-C radiation. J. Biosci. Bioeng. doi:10.1016/j.jbiosc.2018.01.018

Tao, Y., Zhang, X., Au, D.W.T., Mao, X., Yuan, K., 2010. The effects of sub-lethal UV-C irradiation on growth and cell integrity of cyanobacteria and green algae. Chemosphere 78, 541–547. doi:10.1016/j.chemosphere.2009.11.016

Templeton, M.R., Andrews, R.C., Hofmann, R., 2006. Impact of iron particles in groundwater on the UV inactivation of bacteriophages MS2 and T4. J. Appl. Microbiol. 101, 732–41. doi:10.1111/j.1365-2672.2006.02980.x

Torizawa, T., Yamamoto, N., Suzuki, T., Nobuoka, K., Komatsu, Y., Morioka, H., Nikaido, O., Ohtsuka, E., Kato, K., Shimada, I., 2000. DNA binding mode of the Fab fragment of a monoclonal antibody specific for cyclobutane pyrimidine dimer. Nucleic Acids Res. 28, 944–951. doi:10.1093/nar/28.4.944

Tran, T., Racz, L., Grimaila, M.R., Miller, M., Harper, W.F., 2014. Comparison of continuous versus pulsed ultraviolet light emitting diode use for the inactivation of Bacillus globigii spores. Water Sci. Technol. 70, 1473. doi:10.2166/wst.2014.395

Tretyakova, N.Y., Groehler, A., Ji, S., Ji, S., 2015. DNA-Protein Cross-Links: Formation, Structural Identities, and Biological Outcomes. Acc. Chem. Res. 48, 1631–44. doi:10.1021/acs.accounts.5b00056

Ule, J., Jensen, K., Mele, A., Darnell, R.B., 2005. CLIP: A method for identifying protein–RNA interaction sites in living cells. Methods 37, 376–386. doi:10.1016/J.YMETH.2005.07.018

US EPA, 2017. Draft: Innovative Approaches for Validation of Ultraviolet Disinfection Reactors for Drinking Water Systems.

US EPA, 2009. National Primary Drinking Water Regulations.

US EPA, 2006a. Ultraviolet Disinfection Guidance Manual for the Final Long Term 2 Enhanced Surface Water Treatment Rule.

US EPA, 2006b. Long Term 2 Enhanced Surface Water Treatment Rule. US.

US EPA, 2006c. Ground Water Rule. US.

US EPA, 1999. Microbial and Disinfection Byproduct Rules Simultaneous Compliance Guidance Manual.

USCG, 2012. Standards for Living Organisms in Ships' Ballast Water Discharged in U.S. Waters; Final Rule. Federal Register, US.

USEPA, 2001. Male-specific (F+) and Somatic Coliphage in Water by Single Agar Layer (SAL) Procedure.

van Slooten, C., Wijers, T., Buma, A.G.J., Peperzak, L., 2015. Development and testing of a rapid, sensitive ATP assay to detect living organisms in ballast water. J. Appl. Phycol. 27, 2299–2312. doi:10.1007/s10811-014-0518-9

Vazquez-Bravo, B., Gonçalves, K., Shisler, J.L., Mariñas, B.J., 2018. Adenovirus Replication Cycle Disruption from Exposure to Polychromatic Ultraviolet Irradiation. Environ. Sci. Technol. 52, 3652–3659. doi:10.1021/acs.est.7b06082

Wang, D., Oppenländer, T., El-Din, M.G., Bolton, J.R., 2010. Comparison of the disinfection effects of vacuum-UV (VUV) and UV light on Bacillus subtilis spores in aqueous suspensions at 172, 222 and 254 nm. Photochem. Photobiol. 86, 176–81. doi:10.1111/j.1751-1097.2009.00640.x

Weber, S., 2005. Light-driven enzymatic catalysis of DNA repair: a review of recent biophysical studies on photolyase. Biochim. Biophys. Acta - Bioenerg. 1707, 1–23. doi:10.1016/j.bbabio.2004.02.010

Welsh, J., Cantor, C.R., 1984. Protein—DNA cross-linking. Trends Biochem. Sci. 9, 505–508. doi:10.1016/0968-0004(84)90271-8

Wengraitis, S., McCubbin, P., Wade, M.M., Biggs, T.D., Hall, S., Williams, L.I., Zulich, A.W., 2013. Pulsed UV-C disinfection of Escherichia coli with light-emitting diodes, emitted at various repetition rates and duty cycles. Photochem. Photobiol. 89, 127–31. doi:10.1111/j.1751-1097.2012.01203.x

Wigginton, K.R., Kohn, T., 2012. Virus disinfection mechanisms: the role of virus composition, structure, and function. Curr. Opin. Virol. 2, 84–89. doi:10.1016/J.COVIRO.2011.11.003

Wigginton, K.R., Menin, L., Sigstam, T., Gannon, G., Cascella, M., Hamidane, H. Ben, Tsybin, Y.O., Waridel, P., Kohn, T., 2012a. UV Radiation Induces Genome-Mediated, Site-Specific Cleavage in Viral Proteins. ChemBioChem 13, 837–845. doi:10.1002/cbic.201100601

Wigginton, K.R., Pecson, B.M., Sigstam, T., Bosshard, F., Kohn, T., 2012b. Virus Inactivation Mechanisms: Impact of Disinfectants on Virus Function and Structural Integrity. Environ. Sci. Technol. 46, 12069–12078. doi:10.1021/es3029473

Willert, C., Stasicki, B., Klinner, J., Moessner, S., 2010. Pulsed operation of high-power light emitting diodes for imaging flow velocimetry. Meas. Sci. Technol. 21, 075402. doi:10.1088/0957-0233/21/7/075402

WRF, 2015. WRF 4376: Guidance for Implementing Action Spectra Correction with Medium Pressure UV Disinfection.

Wright, D.A., Welschmeyer, N.A., Peperzak, L., 2015. Alternative, indirect measures of ballast water treatment efficacy during a shipboard trial: a case study. J. Mar. Eng. Technol. 14, 1–8. doi:10.1080/20464177.2015.1022379

Wright, H., Heath, M., Bandy, J., 2011. Yikes! What the UVDGM Does Not Address on UV Disinfection. IUVA News 17, 12–18.

Würtele, M.A., Kolbe, T., Lipsz, M., Külberg, A., Weyers, M., Kneissl, M., Jekel, M., 2011. Application of GaN-based ultraviolet-C light emitting diodes--UV LEDs--for water disinfection. Water Res. 45, 1481–9. doi:10.1016/j.watres.2010.11.015

Yates, M. V., Malley, J., Rochelle, P., Hoffman, R., 2006. Effect of Adenovirus Resistance on UV Disinfection Requirements: A Report on the State of Adenovirus Science. J. Am. Water Works Assoc. 98, 93–106.

Young, P.C., Lawryshyn, Y.A., 2017. A computational fluid dynamics analysis of placing UV reactors in series. Water Qual. Res. J. 52, 79–89. doi:10.2166/wqrj.2017.023

Zhang, J.-Y., Boyd, I.W., 2000. Lifetime investigation of excimer UV sources. Appl. Surf. Sci. 168, 296–299. doi:10.1016/S0169-4332(00)00628-0

Zyara, A., Heinonen-Tanski, H., Veijalainen, A.-M., Torvinen, E., 2017. UV-LEDs Efficiently Inactivate DNA and RNA Coliphages. Water 9, 46. doi:10.3390/w9010046

Appendix A

This appendix contains supplementary information for Chapter 2.

There is no supplementary information for Chapter 2.

Appendix B

This appendix contains supplementary information for Chapter 3.

There is no supplementary information for Chapter 3.

Appendix C

This appendix contains supplementary information for Chapter 4.

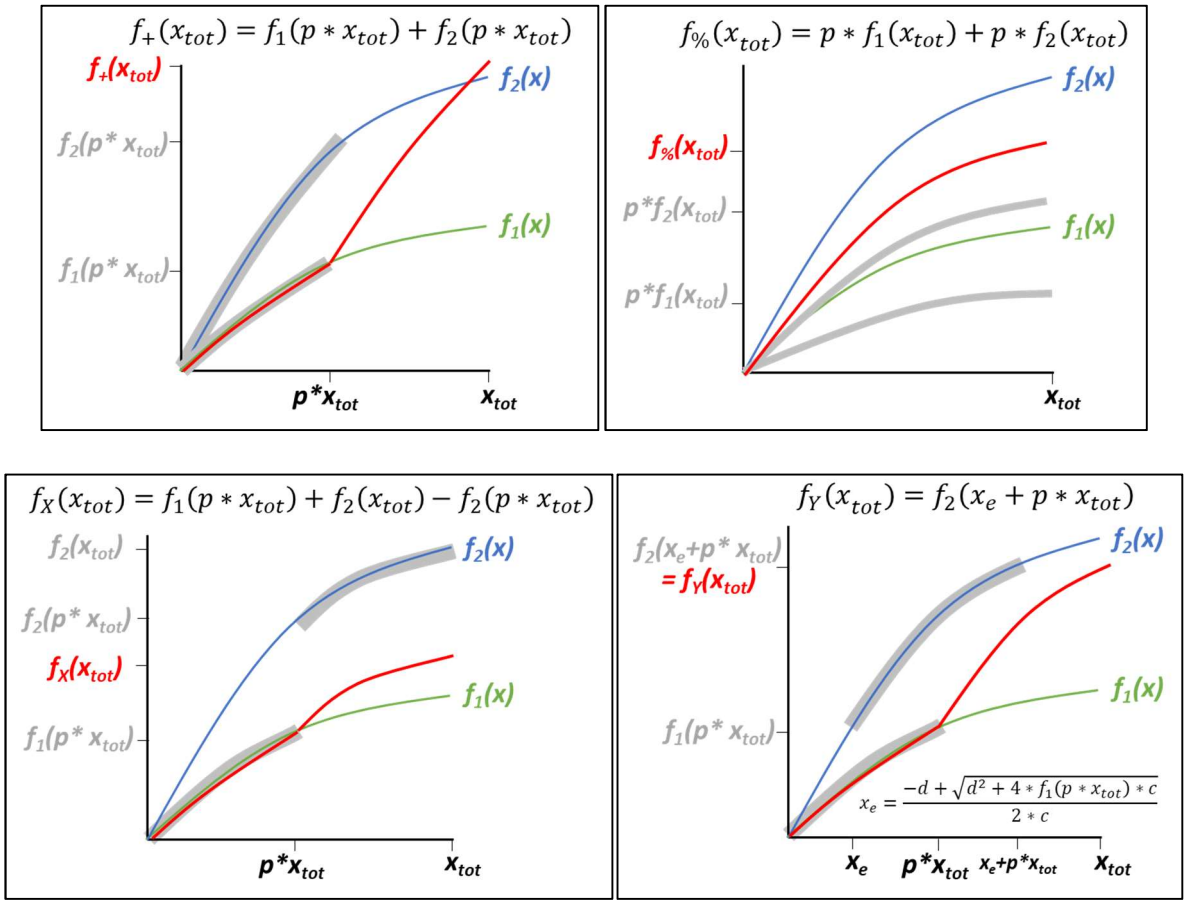

Figure 26 Diagrams for model prediction calculations (f_+, $f_{\%}$, f_X, and f_Y) indicating grey shaded regions of individual UV source dose responses $f_1(x) = ax + bx^2$ and $f_2(x) = cx + dx^2$ summed to predict MS2 $\log_{10}$ reduction for a given x_{tot} = total UV dose in sequential exposures where the proportion of the total dose contributed by each source was half ($p = 50\%$) and order of exposure was UV source 1 followed by UV source 2.

Table 3 MS2 log_{10} reduction model coefficients (for models where $y = a*x + b*x^2$) and their standard error for individual UV dose responses, where y = MS2 log_{10} reduction and x = UV Dose (mJ/cm^2).

	Model coefficient and standard error	
UV Source	a	b
255 nm LED	8.78E-02 ± 4.78E-03	-4.31E-04 ± 9.67E-05
265 nm LED	7.89E-02 ± 4.24E-03	-3.71E-04 ± 8.48E-05
285 nm LED	4.61E-02 ± 2.30E-03	-1.47E-04 ± 2.86E-05
KrCl Excilamp	1.62E-01 ± 1.02E-02	-1.11E-03 ± 2.49E-04
LP Lamp	6.50E-02 ± 1.44E-03	-2.27E-04 ± 1.85E-05

Table 4 MS2 log_{10} reduction model coefficients (for models where $y = a*x + b*x^2$) and their standard error for sequential UV dose responses, where y = MS2 log_{10} reduction and x = UV Dose (mJ/cm^2).

	Model coefficient and standard error	
UV Sources	a	b
LK	1.00E-01 ± 9.63E-03	-7.72E-05 ± 2.37E-04
KL	1.07E-01 ± 9.02E-03	-2.77E-04 ± 2.22E-04
5L	7.14E-02 ± 2.76E-03	-2.63E-04 ± 6.79E-05
L5	9.04E-02 ± 6.53E-03	-5.26E-04 ± 1.55E-04
6L	6.21E-02 ± 4.05E-03	-1.34E-04 ± 9.60E-05
L6	8.15E-02 ± 8.17E-03	-3.73E-04 ± 1.94E-04
8L	4.40E-02 ± 3.70E-03	-3.52E-05 ± 8.76E-05
L8	7.40E-02 ± 8.77E-03	-4.78E-04 ± 2.08E-04
5K	9.99E-02 ± 4.75E-03	-3.37E-04 ± 1.15E-04
K5	1.18E-01 ± 1.27E-02	-5.27E-04 ± 3.00E-04
6K	9.81E-02 ± 3.67E-03	-3.24E-04 ± 8.69E-05
K6	1.19E-01 ± 8.04E-03	-5.52E-04 ± 1.90E-04
8K	7.20E-02 ± 5.67E-03	4.22E-05 ± 1.35E-04
K8	9.50E-02 ± 1.17E-02	-6.72E-05 ± 2.77E-04

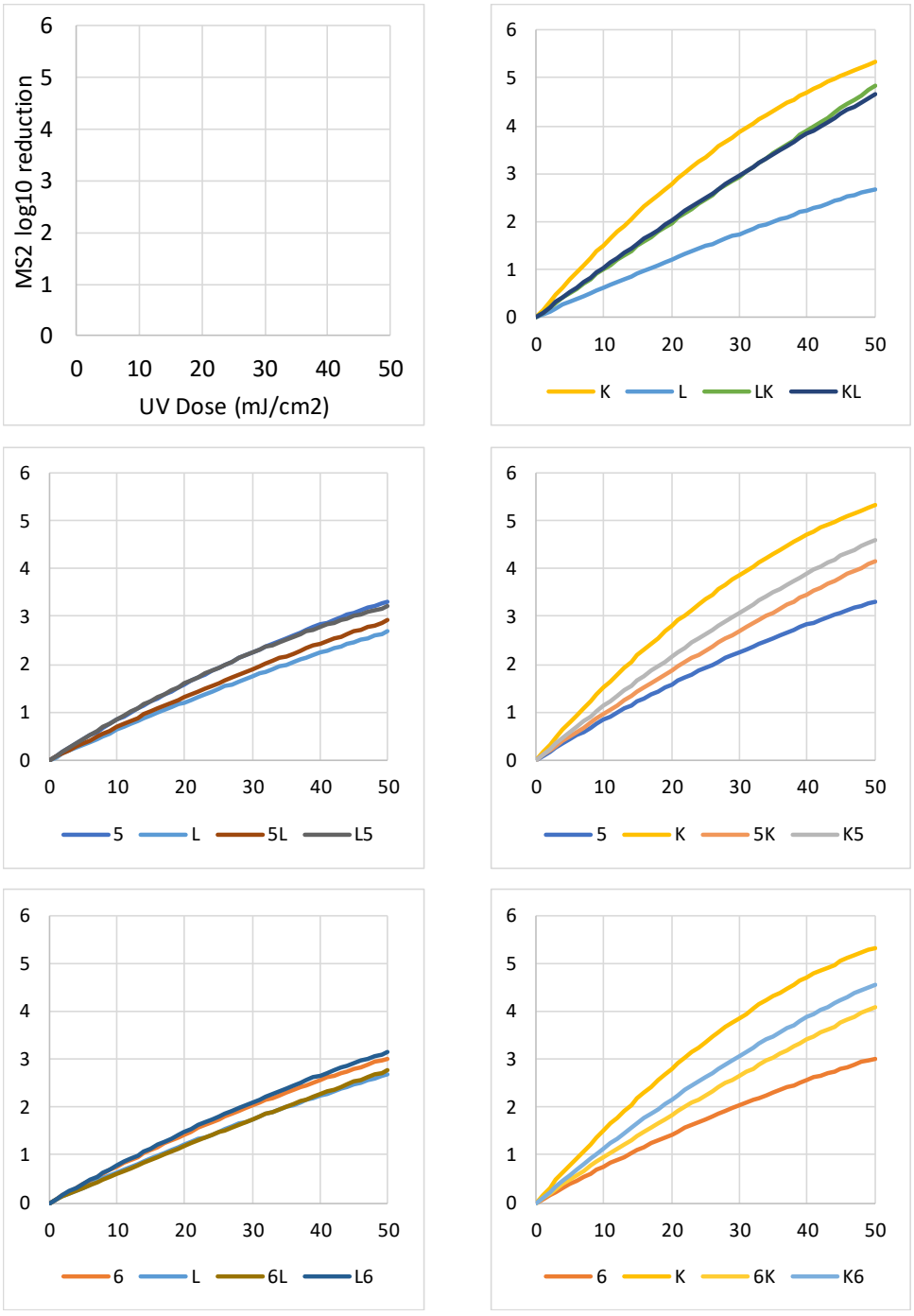

Figure 27 Plots of modeled of MS2 $\log_{10}$ reduction (Appendix C Table 3 and Table 4) for single and sequential UV exposures using the excimer lamp (K), LP lamp (L), 255 nm LED (5), 265 nm LED (6), and 285 nm LED (8). For example, 5K means the sample was exposed first to half the UV Dose from the 255 nm LED and then to half the UV Dose from the excimer lamp, and K5 indicates the exposure order was reversed. The x axis represents the total UV Dose (Fluence), where half was contributed by each source.

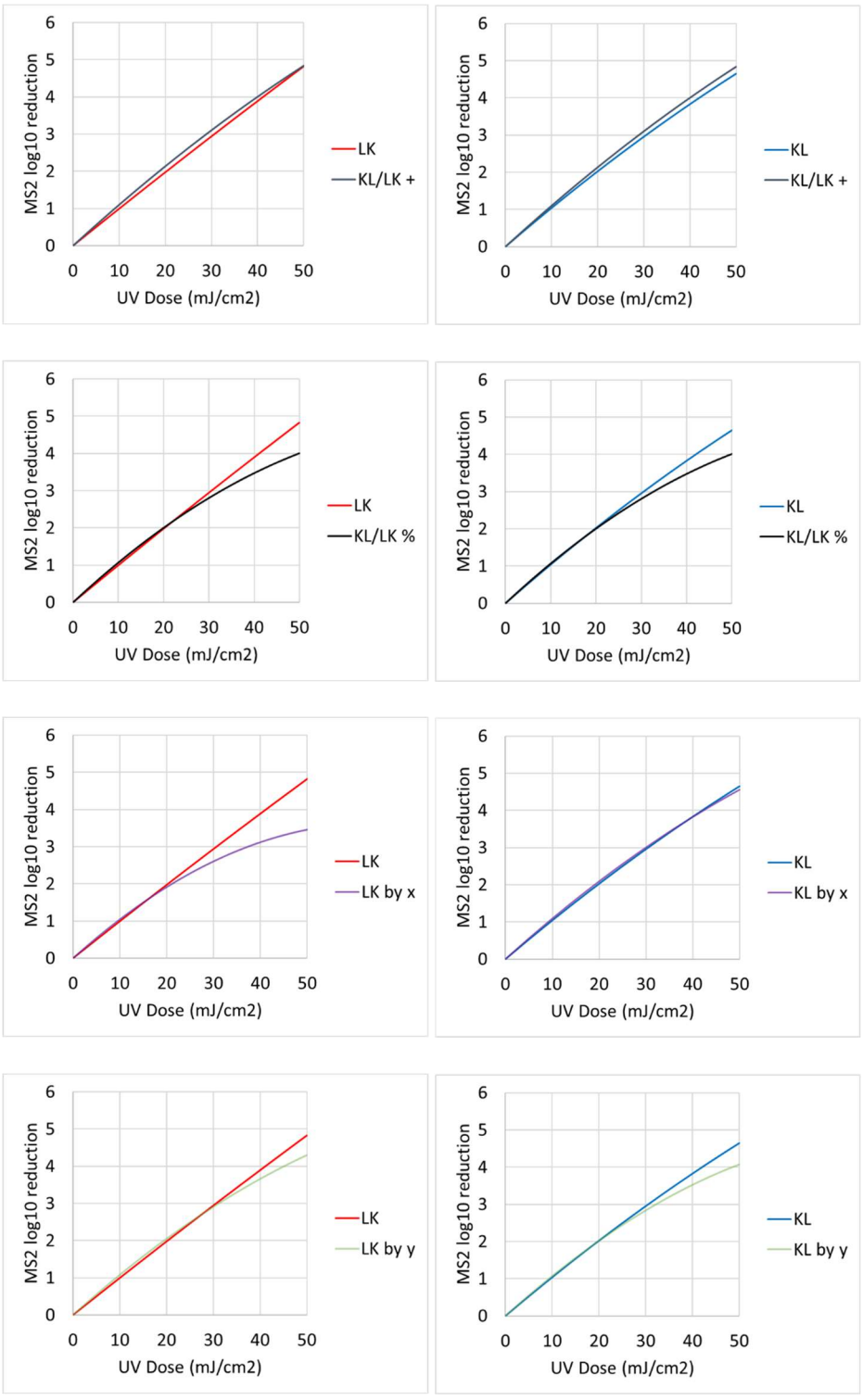

Figure 28 Modeled and predicted (by f_+, $f_\%$, f_X, and f_Y) MS2 log$_{10}$ reduction zero-intercept second order polynomial for sequential UV exposures using the excimer (K) and LP (L) lamps. The x axis represents the total UV Dose (Fluence), where half was contributed by each source.

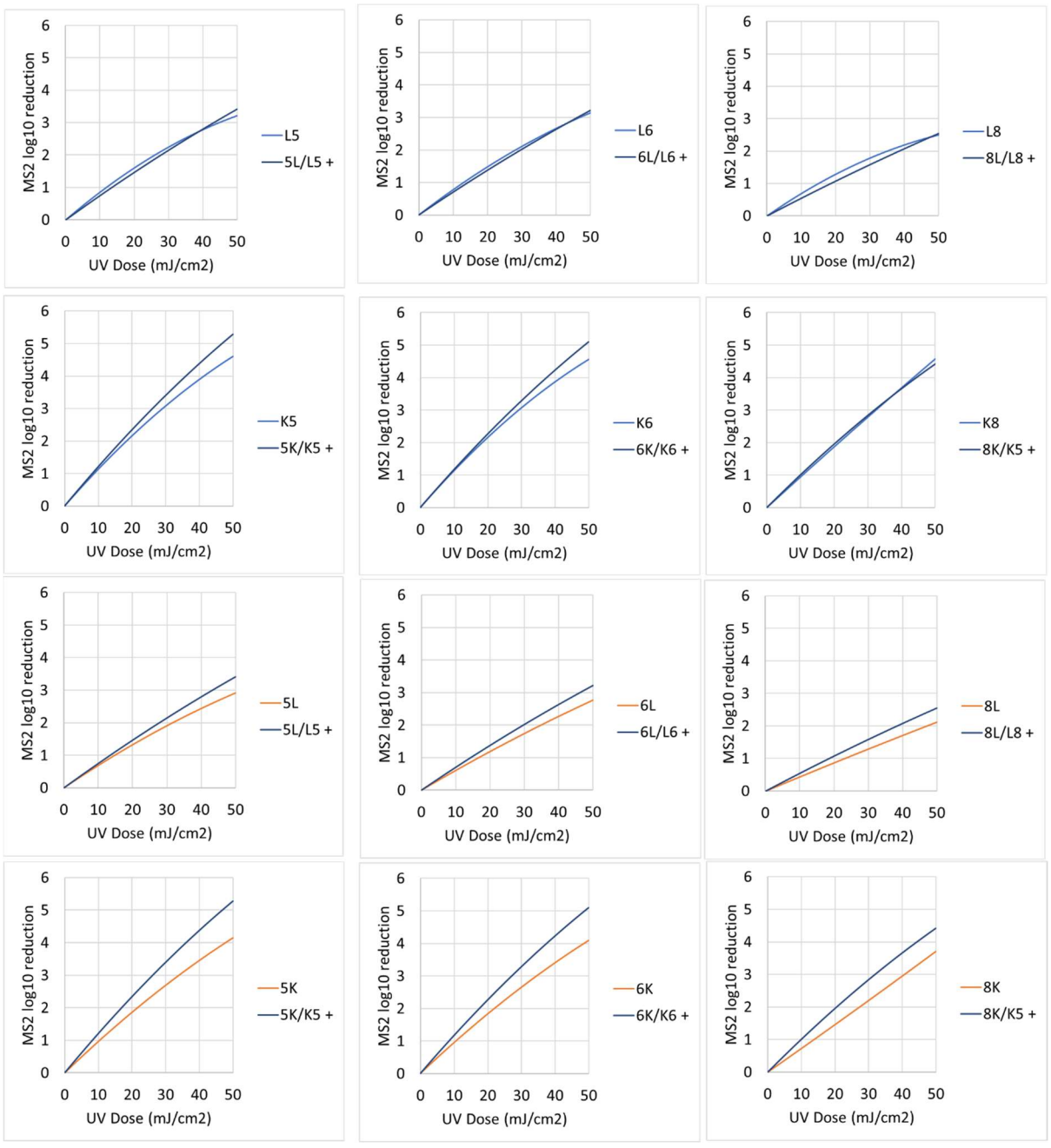

Figure 29 Modeled and predicted (by f_+) MS2 $\log_{10}$ reduction zero-intercept second order polynomial for sequential UV exposures using the excimer (K) and LP (L) lamps combined with the 255 (5), 265 (6), and 285 (8) nm LEDs. The x axis represents the total UV Dose (Fluence), where half was contributed by each source.

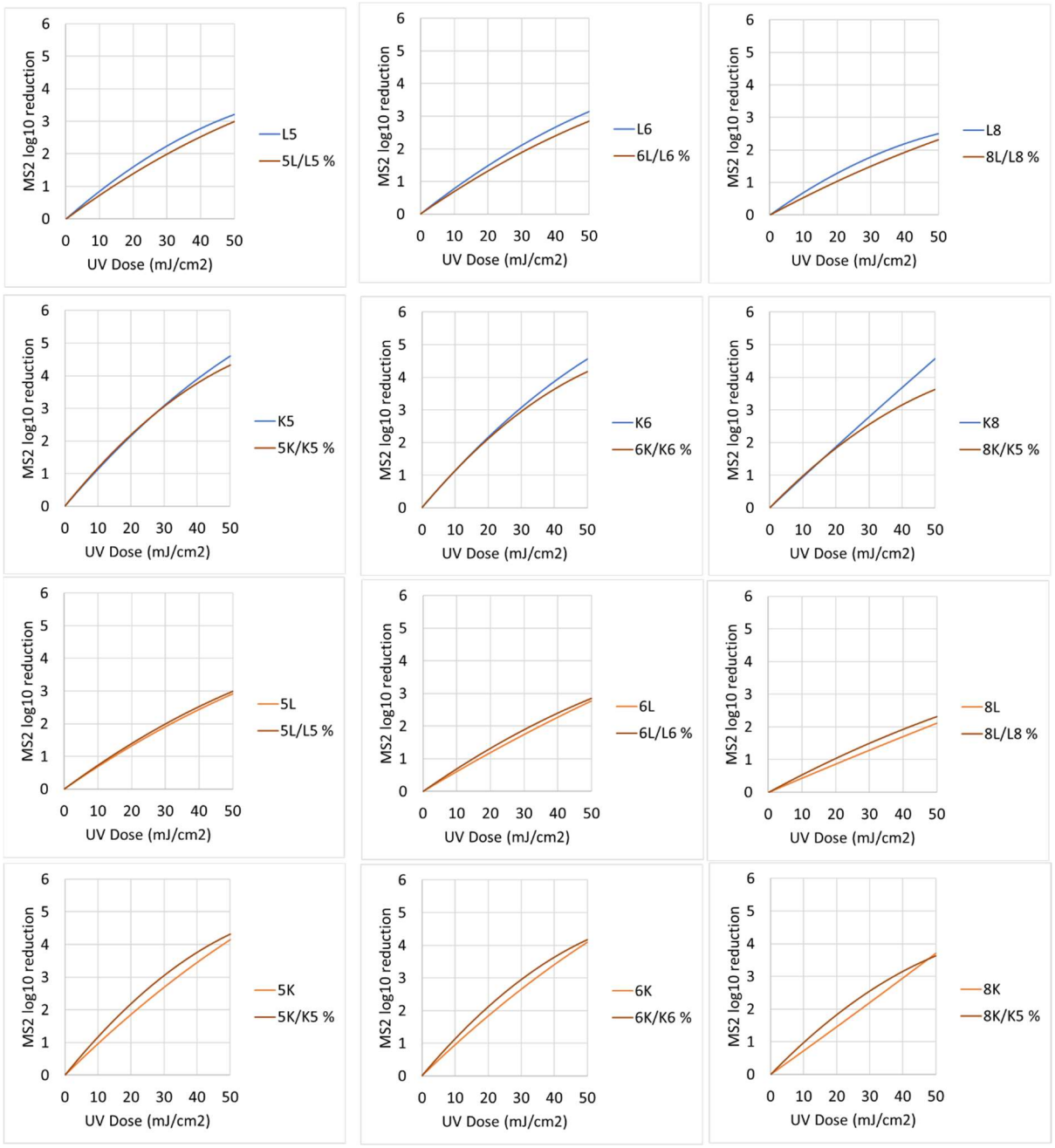

Figure 30 Modeled and predicted (by $f_{\%}$) MS2 $\log_{10}$ reduction zero-intercept second order polynomial for sequential UV exposures using the excimer (K) and LP (L) lamps combined with the 255 (5), 265 (6), and 285 (8) nm LEDs. The x axis represents the total UV Dose (Fluence), where half was contributed by each source.

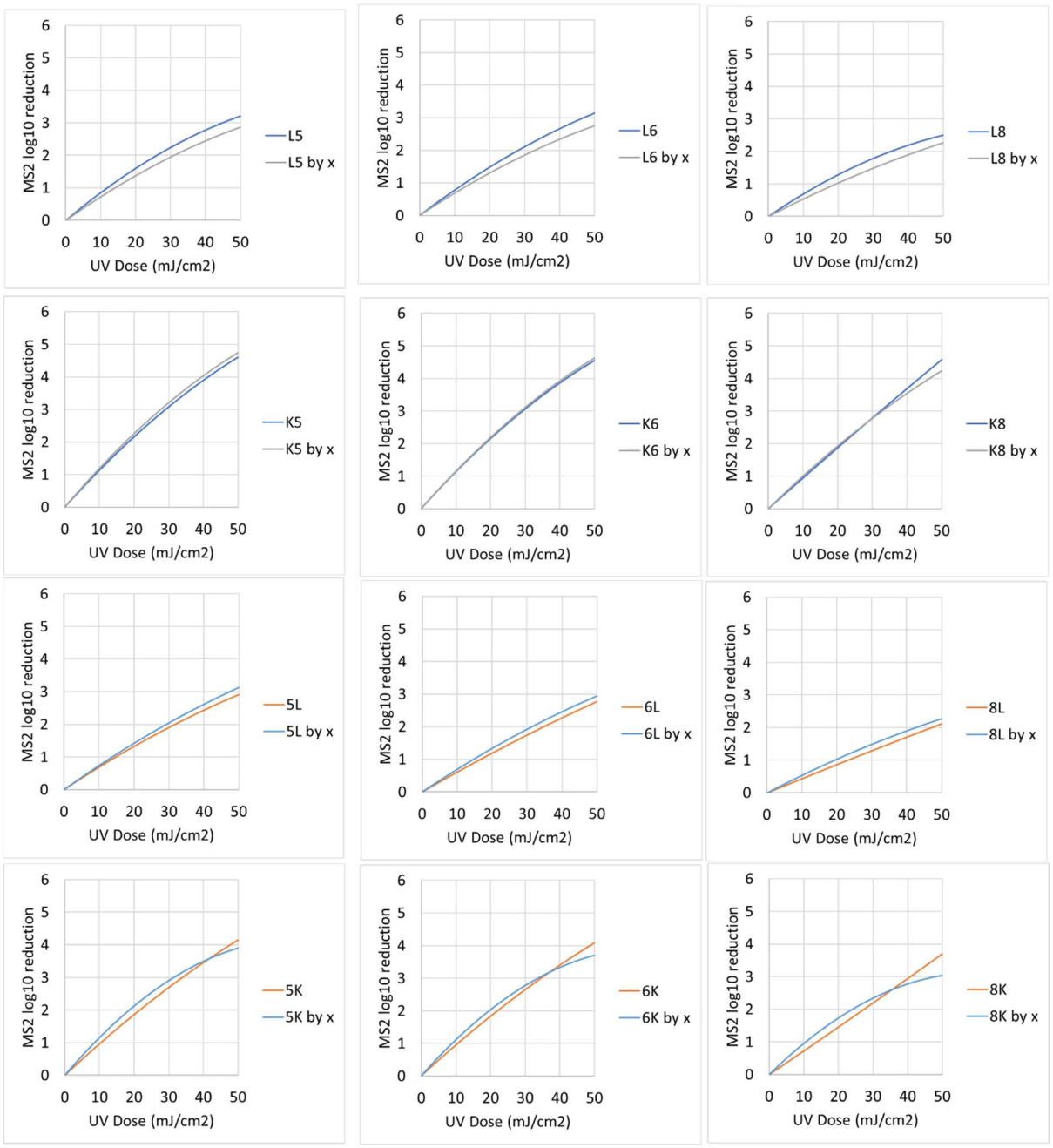

Figure 31 Modeled and predicted (by f_X) MS2 $\log_{10}$ reduction zero-intercept second order polynomial for sequential UV exposures using the excimer (K) and LP (L) lamps combined with the 255 (5), 265 (6), and 285 (8) nm LEDs. The x axis represents the total UV Dose (Fluence), where half was contributed by each source.

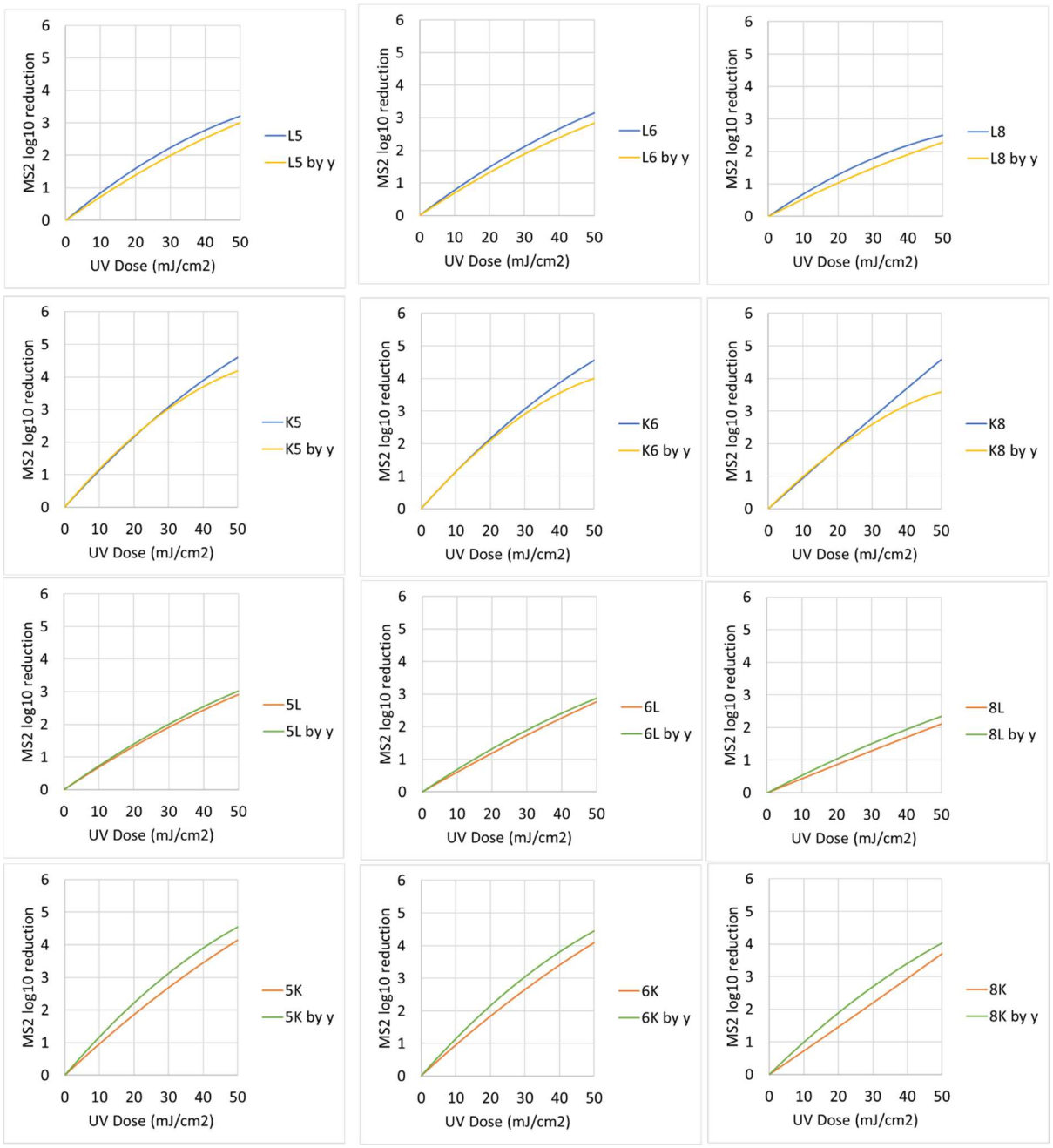

Figure 32 Modeled and predicted (by f_Y) MS2 $\log_{10}$ reduction zero-intercept second order polynomial for sequential UV exposures using the excimer (K) and LP (L) lamps combined with the 255 (5), 265 (6), and 285 (8) nm LEDs. The x axis represents the total UV Dose (Fluence), where half was contributed by each source.

Table 5 Average residuals for sequential exposure dose responses comparing modeled (zero intercept second order polynomial fitted to measured values) versus predicted (f_+, $f_\%$, f_X, and f_Y calculated using individual UV Source dose response models).

UV Sources	f_+	$f_\%$	f_X	f_Y
LK	0.11	-0.17	-0.36	-0.07
KL	0.12	-0.16	0.02	-0.13
L5	-0.05	-0.18	-0.23	-0.18
L6	-0.05	-0.18	-0.21	-0.18
L8	-0.14	-0.22	-0.23	-0.23
K5	0.28	-0.04	0.10	-0.07
K6	0.19	-0.12	0.03	-0.16
K8	0.02	-0.24	-0.04	-0.23
5L	0.21	0.07	0.11	0.08
6L	0.23	0.11	0.14	0.12
8L	0.24	0.16	0.14	0.17
5K	0.58	0.26	0.12	0.34
6K	0.52	0.21	0.05	0.30
8K	0.50	0.24	0.04	0.37

Table 6 Slope for sequential exposure dose responses comparing modeled (zero intercept second order polynomial fitted to measured values) versus predicted (f_+, $f_{\%}$, f_X, and f_Y calculated using individual UV Source dose response models).

UV Sources	f_+	$f_{\%}$	f_X	f_Y
LK	1.0343	0.9051	0.8199	0.9496
KL	1.0466	0.9167	1.0024	0.9298
L5	0.9918	0.9057	0.8790	0.9080
L6	0.9815	0.8989	0.8791	0.8963
L8	0.9251	0.9637	0.8505	0.8555
K5	1.1197	0.9742	1.0382	0.9583
K6	1.0845	0.9442	1.0141	0.9255
K8	0.9971	0.8690	0.9672	0.8723
5L	1.1413	1.0413	1.0723	1.0485
6L	1.1631	1.0644	1.0887	1.0732
8L	1.2188	1.1362	1.1184	1.1487
5K	1.2648	1.0997	1.0272	1.1396
6K	1.2389	1.0778	0.9976	1.1250
8K	1.2516	1.0902	0.9666	1.1725

Table 7 R^2 for sequential exposure dose responses comparing modeled (zero intercept second order polynomial fitted to measured values) versus predicted (f_+, $f_{\%}$, f_X, and f_Y calculated using individual UV Source dose response models).

UV Sources	f_+	$f_{\%}$	f_X	f_Y
LK	0.9975	0.9769	0.9488	0.9887
KL	0.9999	0.9903	0.9987	0.9915
L5	0.9897	0.9977	0.9992	0.9976
L6	0.9958	0.9998	1.0000	0.9999
L8	0.9825	0.9911	0.9927	0.9923
K5	0.9986	0.9968	0.9999	0.9942
K6	0.9981	0.9975	1.0000	0.9944
K8	0.9971	0.9776	0.9947	0.9736
5L	0.9985	0.9997	1.0000	0.9998
6L	1.0000	0.9972	0.9985	0.9978
8L	0.9996	0.9963	0.9949	0.9971
5K	0.9999	0.9922	0.9791	0.9964
6K	1.0000	0.9920	0.9765	0.9969
8K	0.9936	0.9686	0.9199	0.9851

Table 8 Water Factors (WF) and wall plug efficiencies (C) used to calculate electrical energy per order (E_{EN}) required for a given (N) MS2 log_{10} reduction for individual UV sources.

	255	265	285	KrCl	LP
WF min	0.9839	0.9850	0.9884	0.9083	0.9828
WF max	0.9907	0.9914	0.9937	0.9894	0.9983
C min	0.5%	0.5%	0.5%	5.0%	30.0%
C max	10.0%	10.0%	10.0%	15.0%	38.0%
References	(Beck et al., 2017b; Ibrahim et al., 2013; Matafonova and Batoev, 2012; Song et al., 2016)	(Beck et al., 2017b; Ibrahim et al., 2013; Matafonova and Batoev, 2012; Song et al., 2016)	(Beck et al., 2017b; Ibrahim et al., 2013; Matafonova and Batoev, 2012; Song et al., 2016)	(Lomaev et al., 2016, 2012; Matafonova and Batoev, 2012; Oppenlander and Sonsin, 2005; Schalk et al., 2006; Sosnin et al., 2015)	(Beck et al., 2017b; Schaefer et al., 2007; Schalk et al., 2006)

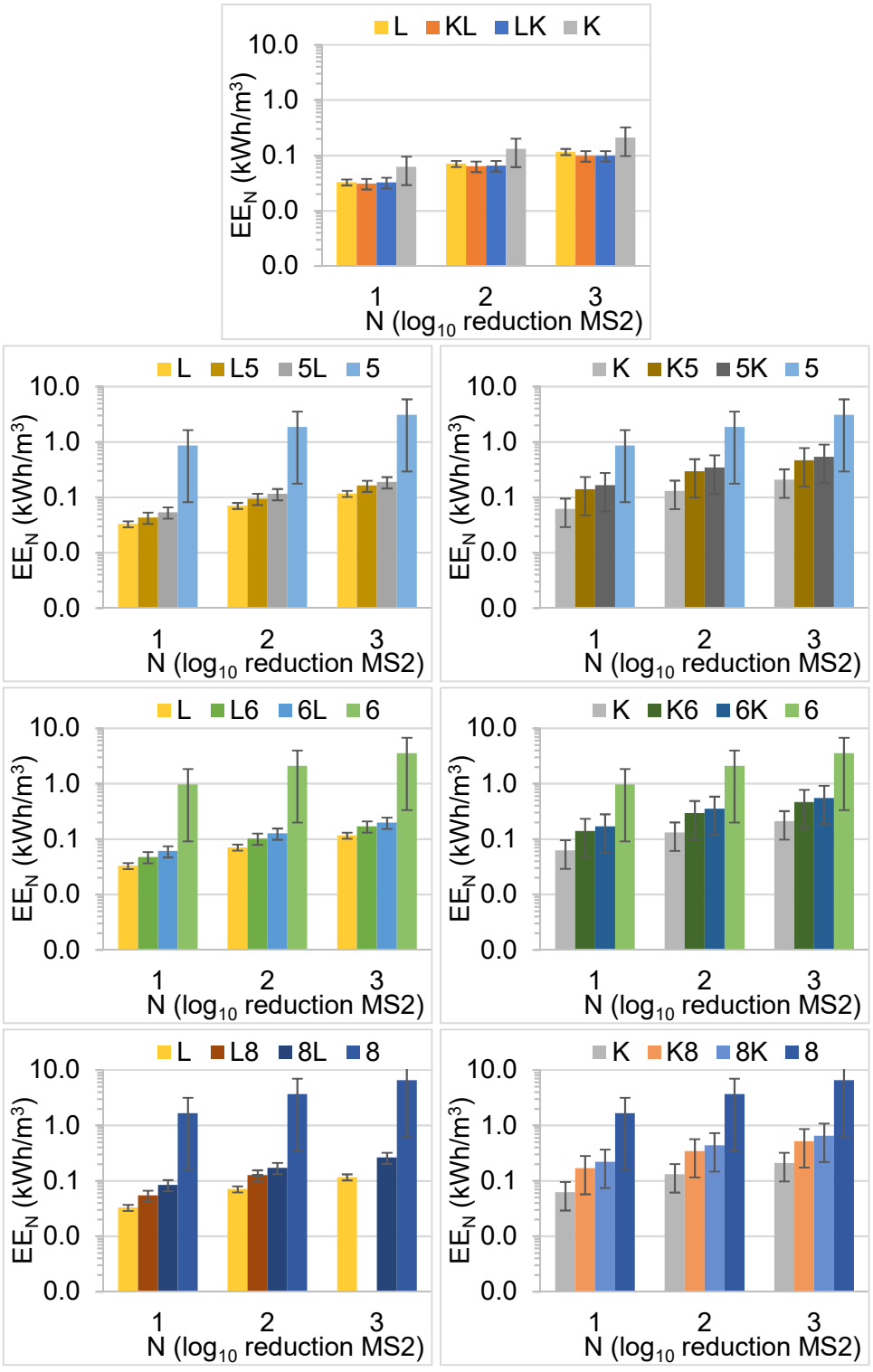

Figure 33 Electrical energy per order (E_{EN}) for single and sequential exposures for each pairwise combination of UV sources.

Appendix D

This Appendix contains supplementary information for Chapter 5.

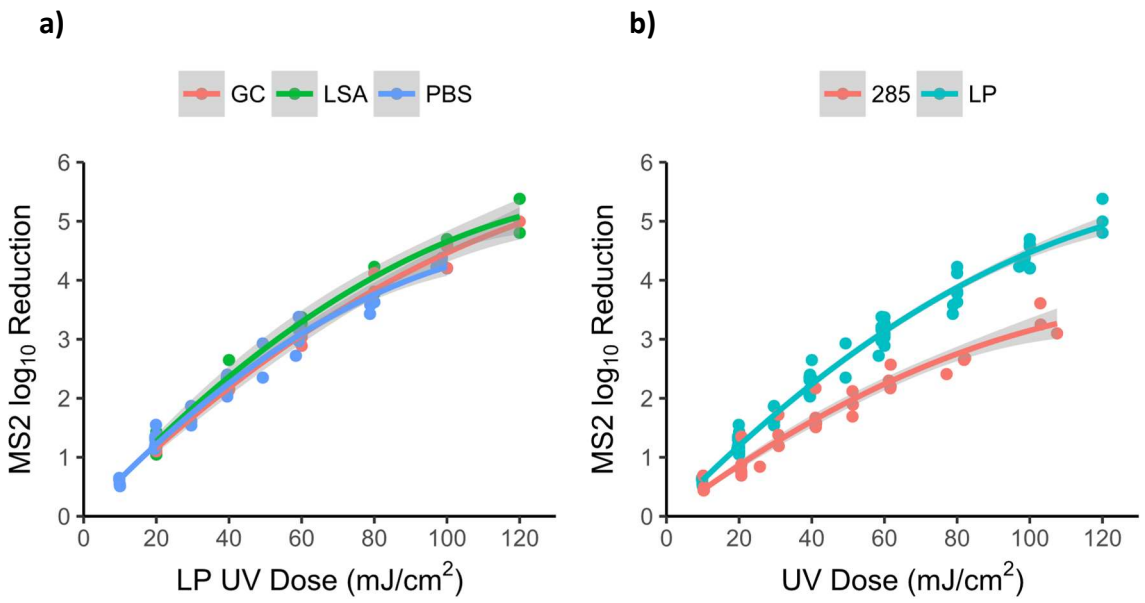

Figure 34 (a) Log_{10} reduction (inactivation) dose responses for MS2 exposed to LP UV in collimated beam studies where water matrices were 1X PBS, dechlorinated tap water treated by granular carbon (GC), or dechlorinated tap water supplemented with UV absorber lignin sulfonate (LSA). PBS data are from Chapter 4 and GC/LSA data were shared by Kaitlyn Mattos. (b) Dose response curves used to calculate MS2 reduction equivalent doses for the 285 nm LED (MS2 was suspended in 1X PBS) and LP UV (for all water matrices in (a).

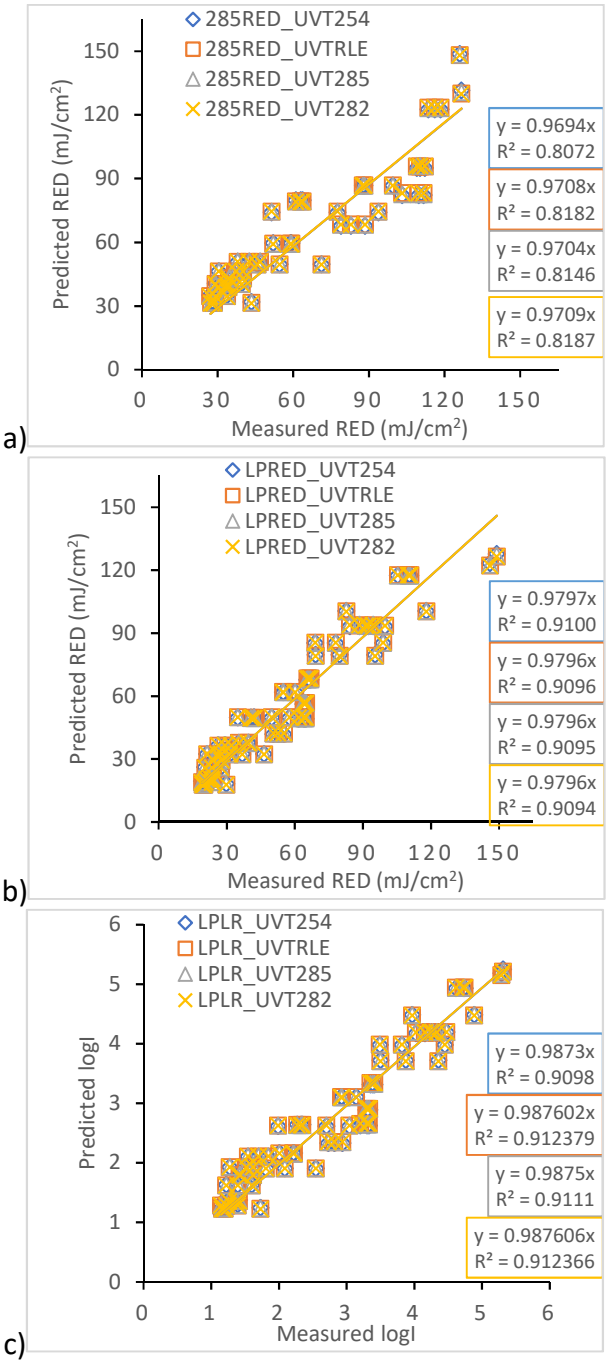

Figure 35 Assessment of combined variable modeling approaches of bench validation by MS2 challenge testing. In (a) RED calculated using the 285 nm LED dose response was modeled as a function of the various UVTs (at 254, 285, or 282 nm, or RLE, relative lamp emission weighted). Only points that could be estimated using the equation for 285 nm LED dose response were included in the model. In (b) RED calculated using LP UV dose responses was modeled as a function of the same UVTs. All data was included in the model. In (c) the same data as used in (b) was used to directly model log reduction (LR) as a function of various UVTs.

Table 9 Inorganic constituents measured in January samples. Elements listed in red had highest concentration in UV LED effluent, except for K and Na which were highest in chlorine effluent, and Si and Zn which were highest in filter effluent. National Primary and Secondary Drinking Water Regulation Maximum Contaminant Levels (MCLs) are shown (www.epa.gov).

Element	Filter Influent	Filter Effluent	Chlorine Effluent	UV LED Effluent	DL	units	MCL
Ag		DL	DL	DL	1	ppb	100*
Al		7.87	3.49	27.12	0.146	ppb	50*
As		DL	DL	DL	0.02	ppb	10
Ba		15.57	11.23	26.13	0.007	ppb	2000
Br	DL	DL	13.8	DL	1.24	ppb	
Ca	6.62	8.61	8.82	8.6	0.062	ppm	
Cd		DL	DL	DL	0.012	ppb	5
Ce		0.03	0.01	0.05	0.001	ppb	
Co		0.08	0.08	0.11	0.003	ppb	
Cr		3.9	3.99	8.32	0.177	ppb	100
Cs		DL	DL	DL	0.002	ppb	
Cu		0.83	1.5	1076	0.249	ppb	1300, 1000*
Dy		DL	DL	DL	0.002	ppb	
Er		DL	DL	DL	0.001	ppb	
Eu		0.01	0.01	0.02	0.003	ppb	
Fe	DL	DL	DL	DL	0.013	ppm	0.3*
Gd		0	DL	DL	0.003	ppb	
Ge		DL	DL	DL	0.02	ppb	
Hf		DL	DL	DL	0.002	ppb	
Ho		DL	DL	DL	0.002	ppb	
I	DL	DL	DL	DL	0.6	ppb	
K*	DL	0.53	0.7	0.58	0.073	ppm	
La		0.01	0.01	0.03	0.002	ppb	
Lu		DL	DL	DL	0.002	ppb	
Mg	1.3	1.51	1.51	1.47	0.007	ppm	
Mn		0.05	DL	0.09	0.038	ppb	50*
Mo		DL	DL	DL	0.472	ppb	
Na*	1.88	1.82	2.86	1.84	0.1	ppm	
Nb		DL	DL	DL	0.061	ppb	
Nd		0.022	0.02	0.029	0.003	ppb	
Ni		1.5	1.35	2.97	0.033	ppb	
P		DL	DL	DL	16	ppb	

Table 9 (continued)

Element	Filter Influent	Filter Effluent	Chlorine Effluent	UV LED Effluent	DL	units	MCL
Pb		DL	DL	0.1	0.002	ppb	15
Pd		DL	DL	DL	0.017	ppb	
Pr		0.001	DL	DL	0.001	ppb	
Pt		DL	DL	DL	0.006	ppb	
Rb		0.428	0.419	0.917	0.002	ppb	
Rh		0.033	0.02	0.095	0.002	ppb	
Ru		0.108	0.07	0.172	0.003	ppb	
Sc		2.23	2.201	4.599	0.039	ppb	
Sb		0.399	0.374	0.223	0.003	ppb	6
Se		DL	DL	0.53	0.11	ppb	50
Si*	4.99	4.66	4.51	4.6	0.047	ppm	
Sm		0.022	0.014	0.032	0.003	ppb	
Sn		DL	DL	DL	0.011	ppb	
Sr		176	125	248	0.008	ppb	
Ta		DL	DL	DL	0.013	ppb	
Tb		DL	DL	DL	0.002	ppb	
Te		DL	DL	DL	0.034	ppb	
Th		0.005	0.002	0.008	0.001	ppb	
Ti		1.05	1.14	2.81	0.071	ppb	
Tl		DL	DL	DL	0.002	ppb	2
Tm		DL	DL	DL	0.001	ppb	
U		0.063	0.055	0.07	0.003	ppb	
V		0.065	0.096	0.104	0.007	ppb	
Y		0.038	0.031	0.041	0.002	ppb	
Yb		DL	DL	DL	0.001	ppb	
Zn*		41.678	13.412	37.214	0.064	ppb	5000*
Zr		0.012	0.01	0.034	0.002	ppb	

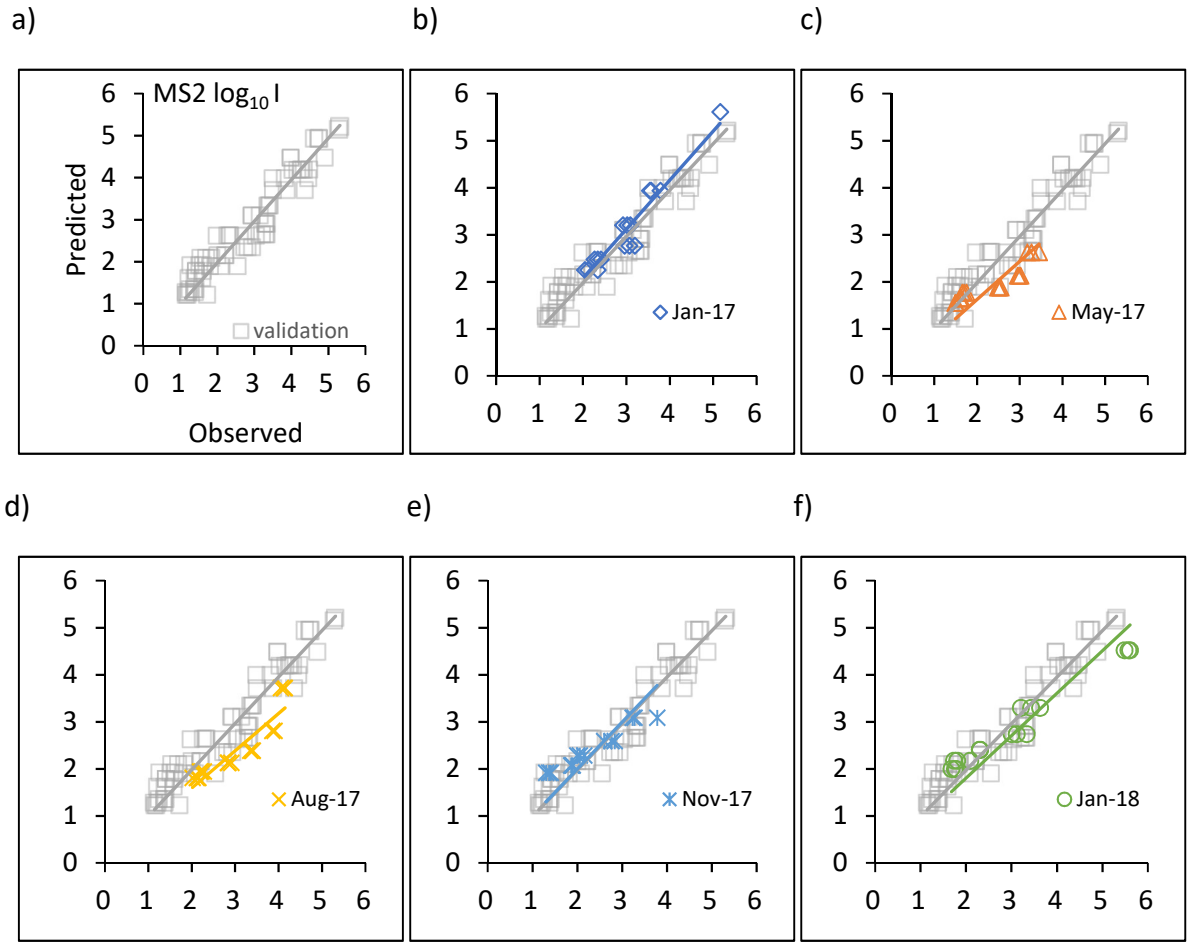

Figure 36 PearlAqua quarterly MS2 challenge testing combined variable model (Equation 12) predictions of MS2 logI as a function of UVT-RLE and flowrate, using bench validation testing model coefficients (Figure 20 reprinted in a with axes labels for quarterly data comparison in b-f).

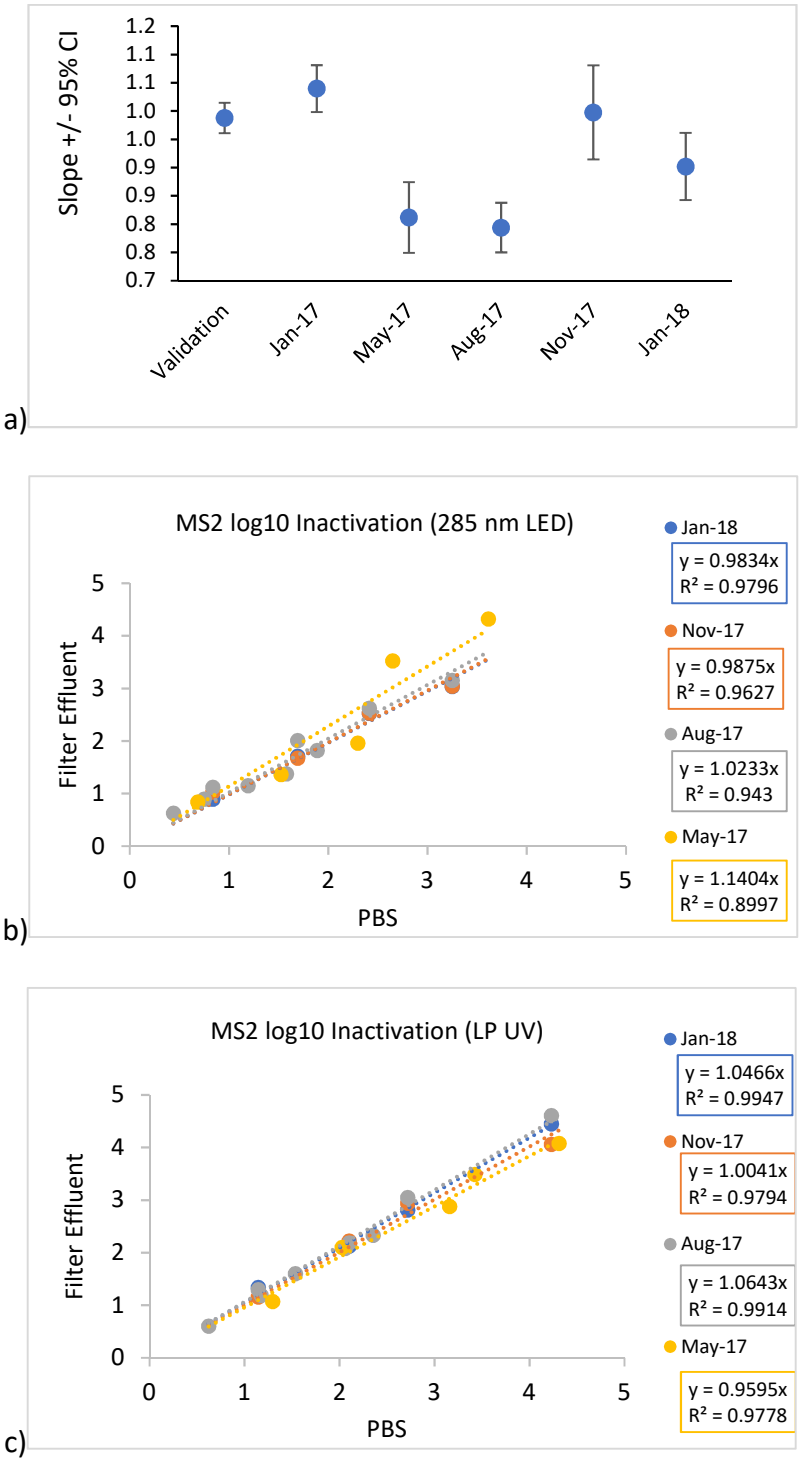

Figure 37 Assessments of quarterly challenge testing models. (a) The slope and 95% confidence interval for each quarterly MS2 challenge testing are shown when calculating predicted MS2 log inactivation using the initial bench testing validation model coefficients. MS2 collimated beam dose responses for the (b) 285 nm LED and (c) LP UV in quarterly challenge testing filter effluent versus in PBS.